Optical properties of thin layers of transition metal dichalcogenides

Maciej Koperski

Communauté
UNIVERSITÉ Grenoble Alpes

UNIWERSYTET WARSZAWSKI

THÈSE

Pour obtenir le grade de

DOCTEUR DE LA COMMUNAUTÉ UNIVERSITÉ GRENOBLE ALPES

préparée dans le cadre d'une cotutelle entre la *Communauté Université Grenoble Alpes* et *l'Université de Varsovie*

Spécialité : **Nanophysique**

Arrêté ministériel : 25 mai 2016

Présentée par

Maciej KOPERSKI

Thèse dirigée par **Marek POTEMSKI**, CNRS et codirigée par **Piotr KOSSACKI**, Université de Varsovie

préparée au sein du **Laboratoire national des champs magnétiques intenses (LNCMI**)
dans **l'École doctorale de Physique**

Propriétés optiques des couches minces de dichalcogénures de métaux de transition

Thèse soutenue publiquement le **5 mai 2017**,
devant le jury composé de :

M. David FERRAND
Professeur, Université Grenoble Alpes, France, (Président)
M. Vladimir FALKO
Professeur, University of Manchester, Angleterre, (Rapporteur)
M. Luis VIÑA
Professeur, Universidad Autónoma de Madrid, Espagne, (Rapporteur)
M. Jacek KOSSUT
Professeur, Instytut Fizyki Polskiej Akademii Nauk, Warszawa, Pologne (Membre)
M. Andrzej WYSMOŁEK
Professeur, Wydział Fizyki Uniwersytetu Warszawskiego, Pologne (Membre)
M. Bernhard URBASZEK
Directeur de recherches au Laboratoire de Physique et Chimie des Nano-objets, Toulouse, France (Membre)

University of Warsaw

Université Grenoble Alpes

Maciej Koperski

Optical properties of thin layers of transition metal dichalcogenides

PhD thesis supervised by

prof. dr hab. Piotr Kossacki and dr. Marek Potemski

May 2017

Contents

List of Figures

Acknowledgements

The decision to pursue the PhD studies in *co-tutelle* formula, in collaboration between the University of Warsaw and High Magnetic Field Laboratory in Grenoble, has vastly affected my research activity during this period of my scientific careerer. From the perspective I have now, I am inclined to say that it has been the right choice.

I must admit that the style of work imposed by the collaborative PhD project was demanding. However, the additional amount of energy and time that had to be spent in order to change labs every half a year was balanced by the benefits of experience and possibilities. The biggest advantage one can indicate is the opportunity to meet and work with a great number of people and, let me say, the scientific output of this work was created only thanks to the involvement of my colleagues. For that I am truly grateful.

First and foremost I would like to thank my supervisors: dr. Marek Potemski and prof. Piotr Kossacki. Their acceptance of following multiple research themes during my studies was admirable. Given the unpredictable nature of experimental sciences, constant readjustments of the schedule were needed, and notably I always got the full support from them. The freedom I was given in my research was of paramount importance to me.

The majority of experiments reported in this thesis were done in Grenoble, where I tightly collaborated with Karol Nogajewski, Maciej Molas and Ashish Arora. The optical pumping experiments were done in Warsaw and in this work Tomasz Smoleński had the leading role together with Tomasz Kazimierczuk and Mateusz Goryca. Ivan Breslavetz always offered technical assistance in High Magnetic Field Laboratory and Artur Slobodeniuk helped with theory.

There is a countless number of people, that I had a pleasure to get to know, but never worked with directly: Milan Orlita, Clément Faugeras, Younes Henni, Zhiguo Chen, Aleksander Bogucki, Krzysztof Gałkowski, Przemysław Leszczyński, Gérard Martinez, Denis Basko, Andrzej Golnik, Wojciech Pacuski, Jan Suffczyński, Johannes Binder, Tomasz Jakubczyk, Rémi Blinder, Aurélien Nicolet an many others. I would also like to thank the administration staff

and the directors of both laboratories for all the help I have received.

Finally, I express my gratitude to prof. Vladimir Falko and prof. Luis Viña for agreeing to become referees of the PhD manuscript and to prof. Jacek Kossut, prof. Andrzej Wysmołek, prof. David Ferrand and dr. Bernhard Urbaszek for participating in the PhD defence jury.

Abstract

The research reported in the thesis entitled 'Optical properties of thin layers of transition metal dichalcogenides' focuses on physical phenomena which emerge in the limit of two-dimensional (2D) miniaturisation when the thickness of fabricated films reaches an atomic scale. The importance of such man-made structures has been revealed by the dynamic research on graphene: a single atomic plane of carbon atoms arranged in honeycomb lattice. Graphene is intrinsically gapless and therefore mainly explored with respect to its electric properties. The investigation of semiconducting materials which can also display the hexagonal crystal structure and which can be thinned down to individual layers, bridges the concepts characteristic of graphene-like systems (K-valley physics) with more conventional properties of semiconductors. This has been indeed demonstrated in a number of recent studies of ultra-thin films of semiconducting transition metal dichalcogenides (sc-TMD). Particularly appealing, from the point of view of optical studies, is a transformation of the bandgap alignment of sc-TMD films, from the indirect bandgap bulk crystals to the direct bandgap system in single layers. The presented thesis work provides a comprehensive optical characterisation of thin structures of sc-TMD crystals. The manuscript is divided into five parts: three main chapters with a preceding introduction and the appendix reporting the supplementary studies of another layered material: hexagonal boron nitride.

Introduction. The fundamental properties of the investigated crystals are presented, especially those which are important from the point of view of optical studies. The discussion includes information on the crystal structure, Brillouin zone and electronic band structure. Also, the general description of the samples' preparation process and experimental set-up is provided.

Chapter 1. ***Basic optical characterisation of excitonic resonances in mono- and multi-layers of sc-TMDs.*** The optical response, as seen in the reflectance and lumines-

cence spectra of thin sc-TMDs is analysed (mostly for $MoSe_2$ and WSe_2 materials). The impact of the number of layers and temperature on the optical resonances is studied and interpreted in details. The complementary time-resolved study is also presented.

Chapter 2. ***Zeeman spectroscopy of excitonic resonances in magnetic fields.*** The evolution of the optical resonances in an external magnetic field, applied perpendicularly to the layers of sc-TMD materials is investigated. Based on these results, a phenomenological model is developed aiming to describe the linear with magnetic field contributions to the energy of individual electronic states in fundamental sub-bands of sc-TMD monolayers. Furthermore, the effects of optical pumping are investigated in WSe_2 monolayers, which can be tuned by tiny magnetic fields.

Chapter 3. ***Single photon sources in thin sc-TMD flakes.*** The uncovering of localised narrow lines emitting centres at the edges of thin exfoliated sc-TMD flakes is discussed. The optical investigations provide information on their fundamental properties. The presented study covers a broad range of topics, such as the impact of temperature and magnetic field on the optical response of the emitting centres, analysis of their polarisation properties and excitation spectra as well as photon correlation measurements.

Appendix A. ***Single photon emitters in boron nitride crystals.*** Hexagonal boron nitride also belongs to the family of layered materials, but it exhibits much larger band gap than semiconducting transition metal dichalcogenides. Narrow lines emitting centres have been observed in boron nitride structures, which reveal multiple similarities to defect centres in wide gap materials. They are characterised in a similar manner as the emitting centres in WSe_2.

Résumé

L'étude intitulée « Propriétés optiques des couches minces de dichalcogénures de métaux de transition » vise les phénomènes physiques émergeant à la limite de la bidimensionnalité, lorsque l'épaisseur du composé ciblé est à l'échelle atomique. Les effets de la dimensionnalité réduite sur les propriétés physiques furent initialement explorés dans le graphène. Les études concernant ce composé se concentrent surtout sur ses propriétés de transport puisque le graphène lui-même n'a pas bande interdite. Les sc-TMD, en plus de présenter une structure atomique et électronique similaire au graphène (vallée aux points K dans la zone de Brillouin), peuvent également être produit sous forme de couche monoatomique. Ainsi, plusieurs études révélèrent que ces composés en couche mince combinent des propriétés découlant de leur caractère 2D en plus des caractéristiques typiques des semi-conducteurs. De plus, la dimensionnalité de ces composés joue un rôle important dans la structure électronique. Plus précisément, les sc-TMD présentent dans le régime tridimensionnel un gap indirect qui devient direct lorsque les composés sont sous la forme d'une monocouche. Cette thèse est une étude complète des propriétés optiques des composés sc-TMD. Le manuscrit en question est divisé en cinq parties : trois sections principales précédées par une introduction. L'ensemble est complété par une annexe présentant des études complémentaires sur un autre composé lamellaire : le nitrure de bore hexagonal (h-BN).

Introduction : Les propriétés fondamentales des composés étudiés sont présentées en mettant l'accent sur celles qui jouent un rôle important dans la réponse optique de sc-TMD. Plus précisément, on y retrouve des informations sur la structure cristalline et la structure de bandes électroniques. Cette section détaille également le processus de préparation des échantillons ainsi que les divers montages expérimentaux utilisés.

Chapitre 1 : ***Caractérisation optique de base des excitons en résonance dans les couches et les multicouches de sc-TMD.*** La réponse optique des composés (surtout le

$MoSe_2$ et le WSe_2) obtenue par spectroscopie de réflexion et par spectroscopie d'émission est interprétée. En particulier, l'impact du nombre de monocouches et de la température sur celle-ci est discuté. De plus, une étude complémentaire de ces propriétés optiques résolue temporellement y est insérée.

Chapitre 2 : ***Spectroscopie Zeeman des excitons résonants sous champ magnétique.*** L'évolution des résonances optiques en fonction d'un champ magnétique appliqué perpendiculairement aux couches est l'objet de cette section. Un modèle phénoménologique décrivant la dépendance en champs magnétique de l'énergie des états électroniques est dérivé directement des résultats expérimentaux présentés dans cette section. L'effet de pompage optique est également étudié dans la monocouche de WSe_2, effet qui est très sensible aux champs magnétiques.

Chapitre 3 : ***Émetteurs de photons uniques dans les couches minces de sc-TMD.*** La découverte de raies d'émission fines et localisées sur de minces cristallites de sc-TMD est présentée, suivie d'une étude approfondie sur leur nature et leurs propriétés. Entre autres, leur évolution en fonction de la température, leur sensibilité aux champs magnétiques appliqués et leur polarisation sont discutées. Finalement, la spectroscopie de corrélation de photon est utilisée pour vérifier le caractére « source de photon unique » de ces émetteurs.

Annexe A : ***Émetteurs de photons uniques dans le nitrure de bore hexagonal.*** Le h-BN partage de nombreuses caractéristiques avec les sc-TMD tout en se distinguant de ceux-ci par la présence d'un gap électronique significativement plus grand. Certaines régions cristallines se comportent comme des défauts ponctuels, dans les matériaux caractérisés par leur large gap, en présentant des raies d'émission fines. Ces régions partagent une similarité frappante avec les émetteurs de photons uniques observés dans le WSe_2.

Streszczenie

Badania opisane w rozprawie pod tytułem "Optyczne własności cienkich warstw dichalkogenków metali przejściowych" dotyczą zjawisk fizycznych, które pojawiają się w granicy dwuwymiarowej miniaturyzacji, gdy grubość struktur osiąga skalę atomową. Znaczenie takich wytworzonych przez człowieka struktur dla zrozumienia podstawowych własności materiałów ujawniło się podczas dynamicznie rozwijających się badań nad grafenem: pojedynczej warstwie atomów węgla ułożonych w strukturę heksagonalną. Grafen, jako materiał bez przerwy energetycznej, był rozpatrywany głównie pod kątem własności elektrycznych. Badania materiałów półprzewodnikowych, również charakteryzujących się strukturą heksagonalną, dla których udało się odizolować pojedyncze warstwy, łączą nowe idee wywodzące się z odkrycia szczególnych cech grafenu (fizyka dolin w punkcie K strefy Brillouina) z wiedzą o bardziej typowych właściwoşciach półprzewodników. Rzeczywiście, nowego typu zjawiska zostały zademonstrowane w licznych, prowadzonych ostatnio, badaniach ultra-cienkich warstw półprzewodnikowych dichalkogenków metali przejściowych. Szczególnie interesujące, z puntu widzenia badań optycznych, wydaje się odkrycie zmiany charakteru przerwy energetycznej, która jest skośna w kryształach objętościowych, ale staje się prosta dla pojedynczej warstwy materiłu. Opisane w tej pracy badania wykorzystują szczegółową charakteryzację optycznych własności cienkich struktur dichalkogenków metali przejściowych jako podstawę do rozważań na temat ich własności elektronowych. Manuskrypt składa się z pięciu części: trzech głównych rozdziałów poprzedzonych wstępem i uzupełnionych dodatkiem, w którym omówione zostały badania dotyczące innego przedstawiciela materiałów warstwowych: heksagonalnego azotku boru.

Wstęp. Przedstawione zostały podstawowe własności badanych kryształów, szczególnie istotne z punktu widzenia badań optycznych. Dyskusja obejmuje informacje o strukturze krystalicznej, strefie Brillouina i elektronowej strukturze pasmowej. Ponadto omówiono ogólnie proces wytwarzania próbek i główne cechy układów doświadczalnych.

Rozdział 1. ***Podstawowe własności optyczne rezonansów ekscytonowych w pojedynczych warstwach i wielowarstwach półprzewodnikowych dichalkogenków metali przejściowych.*** Przeanalizowano optyczną odpowiedź cienkich struktur dwuselenku molibdenu ($MoSe_2$) i dwuselenku wolframu (WSe_2), badaną poprzez pomiary widm odbicia i luminescencji. Szczegółowo zinterpretowano dane doświadczalne dotyczące wpływu liczby warstw oraz temperatury na energię i szerokość optycznych rezonansów. Uwzględniono także uzupełniające badania rozdzielone w czasie.

Rozdział 2. ***Spektroskopia Zeemana rezonansów ekscytonowych w polu magnetycznym.*** Zbadano wpływ pola magnetycznego, przyłożonego prostopadle do powierzchni badanych struktur, na przejścia optyczne. Na podstawie otrzymanych wyników opracowano fenomenologiczny model mający na celu opis liniowych z polem magnetycznym wkładów do energii indywidualnych stanów elektronowych w podstawowych podpasmach pojedynczych warstw dichalkogenków metali przejściowych. Ponadto przeanalizowano efekty związane z pompowaniem optycznym w pojedynczych warstwach WSe_2, którego wydajność można zwiększyć poprzez przyłożenie niewielkiego pola magnetycznego.

Rozdział 3. ***Źródła pojedynczych fotonów w cienkich warstwach półprzewodnikowych dichalkogenków metali przejściowych.*** Przedyskutowano odkrycie centrów emitujących światło w postaci cienkich linii widmowych w eksfoliowanych strukturach dichalkogenków metali przejściowych. Optyczne badania dostarczyły informacji o ich podstawowych własnościach. Przedstawione badania dotyczą wpływu temperatury i pola magnetycznego na optyczną odpowiedź emitujących centrów, własności polaryzacyjnych oraz widm pobudzania jak również pomiarów korelacji fotonów.

Dodatek A. ***Emitery pojedynczych fotonów w kryształach azotku boru.*** Heksagonalny azotek boru również należy do rodziny materiałów warstwowych, lecz charakteryzuje się znacznie większą przerwą energetyczną niż dichalkogenki metali przejściowych. Centra emitujące wąskie linie widmowe także zostały zaobserwowane w strukturach azotku boru. Wykazują one cechy upodabniające je do barwnych centrów w innych materiałach szerokoprzerwowych. Emitery w azotku boru zostały scharakteryzowane podobnie jak emitery w kryształach WSe_2.

Introduction

The investigations of atomically thin layers of semiconductor materials, together with the preceding study of (practically) gapless graphene, constitute a new domain in physics, recently emerging in solid state science **[1]**. This turning point in the general study of condensed matter comes from a simple observation, that at the limit of 2D miniaturisation (when the thickness of structures reaches atomic scale) the material properties may undergo drastic changes. This finding laid the groundwork for a dynamic activity aiming to revisit often widely explored areas of research, which seemingly appear to be developed to a degree that everything is perfectly understood. One example of such tendency is related to the optical studies of semiconducting transition metal dichalcogenides (sc-TMD). The bulk crystals of these materials were investigated a few decades ago in context, e. g., of their potential utility for photovoltaic and photocatalitic applications **[2, 3]**.

Now, several years have passed since the processing of sc-TMD materials has been mastered to a degree, that individual layers can be isolated and incorporated into heterostructures. The importance of this technological step, suffice it to say, is already seen in discovery of numerous appealing features demonstrated uniquely by single and/or a few layers of sc-TMD. The understanding of the electronic properties of these new systems, together with the related physical phenomena, is challenging. It often requires extension of the conventional approach of Schrödinger quantum physics to incorporate new ideas characteristic of quantum electrodynamics (such as massive Dirac electrons **[4]**). Fortunately, a lot of relevant concepts have already been developed during the 'graphene period' and the investigations of sc-TMD structures clearly benefit from them. Still, the introduction of these ideas into semiconductor systems is never straightforward, therefore the vast majority of current research is at the very basic level. It is noteworthy to emphasize, that fabricating thin films of sc-TMD opened up exploration paths extending beyond traditional methods of semiconductor physics. More and more common become approaches inherited from other branches of science, such as soft matter

physics (investigation of membranes **[5,6]**), chemistry (bonds' engineering **[7,8]**) and surface study (tunnelling and atomic force microscopy **[9,10]**). The main driving forces behind these endeavours are to uncover the compendious set of properties, search for new potential functionalities and satisfy the intellectual craving to comprehend the fundamentals of these truly two dimensional systems.

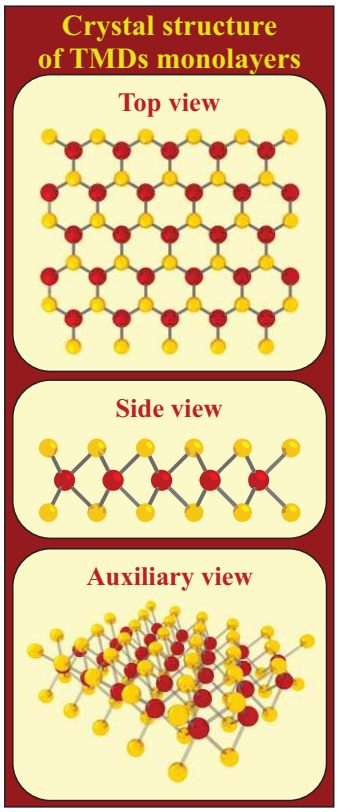

Figure 0-1: **The crystal structure of a monolayer sc-TMD is demonstrated. It is constructed from molecules of chemical formula MX_2, so that the atoms distributed over three separate planes form a hexagonal configuration. The two outer planes contain chalcogen atoms (e. g., S, Se, Te) and the middle plane stretches over metal atoms (e. g., W, Mo). Due to the presence of two different atoms in an elementary cell, the equivalence of the two triangular sublattices is lifted, which has profound consequences for the band structure of sc-TMD structures. Bulk crystals of sc-TMD exist in different phases. They are distinguished by the way, how monolayers are stacked on top of each other.**

The purpose of this thesis is to contribute to this research in terms of comprehensive optical characterisation of mechanically exfoliated sc-TMD structures. The majority of this work will be devoted to the investigation of specimen based on WSe_2 and $MoSe_2$ structures. However, when needed, the analysis will include information about other compounds from sc-TMD family (MoS_2, WS_2, WTe_2). The optical properties of semiconductor systems are inherently linked to their electronic band structure, which is related to the arrangement of atoms (or ions) in the crystal lattice. Therefore the presentation of the crucial information on the crystal structure of the investigated crystals and consequently the characteristics of the electronic states relevant for the fundamental optical transitions is the main purpose of this introduction.

0.1. Crystal structure of sc-TMDs materials; important points in the reciprocal space and thickness-dependent electronic band structure

Sc-TMDs belong to a group of layered materials, in which bulk crystal are composed of well defined stacking units weakly bound by van der Waals forces. A single unit is built of molecules with MX_2 chemical formula, where M stands for a transition metal atom and X for a chalcogen atom, linked together to form an individual layer made of three parallel atomic planes. A schematic representation of the configuration of atoms in such a monolayer is presented in

Figure 0-1. If the metal and chalcogen atoms are projected onto a single plane, they form a hexagonal lattice, however the presence of different atoms in the two triangular sublattices lowers the symmetry of the structure. For instance, out of three rotational symmetries around a hexagon's centre (by 60°, 120° and 180°) which preserve a hexagonal lattice made of a single type of atoms, only one (by 120°) remains valid for the lattice of sc-TMD monolayers. Also the number of mirror symmetries with respect to planes perpendicular to the surface of the monolayer is reduced from six to three. In other words, on could say that the symmetry group D_{6h} characteristic of graphene (in uniform environment) is reduced to D_{3h} for sc-TMD monolayers ($D_{6h} \supset D_{3h}$). Breaking the equivalence of the two triangular sublattices in sc-TMD crystals has profound consequences for their electronic properties. A presence of a band gap in the range roughly from 1 to 2 eV for different materials is perhaps the most important one. The hexagonal form of the crystal structure establishes also a hexagonal shape of the first Brillouin zone in the reciprocal space. The extrema of the electronic bands in mono- and multilayer structures related to the fundamental optical transitions appear at Γ (hexagon's centre), K+/K- (inequivalent hexagon's corners), Λ (located at the line segment connecting Γ and K+ or K- points) and M (located at the line segment connecting closest K+ and K- points).

Sc-TMDs multilayers may be found in various possible configurations determined by the alignment of the consecutive monolayers with respect to each other. The crystals investigated here are in 2H phase, which is likely more stable configuration that the alternative 1T and 3R phases. For 2H alignment the metal and chalcogen atoms appear on top of each other in adjacent monolayers. In this type of stacking the elementary cell of bulk crystals is a prism with a rhombus base containing six atoms (two MX_2 molecules). Therefore, a bilayer may be considered as a basic repeated motif for this kind of crystals. The band structure of sc-TMD in their bulk form is well-established. They have been recognized as indirect band gap systems with the maximum of the valence band located at the Γ point and the minimum of the conduction band at either Λ or K+/K- points, dependent on a particular material. This property alone makes the bulk sc-TMD structures very inefficient emitters of light. However, the transition to thin films, monolayers in particular, can introduce significant changes in their electronic properties. Figure 0-2 presents a concept behind the band structure transformation from multi- to monolayers of sc-TMD. The basic understanding of the evolution of the electronic states in sc-TMD structures with progressively decreasing thickness is related to the

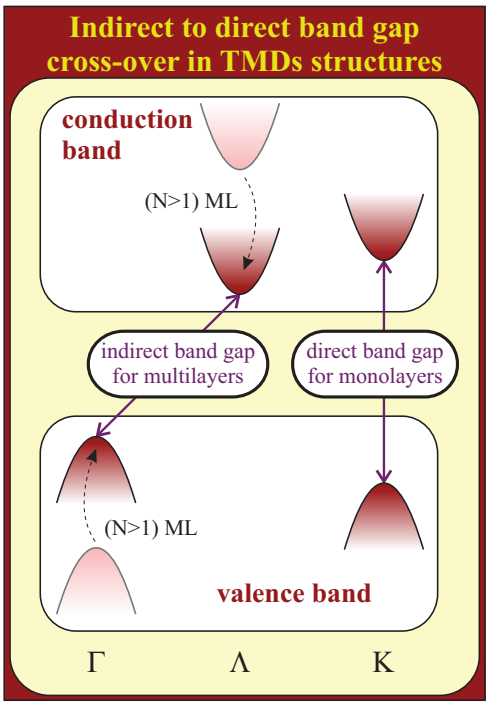

Figure 0-2: **The concept of the transition from indirect band gap character of multilayer sc-TMD structures to a direct band gap system at the limit of monolayer in presented. The basic idea behind this transformation is based on confinement effects. By squeezing the wave function of electrons and holes in the direction perpendicular to the layers of sc-TMD structure, the energy of electronic states is changed. The experimental evidence points out to the conclusion, that the magnitude of the energy shifts of particular states located at the band extrema appears to vary between Γ, Λ and $K\pm$ points in the reciprocal space. In the simplest view this dependence is governed by the inverse of the effective mass of electrons and holes for conduction and valence bands. Therefore, if the carriers occupying $K\pm$ valleys are heavier than their counterparts in other valleys, one can always find a critical thickness, for which the band gap becomes direct. It seems that for most sc-TMD this happens for monolayers (perhaps $MoTe_2$ is an exception, when the transition occurs for bilayers).**

emerging confinement of the carriers. It a simplistic view, the alternation of the energy of the electronic states may be described in terms of an infinite potential well with a barrier width equal to the thickness of the sc-TMD structure. The energies of the electronic states in this canonical problem of quantum mechanics are defined exclusively by the mass of carriers and well thickness d. We can naively extrapolate this picture on the band structure of sc-TMD materials and describe the d-dependant energy of conduction and valence states at relevant band extrema as: $\Delta E_{c/v} \propto 1/\left(m^*_{z_{e/h}} d^2\right)$, where $m^*_{z_{e/h}}$ is the out-of-plane effective mass component of electrons or holes. The transformation of the indirect band gap of bulk crystals into a direct band gap system at monolayer limit for most of the sc-TMD materials is strongly supported by numerous experimental and theoretical investigations. This finding implies that the impact of the thickness reduction on the energy of the electronic states differs starkly for the Γ, Λ and $K\pm$ points in the reciprocal space. Based on invoked arguments, we can therefore speculate that electrons and/or holes occupying the K+/K- valleys have larger our-of-plane mass than their counterparts in Γ or Λ points. In that case, the rise of the gap between valence and conduction states with the decreasing number of layers is least pronounced at K+/K- points and eventually, at certain critical thickness, the character of the band gap has to become direct. It is currently believed than such transformation occurs in the limit of monolayer thickness for most of the sc-TMD materials.

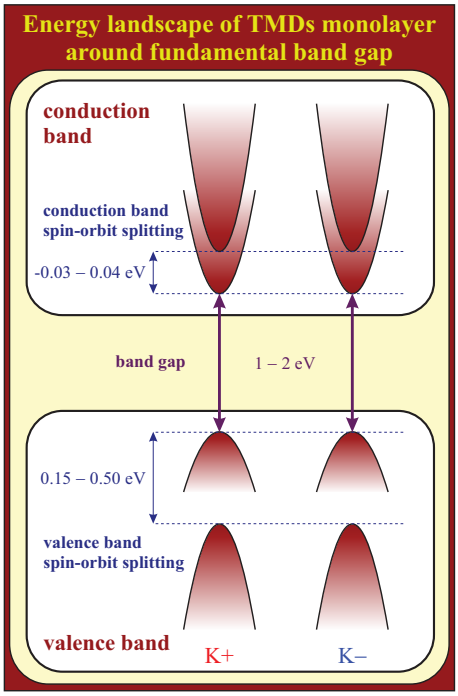

Figure 0-3: **The schematic representation of the alignment of fundamental valence and conduction sub-bands, characteristic of sc-TMD monolayers, is presented. The two inequivalent valleys at K+/K- valleys host massive carriers. The valence and conduction states, separated by the band gap of 1 - 2 eV for various representatives of sc-TMD family, are further split by spin-orbit interaction. The magnitude of this splitting is different for electrons (tens of meV) and holes (hundreds of meV). The negative and positive values of the conduction band splitting reflect the possibility of different distribution of spins between the states in both valleys. In this regard, the spin up and spin down states may be pinned to lower or upper conduction sub-bands in a particular valley.**

0.2. Band structure of monolayers of sc-TMD around fundamental band gap

The direct band gap of sc-TMD monolayers is of vivid interest from the point of view of optical investigations. It opens up the efficient radiative recombination channels leading to observation of robust luminescence from such structures. The feasibility of light emission spans broad temperature range. The low temperature studies, when the emission lines appear as relatively narrow resonances, provide the best access to the electronic properties and are relevant for more advanced fundamental research. Most sc-TMD monolayers exhibit also room temperature emission, which offers attractive opportunities related to optoelectronic functionalities.

In the simplest view, one can think of the band structure of a sc-TMD monolayers around the fundamental band gap as 'gapped graphene'. This description is by far too simplified to confront it with realistic band structures of sc-TMD monolayers, however it may be instructive to use it for the introduction of basic concepts. In this view, the energy of carriers can be expressed as a function of momentum, calculated with respect to the K-point of the Brillouin zone: $\vec{k} = (k_x, k_y) = \vec{k}' - \vec{K}$, where $\vec{k}'$ is the actual momentum of the carriers and $\vec{K}$ is a constant vector pointing to the K-point. Then, a Dirac Hamiltonian for a system with a band gap can be written as follows:

$$\hat{H} = \begin{pmatrix} \Delta/2 & \hbar v k_+ \\ \hbar v k_- & -\Delta/2 \end{pmatrix}$$

where $k_\pm = k_x \pm i k_y$, Δ is the value of the band gap, v is a parameter called Fermi velocity and

$\hbar$ is a reduced Planck constant. In a rigorous approach one should account for the existence of two inequivalent corners of hexagonal Brillouin zone (K+/K-), e. g. by introducing two momentum quantities (k_1 and k_2) corresponding to each valley. However, as far as solely the energy dispersion is concerned, there are no consequences of this distinction. The exact solution for the eigenvalue problem for the presented Hamiltonian are given by:

$$E(k) = \pm\sqrt{\left(\frac{\Delta}{2}\right)^2 + (\hbar v k)^2}$$

For large values of $k^2 = k_x^2 + k_y^2$, away from the K point of the Brillouin zone, the linear dispersion appears in the same form as for graphene. On the other hand, for small k ($|k| \ll \Delta/\hbar v$) one can consider a first order approximation of the exact dispersion relation to recover parabolic character of bands:

$$E(k) \approx \pm\left(\frac{\Delta}{2} + \frac{v^2\hbar^2k^2}{\Delta}\right)$$

For the values of k, which satisfy the condition necessary to obtain the parabolic dispersion, an effective mass (the same for electrons and holes) can be introduced as $m^* = \Delta/2v^2$. Unlike the actual gapped graphene systems (such as graphene deposited on boron nitride with a band gap of tens of meV), the value of the band gap for sc-TMDs is large (1-2 eV). Therefore, the parabolicity of the bands, in this case, is sustained practically for the whole range of momentum relevant for the optical transitions involving K-point states. In is noteworthy to stress, that the consequences of 'gapped graphene' model for sc-TMD monolayers reach beyond the introduction of parabolic bands at K+/K- points of the Brillouin zone. This simple Hamiltonian supports also the basic idea of valley selectivity exploiting the coupling of circularly polarised light with transitions at K+ and K- points **[11]**. In other words, the optical transitions at K+ point are active only in σ^+ polarisation, while the transitions at K- point are active only in σ^- polarisation. Therefore, the optical studies are rightfully designated for exploration of concepts of so called 'valleytronics'.

Any further understanding of the realistic band structure of sc-TMD monolayers requires compilation of experimental investigations with theoretical calculations, which are realised in multiple more or less advanced tight binding or k.p models. The first major divergence from conventional Dirac fermions on a honeycomb lattice is the orbital contribution to the wave functions of electrons and holes in the fundamental sub-bands. They are constructed predominantly from d-orbitals of the transition metal atoms: d_0 in the conduction and $d_{\pm 2}$ in the valence band.

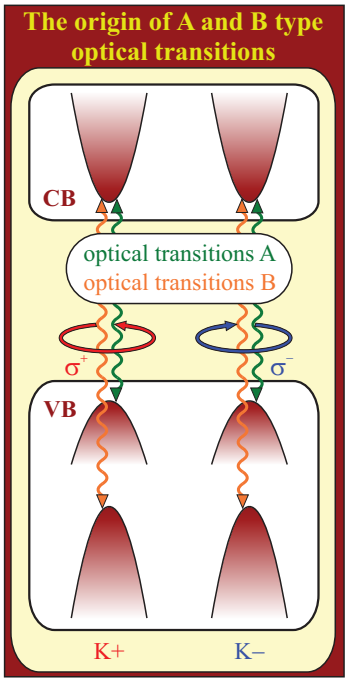

Figure 0-4: **The large spin-orbit splitting in sc-TMD monolayers, particularly robust in the valence band, can be used to classify the optical transitions into two groups. The origin of the distinction between so called transitions A and B is depicted in the scheme. The lower energy transitions A (green arrows) are related to the upper valence band states whereas the higher energy transitions B (orange arrows) are related to the lower valence band states. The spin-orbit splitting for electrons is neglected here in order to emphasize, that the alignment of conduction sub-bands is irrelevant for the introduction of A and B transitions (it may, however, influence their exact energy). Both transitions can typically be observed in absorption-type experiments for most sc-TMD mono- and multi-layers. They appear as two resonances separated energetically by hundreds of meV. It is also important to stress the existence of valley-selective polarisation rules. The helicity of the circularly polarised transitions is determined exclusively by the valley, in which the transition takes place, regardless of it being A or B type.**

For a more accurate description, the minor contribution of chalcogen atoms' p-states may be considered, which originates from the admixture of neighbouring bands in models exceeding a simple two-band approach. The relatively large value of the orbital momentum associated with carriers hosted in K+/K- valleys leads to a robust coupling of the orbital motion of the carriers with their spin, which is further amplified by the presence of heavy metallic atoms in sc-TMD crystals. As a consequence, a large spin-orbit splitting is seen in the conduction and valence sub-bands **[12–15, 18]**. The invoked properties of TMDs monolayers altogether determine their electronic band structure around the band gap. The alignment of fundamental electronic sub-bands, which is now generally acknowledged to represent well the band structure characteristic of sc-TMD monolayers, is demonstrated in Figure 0-3.

The splitting between the valence sub-bands is particularly large, of the order of hundreds of meV, due to the $l_z = \pm 2$ orbitals. That feature leads to a classification of optical transitions into two groups, as presented in Figure 0-4: lower energy transitions A involving holes from the upper valence sub-band and higher energy transitions B involving the lower valence sub-bands. Even though both types of transitions are significantly separated in energy, they still share common valley-selective optical selection rules, which enable a straightforward distinction between the optical transitions taking place in K+ and K- valleys.

0.3. Comments on sample preparation, experimental techniques and set-ups

The samples investigated in this work were prepared by mechanical exfoliation techniques. A set of procedures has been established, tested and gradually improved with time to maximise the efficiency of isolating large area thin sc-TMD structures (down to monolayers) from synthetic bulk crystals. The core steps in the exfoliation process were inspired by the preceding work regarding graphite crystals. These were afterwards adjusted to accommodate parameters (such as strength of adhesion, magnitude/time of applied pressure, etc.) and modifications (e. g., introducing additional transfer from an adhesive tape to an elastomeric stamp) appropriate for particular sc-TMD materials in terms of the resulting quality, size and yield of thin exfoliated flakes **[16]**. The final step in the exfoliation procedure is the deposition of the flakes on the target substrate, Si/SiO_2 in our case. The substrates are always cleaned beforehand by oxygen plasma ashing. Usually, they also have lithographically defined golden markers (with a thin titanium layer underneath for better adherence), which act as a reference when finding the position of the most interesting flakes.

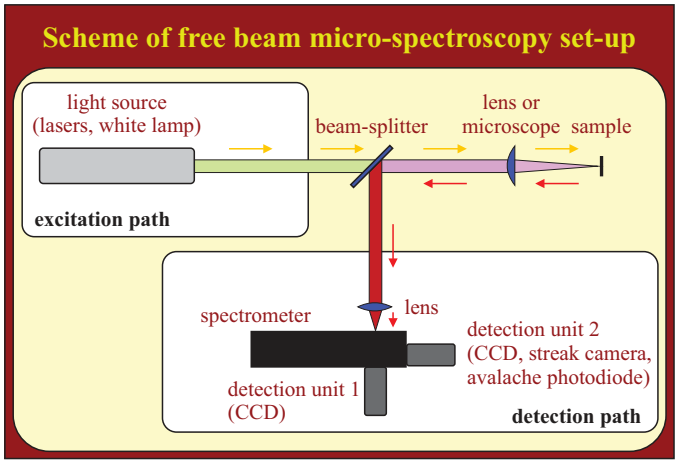

Figure 0-5: **A general scheme of optical micro-spectroscopy set-up is presented. It may be tentatively divided into three parts: excitation/detection path and sample space. The sample usually resides in a cryostat (flow cryostats and helium baths were used), which may be equipped with heaters enabling control of the temperature or superconducting coils providing magnetic field. Different ways of controlling the position of the sample with respect to the excitation beam may be introduced (usually involving more or less precise piezo-stages).**

The newly created samples undergo an initial inspection under an optical microscope. The most promising specimen are preliminarily selected based on their optical contrast with respect to the substrate. In the early stages of development, the thickness of the flakes was verified by atomic force microscopy (AFM) characterisation of the exfoliated flakes. However, the emerging correlation between the actual colours of the flakes appearing in the optical images and their thickness turns out to be surprisingly accurate. The exact correspondence is further supported by the calculations of reflectivity spectra of realistic dielectric stacks by transfer matrix methods, combined with the calibration of the colour palette characteristic of the particular microscope. Eventually, the thinnest structures (monolayers, bilayer, trilayers, etc.) can be

identified exclusively by analysing their optical contrast.

The experiments performed on these samples can generally be labelled as optical micro-spectroscopy study. The choice of realising microscale investigations is not dictated by the small size of the exfoliated flakes as the best exfoliation approaches yielded flakes of lateral dimensions reaching up to hundreds of micrometres. Actually more relevant (almost certainly) is a rather poor quality of the currently available crystals of sc-TMD materials. The exfoliated flakes appear to be strongly inhomogeneous with respect to the the exact energy and intensity of particular resonances seen in the optical spectra and that inconvenience may be avoided/limited by minimising the excitation and/or detection area. Certain attempts have been made to improve the optical signal by chemical treatments (e. g. by passivating the flakes with superacids **[17]**). These approaches lead to the observation of the enhancement of the emission intensity for some sc-TMD materials (mostly sulfur based compounds), however the quality of the optical response is still far from perfect.

Nonetheless, the optical examination brings plentiful of information about the electronic states and related physical phenomena in sc-TMD structures. A general scheme of a standard free beam micro-spectroscopy experimental set-up is presented in Figure 0-5. It may be divided into separate excitation and detection segments, as well as a part, where the excitation beam and the signal (luminescence or scattered/reflected light) coming from the sample spatially overlap. The main unit in the excitation module is a light source. For the study of reflection it is a white lamp. In case of luminescence measurements it is an appropriate laser. Different lasers are used based on the properties of the system (mostly the spectral range of light emission) and desired type of investigation to be performed. In this work we took advantage of the following set of lasers:

- Ar^+ lasers (lines 488.0 nm and 514.5 nm) were used usually for non-resonant excitation.
- Multiple diode lasers, each with a specific emission energy, offer functionalities similar to Ar^+ laser.
- Rhodamine dye laser was used as a tunable source covering roughly the central part of the visible spectral region (560 - 610 nm)
- Continuous wave Ti:Sapph lasers, also tunable, provided excitation at lower energy (690 nm and longer wavelengths). This laser can be used for resonant or quasi-resonant excitation of some sc-TMD materials (e. g. WSe_2, $MoSe_2$).

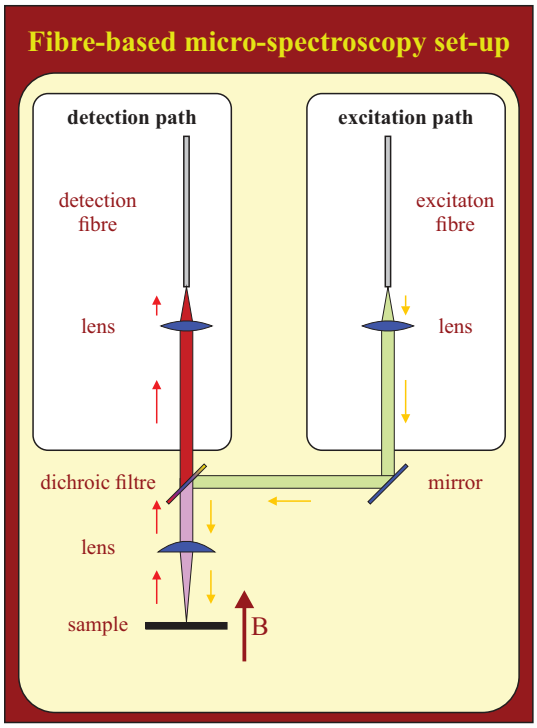

Figure 0-6: **A scheme of the fibre-based optical set-up is presented, which can be compactly realised inside a probe adequate for measurements in high magnetic fields. Different kinds of fibres based on the designated purpose of the particular probe may be used. The probe optimised for measurements of luminescence is usually equipped with monomode excitation fibre (5 μm of core diameter) and multimode detection fibre (50 μm of core diameter). If the excitation fibre is changed into a multimode one with a larger core, then reflectance and luminescence may be measured in the same set-up at the cost of spatial resolution. The sample is mounted on *x*-*y*-*z* controlled piezo-stages in order to provide precise control of its position with respect to the laser beam. The volume inside the probe is filled with helium exchange gas, which mediates the heat transfer. Therefore the sample can be cooled down (to about 10 K) by placing the probe in a helium bath.**

- Pumped optical parametric oscillator (OPO), tunable in broad spectral range in visible region, was used for some of the time-resolved study, mostly involving detection with a streak camera.

The excitation path may also be used to introduce optical elements useful for the control of the geometry of the beam (lenses, diaphragms/pinholes, etc.) and the polarisation properties of light (polarisers and half/quarter wave-plates).

The main component of the detection part is a spectrometer, containing gratings of different density (300, 600, 1800 or 2400 grooves/mm), which spectrally resolves the optical signal coming from the sample. Each spectrometer can be equipped with up to two detectors. Usually one of them is a charged coupled device (CCD) camera (or InGaAs camera for detection of near-infrared light, useful for instance for the study of $MoTe_2$ structures). The other detector, which can be an avalanche photodiode (APD) or a streak camera, usually provides better temporal resolution and/or higher sensitivity than a standard CCD camera. The polarisation properties of the optical signal may be studied by introducing a proper set of wave plates and polarisers before the entrance to the spectrometer.

The application of a magnetic field is possible in a free-beam set-up. It can be realised with split-coil superconducting magnets, but such solution limits the maximum value of the magnetic

field that can be obtained. More complex constructions are needed to reach higher fields. The highest fields used in this work (30 T) were generated by resistive magnets with an outer Bitter coil. In case of such magnets, the samples need to be placed in a specially designed probes with fibre-based optics. The general concept of the set-up is the same as discussed before, but all the elements must be miniaturised to fit a tube of roughly 50 mm diameter. A scheme of such compact configuration of optical elements is presented in Figure 0-6.

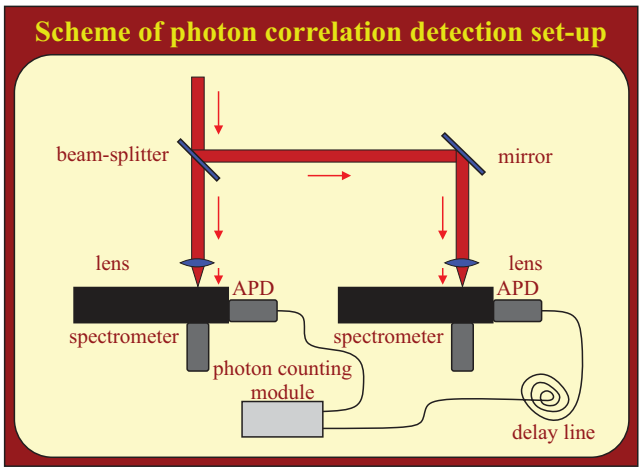

Figure 0-7: **A scheme of a detection set-up for the study of photon correlations is presented. It basically consists of a doubled detection unit, which was used in standard photoluminescence measurements. However, here the luminescence signal is detected by avalanche photodiodes (APDs). The generated electrical signals are further processed by a specialised photon counting module, which is used to measure temporal separation between detection events from both detectors. A delay line, in form of a long coaxial cable, is introduced into one of the detection arms in order to access negative time delays.**

A significant part of this work is devoted to the investigations of the properties of isolated emitting centres found in sc-TMD and boron nitride structures. Both of them reveal single photon emission character, which is studied by designated techniques of optical spectroscopy. A detection set-up used for photon correlation measurements is realised in the Hanbury Brown and Twiss (HBT) configuration, as presented in Figure 0-7. In this case, the luminescence signal is divided into two paths by a beam splitter. Each path ends with a standard detection unit: a spectrometer equipped with an avalanche photodiode (APD). A set of slits, combined with high density gratings in the spectrometer, provides a spacial selection of photons of particular energy, which are directed towards the APDs. Therefore, the APDs can be sensitive to photons corresponding exclusively to a chosen well isolated spectral line originating from the investigated emitter. Upon detecting a single photon, APD sends an electrical signal transmitted to a photon counting module. This device basically works as a high resolution stopwatch, triggered by the electrical signal from the APD in one detection path and stopped by the electrical signal from the APD in the other path. Such measurement is repeated multiple times to investigate the statistical distribution of the time, which elapses between the detection of single photons in the two paths. The result of such a study is *de facto* a histogram of the measured time intervals, which is afterwards confronted with a second-order correlation

function formally defined as $g_2(\tau) = \langle I_a(t)\, I_b(t+\tau)\rangle \,/\, \langle I_a(t)\, I_b(t)\rangle$ where $\langle \ldots \rangle$ may generally be any temporal statistical average, $I_a(t)$ and $I_b(t)$ represent the intensity of light measured by detectors a and b. In case of emitters in solids, the exact formula for the correlation function depends, e. g., on the alignment of the involved electronic levels and dynamical parameters (rates) describing transitions between them. Let us note, that if the emitting specimen is a single photon source, then consequently both APDs cannot detect photons at the same time. In such a case an antibunching appears at zero time delay in the correlation function ($g_2(0) = 0$ for a perfect source).

Chapter 1

Basic optical characterisation of the excitonic resonances in mono- and multilayers of sc-TMD

The possibility of fabricating sc-TMD structures with the precision of individual layers **[1]** offers an unprecedented opportunity to investigate systematically the impact of dimensionality on the fundamental optical excitations. The appearance of resonances of excitonic nature in the optical spectra not only grants insight into the evolution of the sc-TMD band structure with the number of layers, but more importantly reveals a non-trivial influence of the Coulomb interaction **[19–28]**.

A lot of attention has been brought to the fact that the optical response of thin sc-TMD structures critically depends on the number of layers. A very first appealing observation is related to the efficiency of light emission. It is now well established that in the limit of a monolayer (the most basic 'stacking unit' of the thickness of a single MX_2 molecule) the PL signal increases dramatically, practically in all sc-TMD materials **[29–34]**. Such easily fabricated bright light sources, capable of room temperature operation, constitute an attractive research topic, especially if a diverse optical response of various members of sc-TMD family is taken into account. Figure 1-1 presents a miscellany of low temperature PL spectra of most commonly investigated sc-TMD monolayers, which cover a broad spectral range in the visible and near-infrared region. The same crystal structure of various representatives of sc-TMD materials in a monolayer form implies that the value of the band gap is determined predominantly by the strength of the inter-atomic bonds. In this regard, the presence of a chalcogen atom in

a particular compound seems to be a leading factor. The atomic number of sulfur, sellenium and tellurium progressively rises, which elevates the valence electrons to higher orbits ($3s^2 3p^4$, $4s^2 4p^4$ and $5s^2 5p^4$ for S, Se and Te respectively) with smaller binding energy. As a consequence the inter-atomic bonds in the corresponding sc-TMD materials become weaker, a feature which is accompanied by the increase of the lattice constant and the reduction of the band gap.

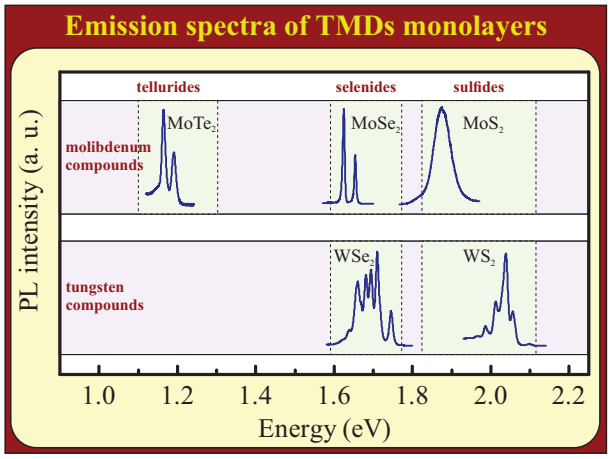

Figure 1-1: **Low temperature PL spectra of commonly investigated sc-TMD monolayers illustrate the diversity of the optical response of different materials. One of the tendencies that emerges from this comparison is a clear correlation between the type of the compound based on the presence of particular chalcogen atoms (S, Se, Te) and the energy of emission originating from monolayer form of the corresponding material.**

Apart from revealing the light emission at different energies, the PL spectra also exhibit distinct characteristics for particular materials. For instance, the relatively simple PL spectra of $MoSe_2$ and $MoTe_2$ monolayers clearly contrast with multi-peak extensive PL bands seen for WSe_2 and WS_2 monolayers. Surely, there is plenty of room for exploration in search for common properties as well as differentiating features of materials belonging to the sc-TMD family.

1.1. Optical signatures of thin structures of sc-TMD

We commence the analysis of the optical response of sc-TMD structures with the comparison of the PL and reflectivity spectra of WSe_2 flakes of various thickness (1-4 monolayers and bulk). Since the very first observation of robust luminescence from monolayer sc-TMD flakes **[29]**, in contrast to weak emission coming from thicker structures, the arguments have been brought up that the sudden enhancement of the PL signal in monolayer limit comes from a particular change of the band structure. It has been speculated that the indirect band gap between Γ and Λ or Γ and K points of the Brillouin zone established for sc-TMD in the bulk form **[35–37]** undergoes a transformation so that monolayers become direct band gap systems with the fundamental optical transitions at the K point of the Brillouin zone. This prediction has been tested against multiple band structure calculations **[14, 38–47]** or angle-resolved photoemission spectroscopy (ARPES) studies **[48]**, which seem to support the initially proposed explanation. The optical

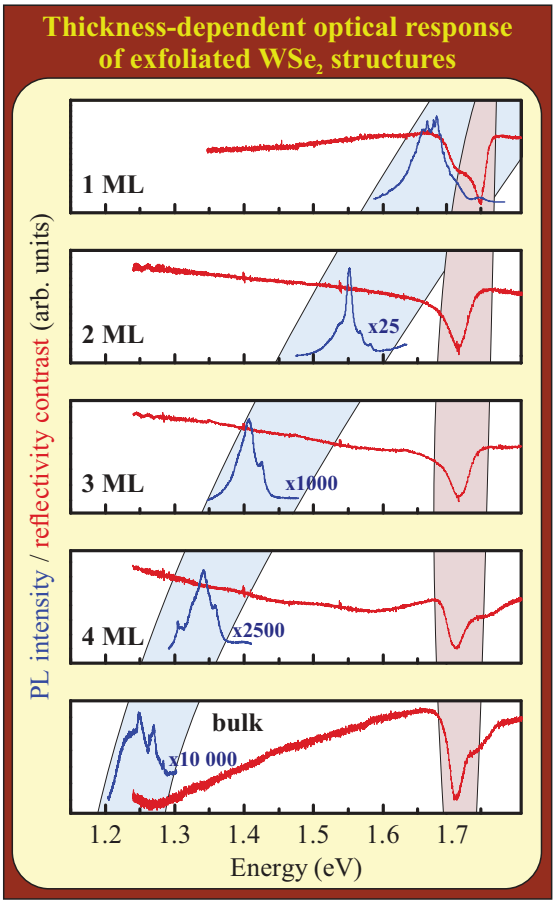

Figure 1-2: **The reflectivity spectra (red curves) are confronted with photoluminescence spectra (blue curves) for exfoliated WSe_2 structures of thickness varying from one to four layers and also in the bulk limit. The reflectance was measured by detecting the light of a white lamp, initially focused on the surface of the sample to a spot of several μm size, reflected from the WSe_2 flake and from nearby Si/SiO_2 substrate. Afterwards the reflectivity contrast was established as: $(R_{flake} - R_{substrate}) / (R_{flake} + R_{substrate})$. The presented reflectivity spectra do not share the vertical axis for consecutive graphs, partially because it is difficult to compare the absorption strength of the excitonic resonances between different structures, as the shape and intensity of absorption lines strongly depends on interferences which are always present in realistic structures. On the contrary, the luminescence spectra, obtained for non-resonant 514 nm laser excitation, are better comparable. They are presented in the same scale, but a multiplying factor was used (which serves also as a measure of the quenching of the emission intensity) to flesh out the detailed structure of the PL spectra.**

spectra for WSe_2 material presented in Figure 1-2 also favour this scenario.

Let us note that the reflectivity spectra in the spectral region, where the absorption band edge appears, are dominated by a single line (in some cases accompanied by lower or higher energy shoulders, which origin is discussed later on), commonly attributed to the resonance related to the lowest energy optical transition at the K point of the Brillouin zone. The position of this resonance is only weakly dependent on the number of layers. It is progressively red-shifted for thicker structures so that the difference in the transition energy between the monolayer and bulk flakes does not exceed 30 meV. In view of the expected significant band structure alternation with the number of layers, especially when the transition from the indirect to direct band gap system appears for monolayers, the observation of almost thickness-independent energy of the fundamental resonance in the absorption-type experiments seems puzzling at first sight. However, the energy of this resonance, excitonic in nature, corresponds to the energy difference between the apparent value of the band gap at the K-point of the Brillouin zone and the exciton binding energy. Clearly, the experimental data hints that the shrinkage of the gap with the increasing number of layers is compensated by the reduction of the exciton binding

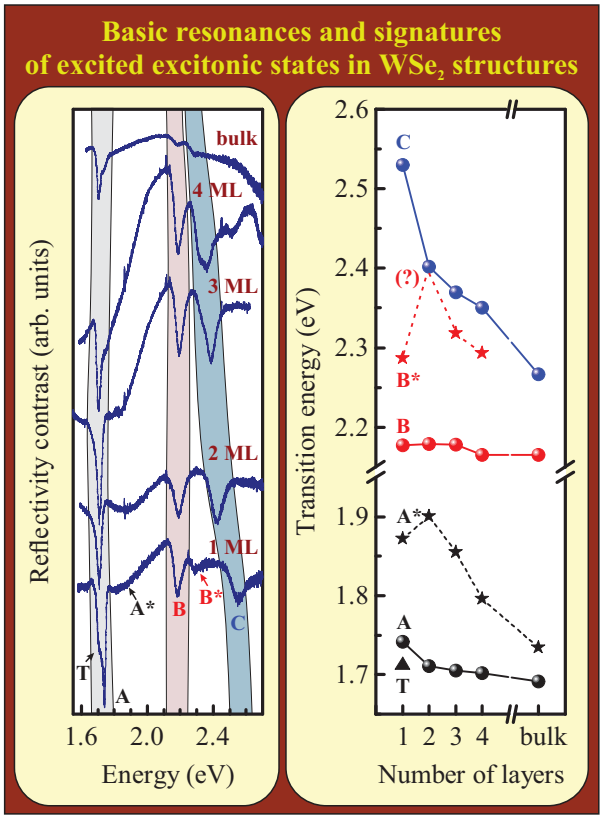

Figure 1-3: **The reflectivity contrast spectra for WSe_2 structures of different thickness (one to four layers and bulk) are shown in broader spectral range. Three major resonances (labelled as A, B and C) dominate the spectra. A and B resonances are accompanied by higher energy shoulders A* and B*. In case of the monolayer flake, on the lower energy side of the resonance A a feature related to a charged exciton (CX) appears. In order to accurately establish the energies of the lines, the spectra were fitted by employing a transfer matrix formalism, in which the presence of resonances is accounted for by Lorentzian contributions to the dielectric function: $\epsilon(E) = \sum_j A_j / \left(E_{0,j}^2 - E^2 - i\gamma_j E\right)$, where $E_{0,j}$ are energies of consecutive resonances. The energy of B* resonance in a bilayer probably coincides with the C resonance, which we speculate on the basis of the evolution of the A* resonance energy with the number of layers.**

energy. The question whether such accurate compensation of these two effects is accidental or originates from specific attributes of the crystals (such as, e. g. symmetry properties) is still up for debate.

More can be said about the band structure changes if the PL and reflectance spectra are comparatively analysed. In case of the WSe_2 material the emission spectra are quite complicated, composed of multi-peak PL bands exhibiting different shapes for flakes of different thickness. Surely, more in-depth studies are needed to comprehend the detailed characteristics of each spectrum, however our main goal is to bring attention to the general tendency of progressively growing energy separation between emission and absorption resonances with the increasing number of layers. Particularly, for monolayer flakes the fundamental absorption resonance is also seen in the emission spectrum, which is a strong argument in favour of a direct band gap system. However, that is no longer the case for structures with the number of layers equal to or larger than two. Instead, the emission signatures appear below the absorption resonance by about 0.15 eV for two layers thick flakes and this shift continuously increases reaching up to about 0.5 eV in the bulk limit. Another feature, also indicative of the direct-indirect band gap cross-over, is the progressive and significant quenching of the PL signal intensity with the increasing number of layers. Overall, the invoked observations and interpretation of the

experimental data provide decent understanding of the band structure evolution for sc-TMD structures and also underline the emerging importance of Coulomb interaction.

Now, we will proceed to the analysis of the reflectivity spectra in a wider spectral range, which are presented in Figure 1-3. The most prominent features in these spectra are three robust resonances. The two lower energy lines, labelled as A and B, are commonly attributed to the transitions at the K point of the Brillouin zone originating from two valence band states, which are significantly split by spin-orbit interaction. The resonance A for monolayer flakes is typically accompanied by a low energy shoulder, which arises due to a charged exciton state (labelled as CX). The third main resonance, subsequently labelled as C, does not have a well-established interpretation, however its energy position in monolayer flakes and the following evolution when increasing layer thickness shows a good correspondence with band structure calculations for a transition at the M point of the Brillouin zone **[49]** (if certain assumptions are made about excitonic effects).

1.2. Appearance of the excited excitonic states in absorption-type experiments

In order to get a complete insight into the excitonic character of these main resonances, they have to be analysed with the inclusion of the information about the excited states. Unfortunately, the contribution of the excited states to the optical spectra in absorption-type experiments performed on exfoliated sc-TMD structures is only weakly pronounced. In our data we observe a type of higher energy shoulder accompanying both A and B resonances (labelled as A* and B*), for which we can assign an energy position by cautiously fitting the reflectivity spectra. Our interpretation is that these additional shoulders arise mostly due to the excited state with a quantum number n = 2, but their spectrally broad signature probably comes from merging of higher energy states with n $\geq$ 2 into a single feature. As a standalone statement, the assumed attribution is rather weakly justified, however confrontation with reports on similar experiments, which sometimes enable resolving excited states with higher quantum numbers for monolayer WSe_2 flakes, e. g. by introducing modulation in reflectivity measurements **[21]** and/or protecting the WSe_2 films by encapsulation **[50]**, shows reasonable agreement.

The energy separation between the A and A* as well as B and B* resonances is very large. It reflects relatively low static dielectric constant ($\epsilon_s \approx 7$) **[51–53]** and high effective masses of electrons (m_e^*) and holes (m_h^*) leading to reduced mass roughly in the range $\mu \approx (0.2\,;\,0.4) \cdot m_0$ **[54]** (m_0 is a free electron mass in vacuum) in sc-TMD materials, which determine the exciton

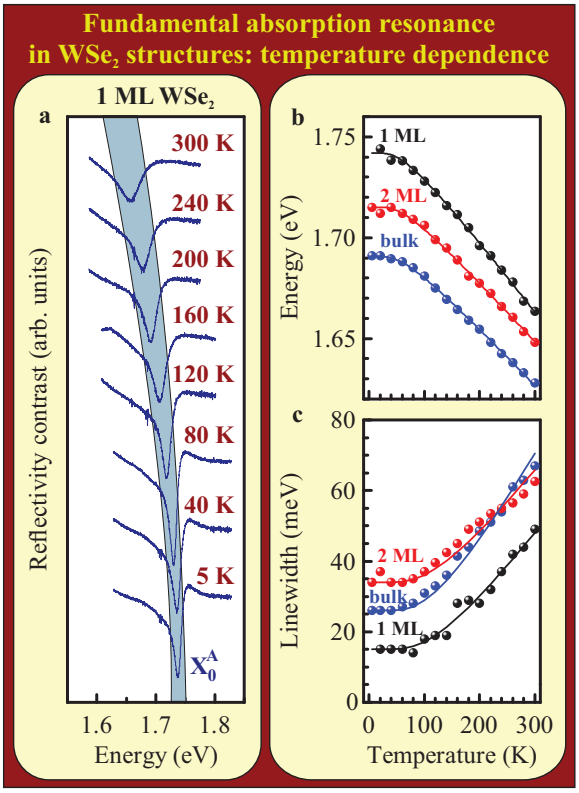

Figure 1-4: **The temperature impact on the fundamental neutral exciton resonance (A) seen in the reflectivity contrast spectra for a WSe_2 monolayer is presented. A transfer matrix method was used to fit the spectra in order to trace the evolution of the resonance. A semi-classical approach of describing intraband transitions in view of a harmonic oscillator model for orbital electrons leads to a contribution to a dielectric funtion: $\epsilon(E) = A/\left(E_0^2 - E^2 - i\gamma E\right)$, where E_0 is the energy of the resonance and γ is responsible for the linewidth as it determines the full width at half maximum (FWHM). The temperature dependence of these two parameters is shown for 1 ML, 2 ML and bulk flakes (spectra for the two latter structures are not shown). The black solid lines are the best fits to the experimental points in terms of least squares method of the formulae discussed in the main text.**

binding energy (E_B) as well as Bohr radius (a_B):

$$E_B \propto \frac{\mu}{\epsilon_s^2} \quad a_B \propto \frac{\epsilon_s}{\mu} \quad \mu = \frac{m_e^* m_h^*}{m_e^* + m_h^*}$$

The excitonic effects in bulk form of sc-TMD can be described in terms of hydrogen-like model, which is usually valid for Wanier-Mott excitons, i. e. when the Bohr radius is significantly larger than the size of the crystal's elementary cell. The enhancement of the binding energy for excitons in thiner structures is clearly not the only factor that determines the energy of excitonic resonances in thin sc-TMD films. That is revealed by the initial enhancement of the energy separation between the A and A* resonances when increasing the thickness from one to two monolayers. For stacks thicker than a bilayer the energy difference progressively decreases until it reaches the value corresponding to the bulk limit. The current understanding of this observation is related to the uncovering of a discrepancy between the energy of excitonic resonances with low quantum numbers n (roughly $n \leq 3$) and the energies corresponding to a Rydberg series for monolayer sc-TMD flakes, which arise most likely due to a non-local character of the screening of Coulomb interaction. This deviation from the hydrogen-like model, most prominent in monolayer structures, pushes the excited states with low n significantly closer to the exciton ground state. With the increase of the number of layers, the Rydberg series of

exciton excited states is recovered, therefore the influence of the transition between two systems of different dimensionality dominates for thicker structures. The presented interpretation of the most important features seen in reflectivity spectra provides some understanding of the excitonic resonances on a qualitative level. More studies are needed on both experimental and theoretical ground, e. g. to expand the comprehension of the influence of different dielectric environments (which can be tuned to a large degree for instance by fabricating suspended films, heterostructures, etc.) on the electron-hole interaction in the thinnest sc-TMD flakes or to learn about the consequences of spin-spin (exchange) interactions on the optical and electronic properties.

1.3. Impact of temperature on the optical response of sc-TMD

For the sake of completeness of the basic optical characterisation, we turn to the analysis of the impact of the temperature on the excitonic resonances seen in reflectivity spectra. Figure 1-4 illustrates the reflictivity contrast spectra in the energy range corresponding to the A neutral exciton resonance in the temperature range from 5 K up to 300 K. A clear tendency appears in form of progressive red-shift and linewidth broadening of the absorption line with the increase of temperature. This is a well-known effect often seen in various semiconductor structures. A detailed analysis of the energy and linewidth of the resonance line, done here for monolayer, bilayer and bulk flakes, allows us to test their temperature evolution against commonly used models developed during studies of more conventional semiconductors **[56, 57]**. The energy shift of the resonances is usually described as a consequence of the band gap closing at higher temperature, which originates from the increase of the average interatomic distance due to the crystal's expansion or from the modulation of the atomic bonds caused by the appearance and/or enhancement of vibrational modes (phonons) which can effectively couple with the electrons occupying the orbital states. This approach holds only if the exciton binding energy remains insensitive to the temperature changes. Such assumption is usually accepted if the temperature dependence of the energy of the excitonic resonances is reasonably well reproduced exclusively by the band gap shrinkage. We use the following formula, which expresses the band gap dependence on the temperature in terms of the mean phonon energy $\langle\hbar\omega\rangle$ and an electron-phonon coupling parameter S:

$$E_g(T) = E_g(0) - S\langle\hbar\omega\rangle\left(\coth\left(\frac{\langle\hbar\omega\rangle}{2kT}\right) - 1\right)$$

Let us note, that the above formula fits acceptably the experimental data for both thin structures (mono- and bilayer) and the bulk crystal, establishing that the presented formalism developed for semiconductors with conventional band structure extrapolates well on sc-TMD materials. The linewidth broadening with the increasing temperature for the exciton ground state resonance (for n=1) is typically accounted for when the coupling of electronic states with longitudinal optical (LO) phonons is considered, proportional to the number of these phonons given by Bose-Einstein distribution. A linear with temperature term, which can be derived for acoustic phonons, is usually of negligible magnitude. Therefore, the formula we used to describe the linewidth changes with temperature was the following:

$$\gamma(T) = \gamma(0) + \frac{\alpha}{\exp\left(\frac{\hbar\omega}{kT}\right) - 1}$$

The agreement with experimental data for the three investigated structures is also decent. In this case, it may be interesting to discuss the dependence of the value of the α parameter, which reflects the probability of the scattering of the excitonic state with the involvement of an LO phonon of the energy 250 $cm^{-1} \approx 31$ meV in WSe_2 material **[31]**, on the thickness of the structure. The value of the α parameter for thin structures was found to be similar, 78 meV for the monolayer and 75 meV for the bilayer), but in the bulk limit it was noticeably increased up to 105 meV. Our interpretation of this tendency is that due to the enhancement of the exciton binding energy in 'more two dimensional' systems, the scattering events can occur only within the ground excitonic state with n=1, so that the process involving the absorption of a phonon elevates the exciton to higher energy states with larger center of mass momentum. However, this limitation may be lifted, when the exciton binding energy decreases in the bulk form of the crystal, eventually opening up an additional scattering channel to the excited states, for which the energetic distance from the ground state becomes comparable with the energy of the LO phonon.

We have explored the topic of the basic optical characterization of sc-TMD structures based on our reflectivity contrast measurements, but now we would shift the focus of our discussion back to the light emission study in order to address the aforementioned diversity of the PL response for different materials belonging to sc-TMD family. Figure 1-5 presents the temperature dependence of the emission spectra of monolayer $MoSe_2$ and WSe_2 flakes. These two materials are representative of the two different types of the emission signature at low temperature. The monolayer $MoSe_2$ flakes give rise to relatively simple spectra composed of two lines, which were

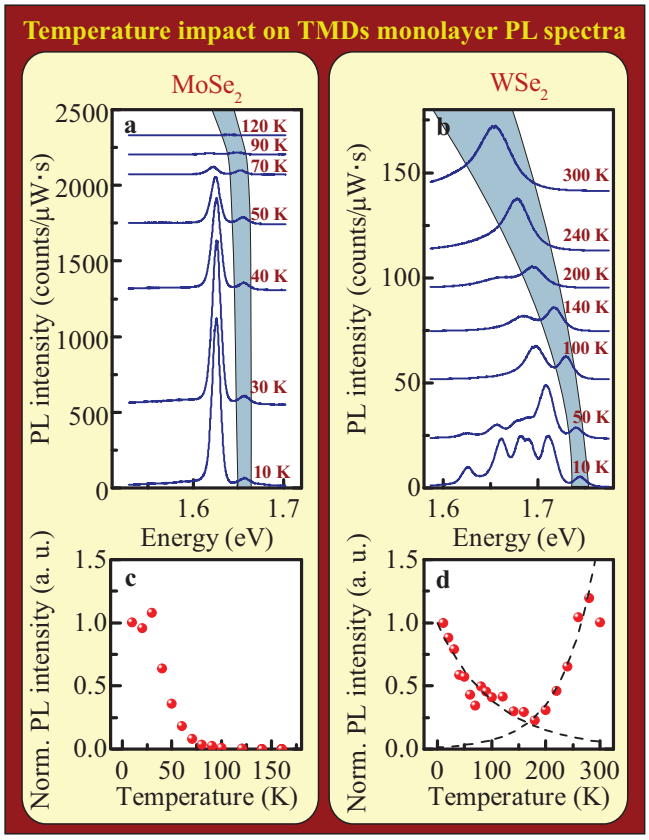

Figure 1-5: **The temperature evolution of the PL spectra for monolayer $MoSe_2$ and WSe_2 flakes reveals features indicative of qualitatively different character of the PL response of both materials. The discrepancy starts at low temperature, when the PL signal of a WSe_2 monolayer appears as multiple peaks forming a complicated pattern in strong contrast with simple two-peak spectra of a $MoSe_2$ monolayer. An increase of temperature impacts the PL spectra in a characteristic manner which differs starkly for both materials. This can be seen for instance in the evolution of the total (integrated) intensity of emission. A $MoSe_2$ monolayer exhibits a typical effect of intensity quenching at higher temperature. In case of the WSe_2 flake, the lower energy PL 'band' quickly disappears (reproduced by a curve $I(T) = I_0 \cdot \exp(-T/T_0)$ with $T_0 = 106$ K), but simultaneously the free neutral exciton gains in intensity (accounted for by a curve $I(T) = I_0 \cdot \exp(T/T_0)$ with $T_0 = 63$ K).**

recognized as neutral and charged exciton resonances. With the increase of temperature the intensity of both lines exhibits a progressive and significant quenching, which is a typical impact of the temperature on the PL signal seen in most of the light emitting semiconductor systems. The case of WSe_2 monolayer is much more complex. In the low temperature spectra, apart from the two free exciton lines, a type of broad multi-peak PL band appears covering an extensive energy range below the free neutral exciton state (often overlapping with the free charged exciton line in our samples). These lower energy resonances have been tentatively baptised as bound/localized excitons based mostly on the time-resolved experiments **[58–60]**, which reveal orders of magnitude longer PL decay times for these 'bound' states (tens of nanoseconds) than for free excitons (single picoseconds). The possible routes to investigate the fast dynamics of free exciton complexes in monolayers of sc-TMD is the measurement of time-resolved Kerr rotation **[59]** or PL transients on a streak camera **[60]**. The latter approach is taken here and allows us to observe the PL decay profiles of the free neutral exciton and the PL band of 'bound' excitons in a WSe_2 monolayer, which are presented in Figure 1-6.

The initial increase of the temperature, roughly from 10 to 100 K causes the decrease of the overall integrated emission intensity due to disappearance of the low energy PL band of 'bound' excitons. However, the free neutral exciton line, which at low energy contributes only weakly

to the total emission, grows in intensity so rapidly that it dominates the spectra at higher temperature. At room temperature, the total intensity comes exclusively from the neutral exciton line and typically exceeds the total intensity at helium temperature, which is quite an unusual feature. In order to provide an interpretation of qualitatively different impact of the temperature on the PL spectra of sc-TMD monolayers, we need to come back to the analysis of the possible configurations of the electronic sub-bands in the vicinity of the K-point of the Brillouin zone. As long as the emission of light is concerned, we may neglect transitions of B type, because the spin-orbit splitting in the valence band (hundreds of meV) significantly exceeds the thermal energy at room temperature (kT $\approx$ 25 meV) therefore the lower valence sub-band can not be occupied in the investigated range of temperature. The spin-orbit splitting in the conduction band is, on the contrary, very much relevant as the alignment of spin in the conduction sub-bands will determine which transitions will be optically allowed. Therefore, the electron involved in the recombination process may come from either the lower or upper conduction band state. We will argue that the existence of two types of optical transitions lies at the origin of the different PL response of sc-TMD monolayers, which can be used to classify the materials into 'bright' and 'darkish' families. For $MoSe_2$ monolayers, their optical properties indicate that the electron from the lower conduction band state participates in the recombination process, which makes $MoSe_2$ a 'bright' material. In that case, the ground state exciton gives rise to the PL signal, what accounts for the general robustness of the emission (the PL signal from $MoSe_2$ monolayer is probably the strongest among all sc-TMD materials).

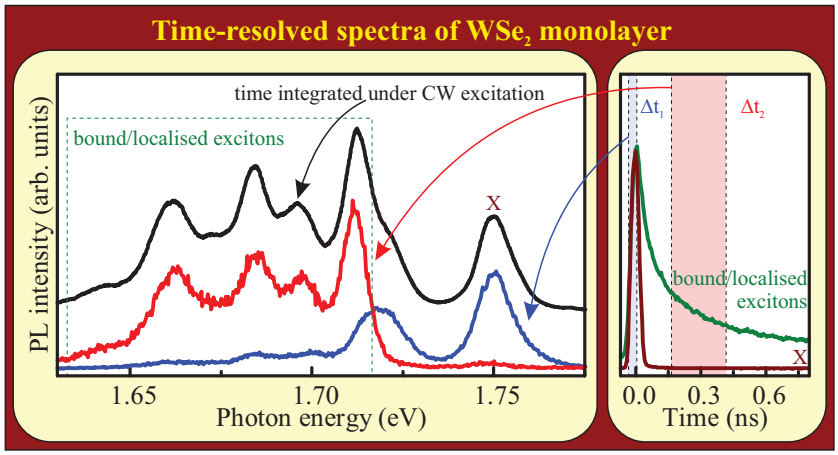

Figure 1-6: **The PL transients of a WSe_2 monolayer were measured with a streak camera coupled with a tunable femtosecond pulsed laser. They reveal a stark contrast between the dynamics of free and 'bound/localised' excitons. A straightforward consequence of significant differences in their decay times is a possibility to observe the PL response separately for free and 'bound/localised' resonances. In the left panel of the figure, three low temperature (T=6.5 K) PL spectra of the same WSe_2 monolayer are presented. The blue and red curves correspond to the PL spectra accumulated over disjoint time intervals after the arrival of the laser pulse, which are marked on the PL decay profiles presented in the right panel. For comparison, the PL spectrum for the continuous wave (CW) excitation is shown (black curve).**

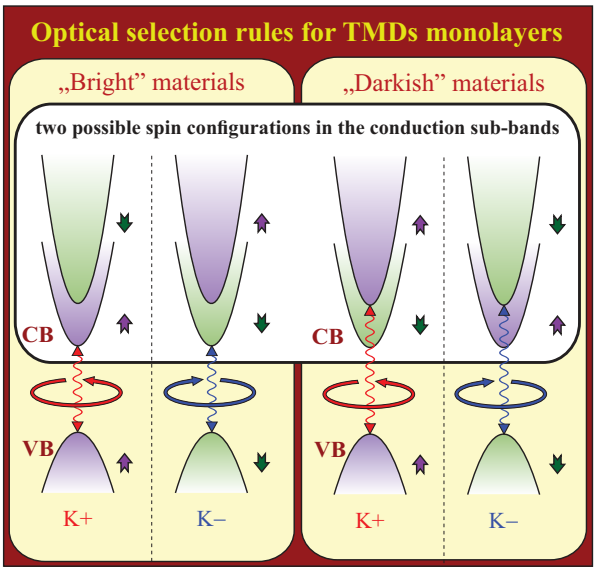

Figure 1-7: **The alignment of spin in the conduction sub-bands of sc-TMD monolayers may have a crucial impact on the optical transitions, what is presented here in form of a cartoon scheme. As a consequence of the optical selection rules, which assume the conservation of spin in the recombination (or absorption) process, the lower energy excitonic resonances (A) seen in the optical spectra can be formed from the electron occupying the lower or the upper conduction sub-band. For that reason, a classification of the sc-TMD materials into 'bright' ($MoSe_2$, $MoTe_2$) and 'darkish' (WSe_2, WS_2) families is introduced, which is relevant in particular for the character of their PL response.**

PL intensity is progressively quenched with the increase of the temperature as the occupation of the excitonic ground state becomes progressively depopulated and the nonradiative processes gain over the radiative recombination.

The properties of WSe_2 monolayers discussed so far are indicative of a 'darkish' character of this material with the electron from the upper conduction state involved in recombination. Particularly, the free neutral exciton resonances seen in the PL spectra is in fact an excited excitonic state, whose occupation is increased at higher temperature. As a consequence, the free neutral exciton resonance would be accompanied by lower energy dark states. Even though, in the first approximation, the recombination of the dark states is forbidden, one can think of multiple brightening mechanisms (activation by disorder/defects, mixing of states with different spin/orbital momentum or recombination with emission/absorption of phonons). The existence of radiative channels for dark excitons, which reside below the free neutral exciton resonance, could potentially be related to the low energy broad PL band seen in low temperature WSe_2 spectra. In this view, the peculiar temperature evolution of the PL spectra of WSe_2 monolayer could be a consequence (at least partially) of the redistribution of electron population between dark and bright states.

Chapter 2

Zeeman spectroscopy of excitonic resonances in magnetic fields

2.1. Empirical model for the magnetic field evolution of the electronic states in a sc-TMD monolayer

The investigation of the magnetic field influence on the excitonic resonances appearing in the optical spectra of the thin layers of sc-TMD constitutes a versatile tool capable to further develop the understanding of their electronic properties. Due to the 2D confinement of the electrons, especially robust in sc-TMD in the monolayer form, the coupling of the orbital motion of the carriers with the external magnetic field is expected to be strongest when the direction of the magnetic field is perpendicular to the surface of the sc-TMD flake. Indeed, the measurements of the magneto-reflectance and magneto-luminescence in such configuration allowed the observation of a Zeeman-type effect **[67–70,96]**, i. e. the splitting of the excitonic resonances into two circularly polarised components. The energy separation, linear with the magnetic field, between the two components is usually used to define a fundamental parameter relevant for the analysis of the electronic states in a magnetic field, which is called a g-factor. Here, we will use the following convention to evaluate the Zeeman energy: $\Delta E = E_{\sigma^+} - E_{\sigma^-} = g\mu_B B$, where $E_{\sigma^{+/-}}$ is the energy of the resonance in a spectrum detected in $\sigma^{+/-}$ polarisation, g is a g-factor, μ_B is the Bohr magneton constant (≈ 0.058 meV/T) and B is the value of a magnetic field. It is important to note, that the g-factor defined in this way is related to a particular optical transition between the electronic states in a valence and conduction bands. However, one can assign a g-factor value to any individual electronic state as well. Therefore,

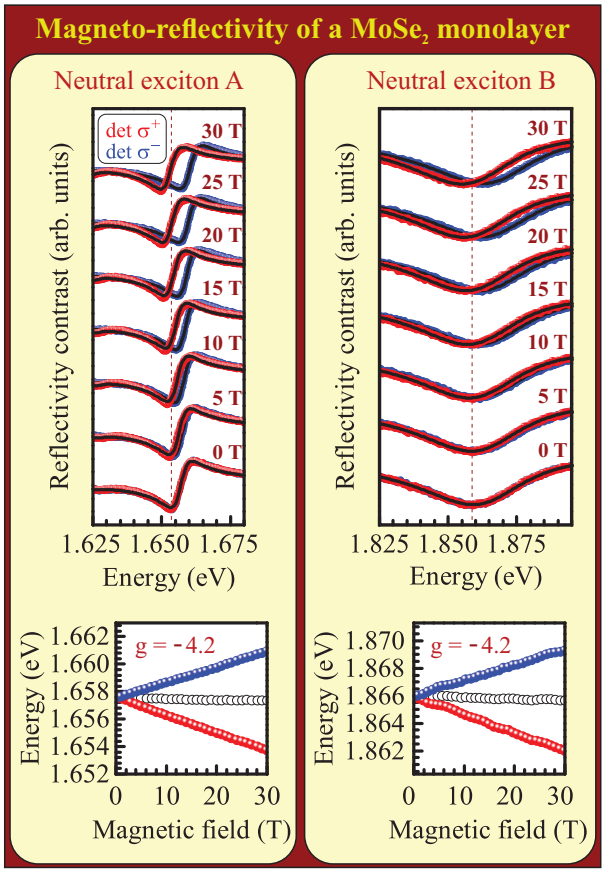

Figure 2-1: **Reflectivity contrast spectra are presented as a function of the magnetic field applied perpendicular to the surface of a monolayer $MoSe_2$ flake. A circualar polarisation analiser was placed in the detection path and the particular component of the polarisation (σ^+ vs σ^-) was chosen by the direction of the field vector. The spectra show two fundamental resonances seen in monolayer sc-TMDs flakes: the lower energy neutral exciton A (left panel) and the higher energy neutral exciton B (right panel). The fitted curves come from the same procedure, which was applied in the analysis of zero-field spectra (transfer matrix method with Lorentzian contributions for the excitons). The position of the resonances were established as a functuion of the magnetic field seperately for σ^+ (red points) and σ^- (blue points) components. Open circles represent the avarage value of the energy of both transitions $^1/_2(E_{\sigma^+} + E_{\sigma^-})$. They are presented here to demonstrate that the diamagnetic shift (quadratic with B term) is not seen in our data in the investigated magnetic field range.**

the g-factor obtained directly from the magnetic field evolution of the excitonic resonances, as they are seen in the optical spectra, can be considered as a differential g-factor between two electronic states. Nevertheless, we will argue that the detailed analysis of the magneto-optical data can also provide an estimation for the g-factors of individual electronic states. There are three parameters, i. e. spin and orbital momentum as well as valley degree of freedom which determine Zeeman effects of electronic states (and optical transitions) in sc-TMD monolayers. Notably, the σ^+ and σ^- optical transitions in sc-TMD monolayers are valley selective but at the same time involve also the electronic states with different spin and orbital momentum.

The presentation of the magneto-optical study of sc-TMD monolayers will be focused on the properties of the most fundamental transitions. Our initial goal will be to establish a description of the magnetic field evolution of the relevant electronic states. It is important to stress, that the incorporation of all possible contributions to the Zeeman effect into a single self-consistent band model, either in k.p or tight-binding theory, is complicated. Various approaches may yield significantly different values of calculated g-factors **[72,73]**, which in most basic cases can even lead to a complete disappearance of the excitonic Zeeman effect **[70]**. As the discrepancies between the band models and the experimental results still remain controversial, we here propose

an alternative route to construct an empirical description of the Zeeman effects based on the experimental findings and symmetry properties.

material	neutral exciton A g-factor	neutral exciton B g-factor
MoS_2	−4.0* *(reflectance)*	−4.2* *(reflectance)*
$MoSe_2$	−4.2 *(reflectance)*	−4.2 *(reflectance)*
$MoTe_2$	−4.8** *(reflectance)*	−3.8** *(reflectance)*
WS_2	−4.3* *(transmission)* −3.9 *(reflectance)*	−4.3* *(transmission)* −4.0 *(reflectance)*
WSe_2	−3.8 *(reflectance)*	−3.9 *(reflectance)*

– „darkish" materials – bright materials

* - data from A. V. Stier, et al., Nat. Comm. **7**, 10643 (2016)
** - data from A. Arora, et al., Nano Lett. **16 (6)**, 3624 (2016)

Table 2.1: **The values of the g-factors of neutral excitons A and B measured for monolayers of different sc-TMD materials are presented in the table. The data come from absorption type experiments, in which reflectance or transmission was measured. The background colours indicate, whether the particular matieral is classified as 'darkish' or bright. The case of MoS_2 is exceptionally highlighet by dual-colour background, as multiple theoretical predictions suggest significantly smaller conduction band spin-orbit splitting in MoS_2 with respect to other sc-TMD representatives.**

Let us begin with a remark that even though the excitons in sc-TMD are spatially strongly bound and therefore their wave functions extend broadly in the momentum space, we will still describe the optical transition as if they were originating only from the states located exactly at the corners of the Brilloun zone in the K+/K− points. The theoretical estimations of the contribution to the g-factor value coming from the surrounding states show that it can be treated as a small perturbation and in the first approximation can be neglected. In this view, we can commence the construction of our description by considering 2 sub-bands composed altogether of 4 non-degenerate individual electronic states around both K+ and K− corners of the Brillouin zone, essential to account for all A and B transitions appearing in the optical spectra of sc-TMD monolayers. A straightforward way to establish a relation between the magnetic field evolution of the electronic states at the K+ and K− points comes from the consideration of time reversal symmetry properties. As the time reversal transformation changes the direction of the momentum, spin and the magnetic field ($p \to -p, \uparrow \to \downarrow, B \to -B$), the arguments have been put up (based on the analysis of the properties of the Hamiltonian in either k.p or tight binding theory) that the linear with the magnetic field energy shift of the corresponding states in both valleys (i. e. of the same energy in the absence of a magnetic field) must be of an equal magnitude and an opposite sign. This condition may be expressed in a following manner: $\Delta E^{K+}_{c(v),\uparrow(\downarrow)}(B) = -\Delta E^{K-}_{c(v),\downarrow(\uparrow)}(B)$, where $\Delta E^{K+(-)}_{c(v),\uparrow(\downarrow)}(B)$ is the energy shift in a magnetic field B of the conduction (c) or valence (v) band state with a spin up (↑) or down (↓) in the K+ or K− point of the Brillouin zone. This allows us to parametrize the magnetic field evolution of the electronic states in one valley only. We could introduce 4 parameters now and carry on with the analysis of their impact on the

magneto-optical properties, nevertheless we will take advantage of a simple experimental observation, based on the investigation of the excitonic resonances appearing in the reflectivity spectra, to further simplify that description.

In the absorption spectra of sc-TMD monolayers, which can be studied either by the measurements of reflectivity **[74]** or transmission **[75–77]**, the two most robust resonances arise due to the neutral exciton A and B states. In Figure 2-1 the magnetic field evolution of the reflectivity contrast spectra are presented for a $MoSe_2$ monolayer, which reveal the presence of the neutral exciton A at the energy $\sim$1.65 eV and neutral exciton B at $\sim$1.86 eV. These two resonances exhibit a similar behaviour in the magnetic field. They split into two circularly polarised components so that the g-factor value may be obtained by the analysis of the magnitude of the splitting in a broad rage of the magnetic field. For a $MoSe_2$ monolayer, the g-factor values for both neutral exciton A and B were found to be equal to -4.2. The equal value of the g-factors of these two resonances in monolayer structures seems to be a common property for majority of materials belonging to sc-TMD family which can be seen in the data originating from the measurements of magneto-reflectance and magneto-transmission, summarized in Table 2.1. That property allows us to introduce an additional constraint for the magnetic field evolution of the particular electronic states, namely $\Delta \mathrm{E}^{\mathrm{K}\pm}_{\mathrm{c},\uparrow}(\mathrm{B}) - \Delta \mathrm{E}^{\mathrm{K}\pm}_{\mathrm{v},\uparrow}(\mathrm{B}) = \Delta \mathrm{E}^{\mathrm{K}\pm}_{\mathrm{c},\downarrow}(\mathrm{B}) - \Delta \mathrm{E}^{\mathrm{K}\pm}_{\mathrm{v},\downarrow}(\mathrm{B})$. Thus, symmetry arguments and the experimentally observed similar g-factors for excitons A and B imply that the number of parameters used in the description of Zeeman effects in sc-TMD monolayers can be reduced to three. However, these condition are not strong enough to impose a unique parametrization. Our strategy will be to choose one that satisfies the relations, for which the appearing parameters may be related to physical quantities. Therefore we will express the magnetic field evolution of the energy of the electronic states in the following manner:

$$\begin{cases} \Delta E^{K\pm}_{c,\uparrow}(B) = \pm E_V + E_S \\ \Delta E^{K\pm}_{c,\downarrow}(B) = \pm E_V - E_S \\ \Delta E^{K\pm}_{v,\uparrow}(B) = \pm E_V + E_S \pm E_{d_2} \\ \Delta E^{K\pm}_{v,\downarrow}(B) = \pm E_V - E_S \pm E_{d_2} \end{cases}$$

where we assume that E_S, E_V and E_{d_2} are all positive and introduce the corresponding set of associated g-factors:

$$\begin{cases} E_V = g_V \mu_B B \\ E_S = g_S \mu_B B \\ E_{d_2} = g_{d_2} \mu_B B \end{cases}$$

In this representation E_V is a valley selective Zeeman term. It shifts equally all the states in one valley in the same direction towards higher or lower energy in K+ or K− valleys, respectively. E_S is a spin term, which acts on the electronic states accordingly to the orientation of their spin with the convention that spin up (↑) states are shifted to higher energy and spin down states (↓) are shifted to lower energy in a magnetic field. Finally, E_{d_2} is an orbital term which acts in the same way as the valley term but only in the valence band. The reason behind this is the composition of the valence and conduction band wave functions. In the first approximation, they are created from d-orbitals with a projection of the orbital momentum $l_z = 2$ in the valence band and $l_z = 0$ in the conduction band. Therefore in the simple approach we can neglect the influence of the orbital effects on the magnetic field evolution of the conduction states. Figure 2-2 offers a pictorial illustration of the energy landscape for the fundamental sub-bands of monolayer sc-TMD in a magnetic field. The general knowledge about the magneto-optical properties of various representatives of sc-TMD **[67–70,75–77,96]** makes us believe, that the described picture is valid on a qualitative level for monolayers of most of these materials (perhaps with the exepction of $MoTe_2$, for which the condition of equal g-factors for the excitons A and B does not hold). However, it is noteworthy to stress that the two possible spin alignments in the conduction sub-bands for 'bright' and 'darkish' monolayers **[61–63]** may lead to distinct properties of particular materials. In the next section we will compare the properties of 'bright' $MoSe_2$ and 'darkish' WSe_2 monolayers to illustrate the possible impact of different spin configurations on the magneto-optical spectra and ultimately take advantage of their analysis to obtain an estimation of the 3 parameters we have introduced to describe the magnetic field evolution of the electronic states.

2.2. Estimation of the orbital, spin and valley terms

The introduced description of the Zeeman effects in sc-TMD monolayers offers a straightforward way to determine one of the parameters. The value of the neutral exciton A and B g-factor, e. g. obtained from the splitting of the resonance in the reflectivity spectra, comes exclusively

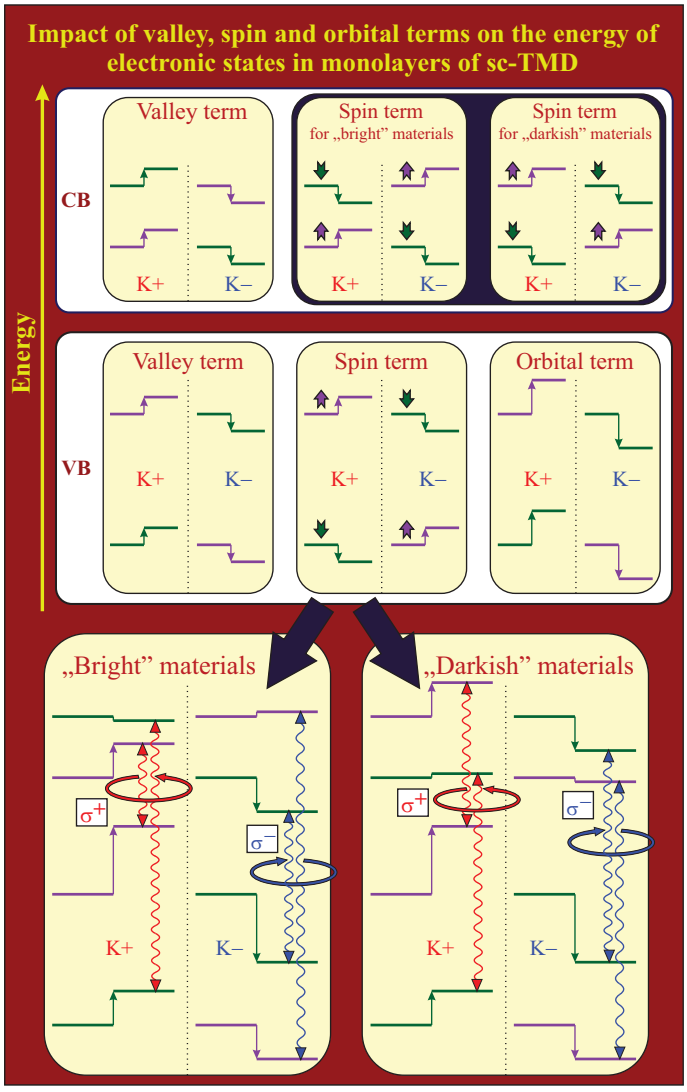

Figure 2-2: **The linear with magnetic field contributions to the energy of the fundamental electronic states exactly at the K+/K- points of the Brillouin zone is presented in form or simple cartoons. Three terms (valley, orbital and spin) are considered separately for the conduction band (CB) and the valence band (VB). Furthermore, the distinction between 'bright' and 'darkish' materials is taken into account for the spin contribution. The actual value of the spin is colour-coded, so that the states marked with green bars correspond to spin-down states and purple bars correspond to spin-up states. Additionally, the direction of spin is represented by supplementary arrows. The two bottom cartoons show the magnetic-field-induced shifts of the individual electronic states in K+/K- valleys, when all three contributions are taken into account. The difference between the 'bright' and 'darkish' materials comes from the alignment of spin in the conduction band. The configuration of spin impacts the circularly polarised optical transitions for both excitons A and B, which are represented here by red and blue arrows.**

from the orbital term: $g_{X_A^0} = g_{X_B^0} = -2E_{d_2}$. The spin and valley term alter the energy of the electronic states in valence and conduction bands in the same manner, therefore they cancel out when the excitonic (i. e. differential) g-factor is considered. The same argument applies for the charged exciton resonance, which in the first approximation has the same g-factor value as the neutral exciton resonance. Therefore we will need to gain access to the g-factor value of individual electronic states, if we are to estimate the other 2 parameters.

A possible route to investigate the state of a single electron is through the measurements of the negatively charged exciton absorption resonance **[64–66]**, e. g. in the reflectance spectrum. In the absorption process, when the charged exciton is created, a single carrier is present in the initial state of the transition. If the application of a magnetic field induces a splitting of its state, then the redistribution of its population will lead to the enhancement of the absorption strength of the transition in the presence of the carrier in its lower energy state (seen in one circular polarisation) at the cost of the transition in the presence of the carrier in the higher

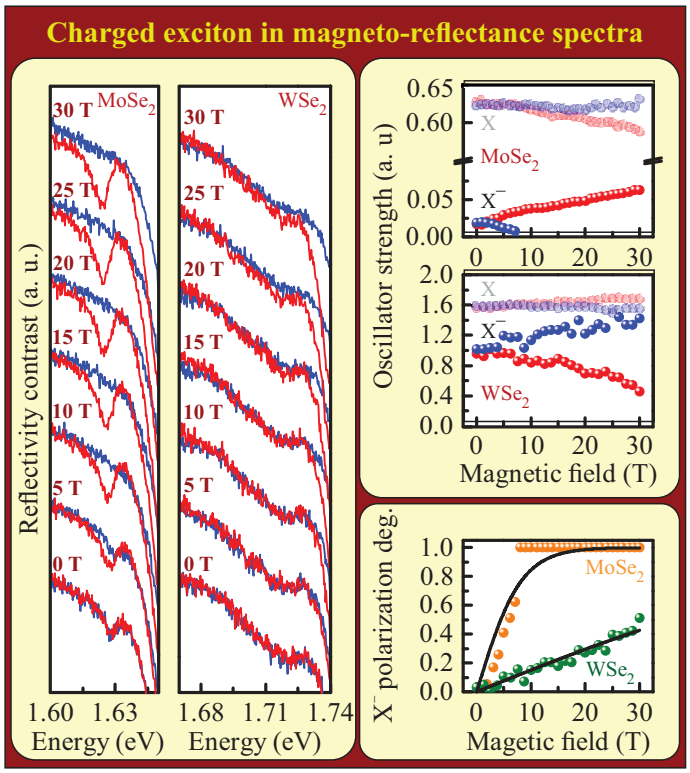

Figure 2-3: **The magneto-reflectance spectra are presented in a narrow spectral range to highlight the weak negatively charged exciton (X^-) resonance in $MoSe_2$ and WSe_2 monolayers. The presence of a circular polarisation analyser allows the detection of the reflected light separately for σ^+ and σ^- polarisations. The transfer matrix analysis is used to estimate the polarisation-resolved oscillator strength of the negatively charged exciton state in both materials. The data for the neutral exciton is also presented to show a small degree of oscillator strength transfer between the neutral and charged states. Finally, the magnetic field evolution of the polarisation degree of the charged exciton state is obtained for WSe_2 and $MoSe_2$ monolayers and fitted with functions derived in the main text.**

energy state (seen in the opposite circular polarisation). Indeed, the experimental data for monolayer $MoSe_2$ and WSe_2 flakes reveal such tendency, as can be seen in Fig. 2-3. The charged exciton resonance in the reflectance spectra appears as a rather weak absorption line at the lower energy tail of the neutral exciton resonance. It is seen at 1.628 eV for a $MoSe_2$ monolayer and at 1.713 eV for a WSe_2 monolayer. It is important to note that even though there is an apparent difference in the quality of the optical response of the charged exciton state between the 2 materials, as the width of absorption line for $MoSe_2$ is significantly smaller than for WSe_2 material, a careful fitting of the spectra allows us to determine the magnetic field dependence of the oscillator strength of the charged exciton transition in σ^+/σ^- polarisations for both materials. A striking finding comes out from this analysis, as for the $MoSe_2$ monolayer the lower energy σ^+ transition gains in intensity with the increase of the magnetic field while for the WSe_2 monolayer the opposite transition - the higher energy σ^- one is enhanced at higher fields. Apart from this clear qualitative difference, also the rate at which the charged exciton becomes polarised in a magnetic field varies strongly for both materials. That is vividly seen in the magnetic field dependence of the polarisation degree of the charged exciton resonance. In order to interpret these observations we will consider how a charged exciton state can be constructed given the electronic states structure in sc-TMD monolayers.

Firstly, let us note the pair of electrons in the considered system can form a singlet

or a triplet state in a intra- or inter-valley configuration. As a consequence, the existence of 4 qualitatively different negatively charged excitons A may in principle manifest itself in the optical spectra. However, the measurements of reflectivity reveal the signature of only one resonance which we can associate with a charged exciton state, therefore we will make an assumption that it arises due to a singlet state. Which configuration of electrons is actually realised when forming a charged exciton in sc-TMD monolayers is up for debate, however, surely the two possible alignments of conduction sub-bands are relevant for this problem. We will argue that in 'bright' and 'darkish' systems a different charge exciton state is seen in the absorption. This claim originates from the strikingly different magnetic field evolution of polarisation-resolved reflectivity spectra of the 'bright' $MoSe_2$ monolayers and 'darkish' WSe_2 monolayers.

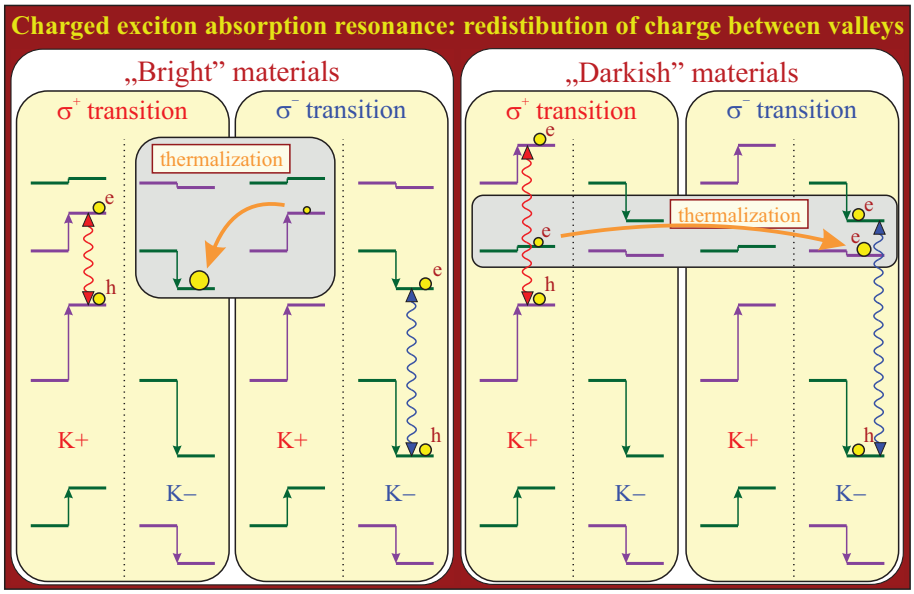

Figure 2-4: **Schematic representation of the absorption process leading to the creation of negatively charged exciton A in sc-TMD monolayers, presented separately for 'bright' and 'darkish' materials. The assumptions regarding this process, based on the experimental data from the magneto-reflectivity measurements, include the formation of a singlet state of a pair of conduction band electrons. Additionally, due to the low temperature of the sample (about 10 K) we take into account solely the occupation of the lower energy conduction band states for the additional electron. The highlighted thermalisation process of the additional electron, originating from the Zeeman splitting of its state, plays a crucial role for the magnetic field evolution of the absorption strength of circularly polarised transitions. Noteworthy is the fact, that in the presented picture, the transitions of opposite helicity are enhanced for 'bright' and 'darkish' materials. Moreover, the rate of the increase of the polarisation degree should be substantially different due to much larger magnitude of the Zeeman splitting of the additional electron's state for 'bright' than for 'darkish' monolayers.**

The task of uncovering the state of the charged exciton created in the absorption process basically comes down to indicating, which electron accompanies the photo-created electron-hole pair. As our experiments are performed at low temperature of about 10 K, we can expect that only the lower energy conduction band state is occupied. Nevertheless, still two possibilities,

of creating either a singlet or a triplet state, remain. We do not have solid arguments accounting for the observation of only a single charged exciton state in the reflectance spectra, therefore we will undertake a phenomenological approach. In order to stay consistent with the experimental data we will assume that the experimentally identified charged exciton resonance is formed from the singlet state of electrons. If that is the case, then for 'bright' monolayers the two electrons are located in the opposite valleys as the photo-created electron occupies the lower energy conduction band state. On the other hand, for 'darkish' monolayers the two electrons should be in the same valley. The Figure 2-4 shows a schematic representation of how the singlet state of the charged exciton is created in the absorption process in 'bright' and 'darkish' sc-TMD monolayers within the framework of our description of the magnetic field evolution of the electronic states. This simple illustration of the considered electronic configurations of carriers may be useful for understanding the polarisation properties of the charged exciton resonance in the reflectivity spectra. As it was mentioned before, the charged exciton resonance becomes polarised in the magnetic field due to the redistribution of charge between the two valleys induced by the thermal population of excess electrons. Therefore the Zeeman splitting of the state of the excess electron, which constitutes the initial state of the absorption process determines which transition is enhanced at higher magnetic field. As we can see in the scheme (Fig. 2-4), the choice of constructing a singlet charged exciton state ensured that the σ^+ polarised transition is enhanced for 'bright' monolayers and σ^- polarised transition is enhanced for 'darkish' monolayers, consistently with the experimental data. Moreover, the presented description accounts also for the significant difference between the rate at which the charged exciton becomes polarised in the magnetic field in 'bright' and 'darkish' systems. Its value is governed directly by the magnetic-field-induced splitting of the single electronic state, which can be conveniently expressed by a g-factor. In the framework of our description of the magnetic field evolution of the electronic states, this g-factor is equal to:

$$\begin{cases} g = g_S + g_V, \text{ for 'bright' monolayers} \\ g = g_S - g_V, \text{ for 'darkish' monolayers} \end{cases}$$

Indeed, the condition $g_{\text{'bright'}} \gg g_{\text{'darkish'}}$ explains the much faster polarisation rate of the charged exciton in $MoSe_2$ monolayers with respect to the WSe_2 monolayers. Therefore, this observation will be our gateway for estimating the value of the spin and valley terms. The information about the value of the g-factor will be obtained from the analysis of the magnetic field evolution

		Experimental data/assumptions						Parameters		
Nr	Material	g_V	g_S	g_{d_2}	$g_V - g_S$	$g_V + g_S$	$g_V + g_S + g_{d_2}$	g_V	g_S	g_{d_2}
1	$MoSe_2$	$g_{V,MoSe_2}$ = g_{V,WSe_2}	$g_{S,MoSe_2}$ = g_{S,WSe_2}	2.1 (exp)	0.22 (exp)	1.84 (exp)		1.03	0.81	2.1
	WSe_2			1.9 (exp)				1.03	0.81	1.9
2	$MoSe_2$		1 (assump.)	2.1 (exp)	0.22 (exp)	1.84 (exp)		0.84	1	2.1
	WSe_2			1.9 (exp)				1.22	1	1.9
3	$MoSe_2$		1 (assump.)	2.1 (exp)			4.4 (assump.)	1.3	1	2.1
	WSe_2			1.9 (exp)			4.4* (exp)	1.5	1	1.9
4	$MoSe_2$	$g_{V,MoSe_2}$ = g_{V,WSe_2}	$g_{S,MoSe_2}$ = g_{S,WSe_2}	2.1 (exp)	$\frac{g_V + g_S}{g_V - g_S}$ =8.7(exp)		4.6 (assump.)	1.45	1.15	2.1
	WSe_2			1.9 (exp)			4.4* (exp)	1.45	1.15	1.9

* - based on the interpretation of SdH oscillations data from B. Fallahazad, et al., PRL **116**, 086601 (2016)

Table 2.2: **Four different approaches of estimating the linear with magnetic field contributions to the Zeeman splitting in sc-TMD monolayers are presented. The combination of the analysis of experimental (exp) data (reflectivity spectra or Shubnikov-de Haas oscillations) with certain assumptions allows the determination of valley, spin and orbital terms for WSe_2 and $MoSe_2$ materials. The detailed discussion of all four methods can be found in the main text. The key conclusion is that regardless of the types of experiments used to access information about the Zeeman splitting of individual electronic states in sc-TMD monolayers, the interpretation of the results may lead to the determination of similar values of the three introduced contributions.**

of the polarisation degree of the charged exciton. As we lack the knowledge of the value of the Fermi energy in our samples, we cannot use the exact expression for the occupation of the electronic states given by Fermi-Dirac statistics. Instead, we will apply a Boltzmann distribution approximation to describe the number of carriers in the conduction band (which is valid as long as the Fermi energy is smaller than the thermal energy of carriers ($E_F \ll kT$)). This allows us to determine the formula for the spin polarisation degree, which yields in such case:

$$\left|\frac{I_{\sigma_+} - I_{\sigma_-}}{I_{\sigma_+} + I_{\sigma_-}}\right| = \tanh\left(\frac{g\mu_B B}{kT}\right)$$

where g is the g-factor of the adequate individual electronic state, μ_B is a Bohr magneton, B is the magnitude of the magnetic field and kT is the thermal energy. The fitting of this formula provides the ratio g/T separately for WSe_2 and $MoSe_2$ materials. For our data we obtained the values:

$$\begin{cases} g/T \approx 0.184\ K^{-1}, \text{ for } MoSe_2 \text{ monolayer} \\ g/T \approx -0.022\ K^{-1}, \text{ for } WSe_2 \text{ monolayer} \end{cases}$$

There are multiple ways to use our experimental data for the estimation of the values of the valley, spin and orbital terms. However, all of them are unavoidably based on certain assumptions, which are rather speculative. Therefore we will consider four different approaches to demonstrate that independently on the chosen route, the values of the estimated parameters are similar to a reasonable extent. Table 2.2 summarises the data and/or assumptions used in every approach and presents the resulting values of the valley, spin and orbital parameters. For each scenario, the value of the orbital term comes directly from the measurements of the Zeeman splitting of the neutral exciton A seen in the reflectance spectra. We will now discuss the four possible routes to estimate the remaining two parameters:

1. We assume that the temperature of the electron gas in the investigated sc-TMD monolayers is the same as the sample bath temperature, and equals 10 K, as we estimated in multiple experiments using our experimental arrangements. This assumption allows us to obtain the g-factors of an individual electronic state separately for WSe_2 and $MoSe_2$ monolayers. In such a case, we have a simple linear equation:

$$\begin{cases} g_S + g_V = 1.84\ , \text{ for } MoSe_2 \text{ monolayer} \\ g_S - g_V = -0.22\ , \text{ for } WSe_2 \text{ monolayer} \end{cases}$$

which we can solve if we assume that the g_S and g_V parameters are the same for WSe_2 and $MoSe_2$ monolayers. Under such conditions:

$$\begin{cases} g_V = 1.03 \\ g_S = 0.81 \quad \textbf{(MoSe}_2\textbf{)} \\ g_{d_2} = 2.1 \end{cases} \qquad \begin{cases} g_V = 1.03 \\ g_S = 0.81 \quad \textbf{(WSe}_2\textbf{)} \\ g_{d_2} = 1.9 \end{cases}$$

2. The assumption about the same values of spin and valley parameters for WSe_2 and $MoSe_2$ materials may seem to be excessively rigid. In order to avoid it, we can take an alternative approach, in which the spin contribution takes the form adequate for a free electron in vacuum. Therefore, we set the value $g_S = 1$ and keep the assumption about the electron

gas temperature being equal to 10 K. Then, we can estimate the valley terms separately for WSe_2 and $MoSe_2$ monolayers. Such approach provides:

$$\begin{cases} g_V = 0.84 \\ g_S = 1 \\ g_{d_2} = 2.1 \end{cases} \quad \textbf{(MoSe}_2\textbf{)} \qquad \begin{cases} g_V = 1.22 \\ g_S = 1 \\ g_{d_2} = 1.9 \end{cases} \quad \textbf{(WSe}_2\textbf{)}$$

3. The information on the Zeeman splitting of individual electronic states is accessible in transport measurements as well. Recent report on the observation of Shubinkov-de Haas (SdH) oscillations in p-doped WSe_2 monolayers **[78]** provides a way to estimate the value of the g-factor of the upper valence sub-band state. The level of doping in the investigated samples was rather high with the hole concentration $p = 7.9 * 10^{12}$ cm^{-2}. Therefore the position of the Fermi energy in the valence band implied the occupancy of multiple Landau levels even at higher magnetic fields (the data up to 14 T is presented, with the smallest Landau level filling factor $\nu = 26$). The appearance of even values of the filling factor numbers in the investigated field range, consistent with the Hall voltage measurements, reveals the double degeneracy of the Landau levels. This results reminds the typical observations for two dimensional electron gas in GaAs structures. In conventional systems, such as GaAs quantum wells, the Zeeman splitting of the hole state is much smaller than the cyclotron energy ($g\mu_B B \ll \hbar\omega_C = \hbar eB/m^*$), which accounts for the double degeneracy. However, our previous findings point out to rather high value of the Zeeman spitting of the upper valence sub-band state in sc-TMD monolayers therefore the condition $g\mu_B B = (g_S + g_{d_2} + g_V)\,\mu_B B \approx N\hbar\omega_C$ may in fact hold not for $N = 0$, but for an even integer number ($N = 2, 4, \ldots$). For the sake of our analysis we will assume that the condition $(g_S + g_{d_2} + g_V)\,\mu_B B = 2\hbar\omega_C$ is realised, which is most likely valid unless the valley term E_V is anomalously large. For the effective mass of holes equal to $m^* = 0.45\,m_0$, estimated from the temperature dependence of the amplitude of SdH oscillations, we can obtain a new formula $(g_S + g_{d_2} + g_V) = 4.4$ for WSe_2 monolayer. With this information, we can repeat the assumptions about the spin term ($g_S = 1$) and equal values of the valley terms for WSe_2 and $MoSe_2$ monolayers to provide estimation for all three contributions:

$$\begin{cases} g_V = 1.3 \\ g_S = 1 \\ g_{d_2} = 2.1 \end{cases} \quad (\mathbf{MoSe_2}) \qquad \begin{cases} g_V = 1.5 \\ g_S = 1 \\ g_{d_2} = 1.9 \end{cases} \quad (\mathbf{WSe_2})$$

4. In our final approach we will attempt to utilise mostly the experimental data. The only assumption will be an equal value of the spin and valley term in WSe_2 and $MoSe_2$ monolayers. Then, the information about the Zeeman splitting of the upper valence sub-band state coming from the SdH oscillations combined with the ratio between the g-factors of the upper and lower conduction band states, which we know directly from the analysis of the charged exciton polarisation rate in WSe_2 and $MoSe_2$ monolayers, is sufficient to obtain the values of the three parameters. In this case:

$$\begin{cases} g_V = 1.45 \\ g_S = 1.15 \\ g_{d_2} = 2.1 \end{cases} \quad (\mathbf{MoSe_2}) \qquad \begin{cases} g_V = 1.45 \\ g_S = 1.15 \\ g_{d_2} = 1.9 \end{cases} \quad (\mathbf{WSe_2})$$

As summarised in Table 2.2, the general conclusion from the presented analysis is that, independently on the chosen method, the obtained values of the valley, spin and orbital terms are reasonably similar. The rough estimates yield $E_V \approx 1\mu_B B$, $E_S \approx 1\mu_B B$ and $E_{d_2} \approx 2\mu_B B$. The consistency of the results coming from different approaches supports the validity of the proposed description of the Zeeman effects in sc-TMD monolayers.

2.3. Magneto-photoluminescence studies

Now we proceed to the analysis of the magneto-PL data, which provide a complementary test for our proposed description of Zeeman effects in sc-TMD monolayers. Unlike the reflectance spectra, which qualitatively share the same features among various representatives of sc-TMD family, the PL response of $MoSe_2$ and WSe_2 monolayers differs starkly. The main zero-field discrepancies have been discussed in the previous chapter, but here we will extend the presented view by analysing the impact of the magnetic field on the emission lines. The spectra detected with circular polarisation resolution in the magnetic field range 0 - 30 T for $MoSe_2$ and WSe_2 monolayers are demonstrated in Figure 2-5. In case of a $MoSe_2$ monolayer, the PL spectrum

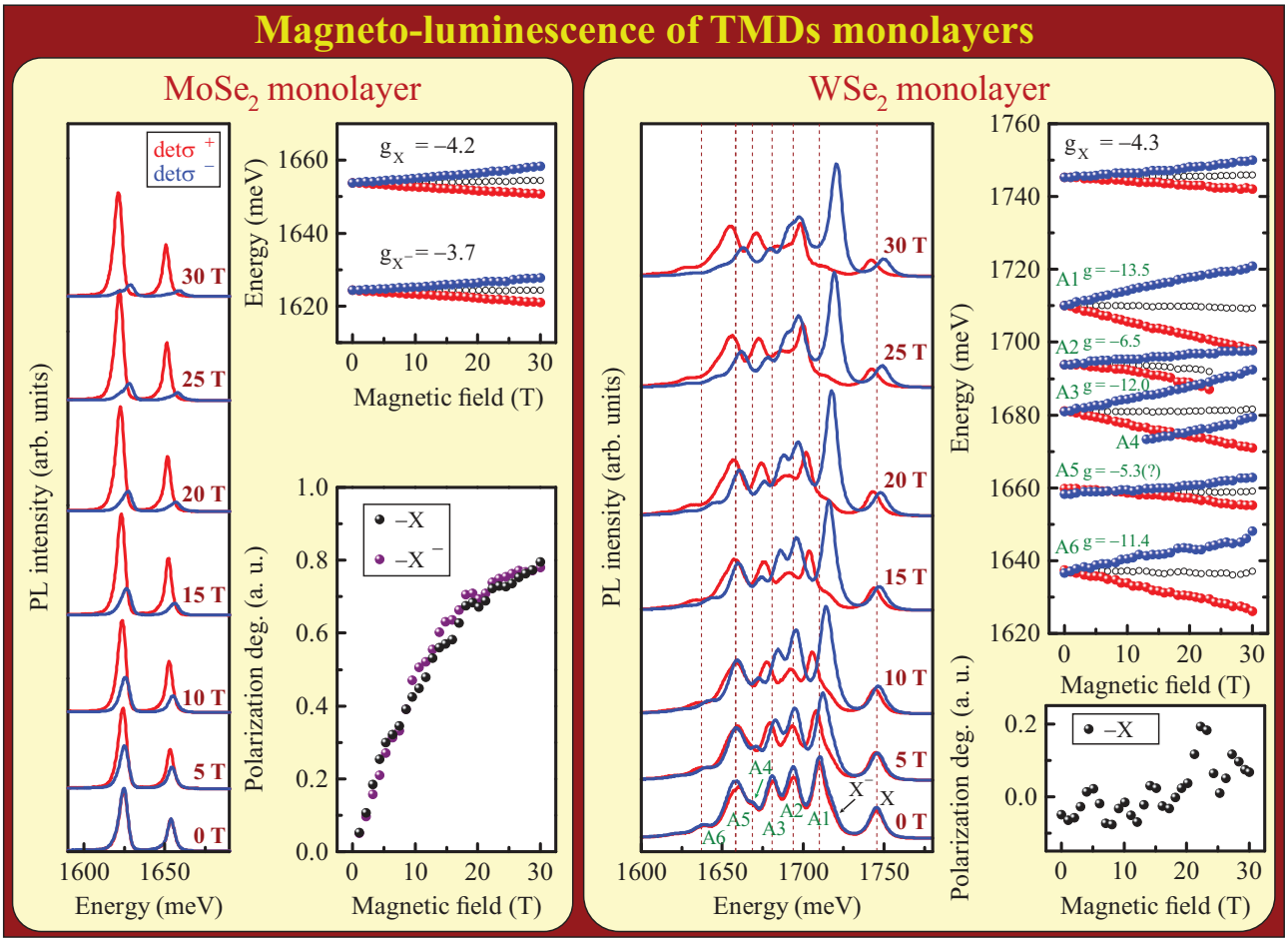

Figure 2-5: **The results of magneto-PL investigations are presented for $MoSe_2$ (left panel) and WSe_2 (right panel) monolayers. The demonstrated PL spectra are measured for non-resonant excitation with linearly polarised 514 nm argon laser line. A circular polarisation analyser was present in the detection path. The spectra were fitted with gaussian profiles to determine the energy of the resonances and in case of free exciton resonances (except for charged exciton in WSe_2 monolayer) also the PL intensity. The energy of σ^+/σ^- components are presented as the red/blue dots and their avarage value $1/2(E_{\sigma+} + E_{\sigma-})$ is denoted by open circles. The value of the g-factor for each resonance is given. The PL lines, especially in $MoSe_2$ monolayer, become polarised at higher field. The magnetic field evolution of the polarisation degree, defined as $(I_{\sigma+} - I_{\sigma-})/(I_{\sigma+} + I_{\sigma-})$, is presented for neutral and charged excitons in $MoSe_2$ monolayer and neutral exciton in WSe_2 monolayer.**

consists of two robust emission lines. Their energetic positions correspond well to the resonances observed in the reflectivity spectrum. Following the previous attribution, we note that the higher energy line comes from the recombination of the neutral exciton A and the lower energy one from the recombination of the charged exciton A. The application of the magnetic field, similarly to the resonances observed in reflectivity spectra, leads to the splitting of both lines. The values of the g-factors are obtained by fitting Gaussian line shapes to both lines. We find the values of $g_X = -4.2 \pm 0.4$ and $g_{X^-} = -3.7 \pm 0.5$. In this case, however, both lines

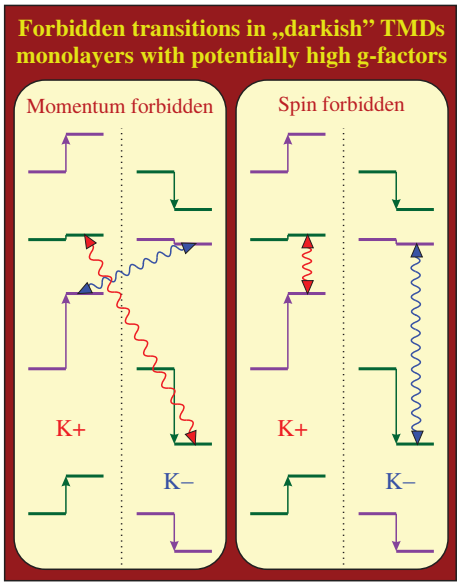

Figure 2-6: **Two simple diagrams demonstrate the examples of optical transitions in 'darkish' sc-TMD monolayers, which could possibly exhibit large g-factor values. These recombination channels are in the first approximation forbidden, nevertheless various mechanisms of their brightening could be considered. The left panel shows inter-valley transitions, which are not allowed due to the conservation of momentum principle, unless these processes involve emission of phonons. The value of the g-factor (in the framework of our description of Zeeman effects in terms of $g_V = 1$, $g_S = 1$ and $g_{d_2} = 2$) in this case yields: $g = 2\,(g_{d_2} + 2g_V) \approx 8$. In the right panel, an intra-valley spin-forbidden transitions are presented. A possible brightening mechanism could origin from inter-valley and/or spin mixing of states. In this scenario the same value of the g-factor is obtained: $g = 2\,(g_{d_2} + 2g_s) \approx 8$.**

become strongly polarised in a magnetic field, so that the lower energy component (σ^+) gains in intensity, while the higher energy one (σ^-) disappears. Such redistribution of intensity between the circularly polarised emission lines originates from the thermalisation of the neutral and charged exciton states in a magnetic field. This feature hinders the precise estimation of the value of the g-factors, as the higher energy line (σ^-) becomes rather weakly pronounced in higher fields. Additionally, the lower energy line progressively gains in intensity and, due to imperfect polarisation selectivity in the experimental set-up, eventually starts to show up in the spectrum detected in opposite polarisation. As a consequence, the values of g-factors determined in PL measurements are subjected to larger uncertainty than one can achieve by analysing the reflectivity spectra. Therefore, the discrepancy between the values of the g-factors of neutral and charged excitons, as seen in the magneto-PL spectra, may result from lesser accuracy of the method with respect to one achievable in the absorption-type experiments. The general conclusion from the analysis of the magneto-PL properties of $MoSe_2$ monolayer film is that the observed features are quite typical for a 2D semiconductor system.

By contrast, the magneto-PL spectra of a WSe_2 monolayer are much more complex and reveal surprising features, which make this system intriguing. Firstly, we have to note that the lower energy band of additional PL lines in our samples is rather broad and obscures efficiently the charged exciton line, which appears as a barely distinguishable shoulder of a more robust lower energy line (an observation supported by the comparison of the energy of the resonances in the reflectivity spectra with the positions of the lines in the PL spectra). The broad PL band, residing below the neutral and charged exciton A lines and dominating the spectra at

low temperature, is the feature which exhibits peculiar behaviour in a magnetic field. An analysis of the positions of the lines reveals, that the values of the g-factors of all resolvable lines in the PL band are significantly larger in magnitude than -4, in some cases even reaching -13. As already mentioned, we speculate that numerous emission peaks appearing in optically 'darkish' systems, such as the WSe_2 monolayer, may be due to recombination of dark excitons, allowed by disorder or phonon-assisted processes. As illustrated in Figure 2-6, the imaginable recombination processes which violate the k-vector or spin selection rules would, in accordance with the proposed scheme of the Zeeman effect in sc-TMD monolayers, result in anomalously large g-factors for the emission lines in 'darkish' systems.

2.4. From high to tiny fields: optical pumping controlled by magnetic field

Optically active excitations is solids must fulfil a set of selection rules regarding the conservation of fundamental physical quantities. One of them is the angular momentum, easily controlled in case of photons which may be used to induce inter-band transitions leading to creation of electrons and holes. Afterwards, depending on the conditions of the excitation determined by the alignment of the bands and the character of electronic states, the photo-created carriers may recombine directly or after a series of relaxation processes. Either way, upon the excitation with circularly polarised light there is a possibility of preservation, to a certain degree, of the angular momentum until the radiative recombination. A quantitative measure of the efficiency of the optical orientation may be defined as a normalised difference between the emission intensity in the co-polarisation and the cross-polarisation configurations. It is practically realised by the measurement of two spectra in a way that excitation light is circularly polarised (σ^+ or σ^-) and the emitted light is detected in both circular polarisations (σ^+ and σ^-). Then, if the excitation is, for example, σ^+ polarised, the polarisation degree, for a particular energy of emission, is determined as follows:

$$P(E) = \left| \frac{I_{\sigma^+}(E) - I_{\sigma^-}(E)}{I_{\sigma^+}(E) + I_{\sigma^-}(E)} \right|$$

where $P(E)$ stands for the polarisation degree (can be in principle energy-dependent), $I_{\sigma^+}(E)$ and $I_{\sigma^-}(E)$ correspond to the intensity of emission detected in σ^+ and σ^- polarisation, respectively. Phenomena related to the optical orientation have been widely explored in zinc-blend semiconductors **[79]**. In sc-TMD structures, they may be especially important, as the circularly

polarised light is associated with the valley degree of freedom **[80–82]**.

The possibility of the optical orientation of the valley pseudo-spin has already been demonstrated for several representatives of sc-TMD materials, in some cases (for MoS_2) up to room temperature. It is worth noting that the concept of optical pumping is not limited to states of photons with ± 1 angular momentum corresponding to circularly polarised light of $\sigma^{\pm}$ helicity. WSe_2 monolayers, for instance, revealed the capabilities of preserving linear polarisation of light as well **[83]**. In the view of their band structure this uncommon feature signifies that coherent superpositions of states from two inequivalent valleys at K+ and K- points of the Brillouin zone may be created and sustained until recombination.

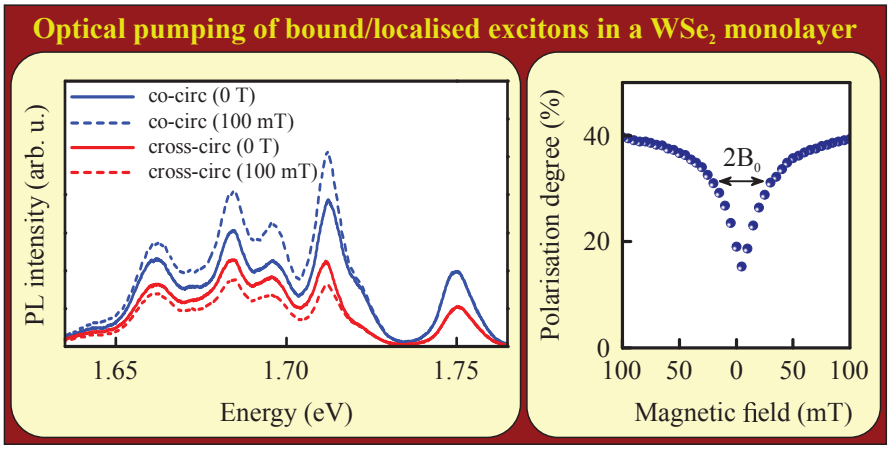

Figure 2-7: **The monolayer WSe_2 spectra detected in σ^+ and σ^- polarisations without magnetic field and at a tiny field of 100 mT applied perpendicularly to its surface are shown in the left graph. The luminescence signal was excitated with circularly polarised laser light of σ^- helicity at the energy of 1.915 eV (non-resonant excitation between the energy of neutral A and B excitons). A clear impact of the magnetic field on the polarisation decgree of the 'bound/localised' exciton states is observed. The precise measurement of the magnetic field dependence of the polarisation degree of the light integrated over the spectral region covering the entire 'bound/localised' excitons band, is presented in the right graph. The data for both directions of the field vector (negative and positive values) are presented. They illustrate a progressive growth of the polarisation degree, untill a saturation value is reached at about 100 mT. A characteristic value of a magnetic field $2B_0$ can be established as a full width at half maximum (FWHM).**

Here, we would like to bring attention to the observation that the efficiency of the optical orientation of the valley pseudo-spin may be controlled by the application of a tiny external magnetic field **[84]**. Representative PL spectra of a WSe_2 monolayer, detected in co- and cross-polarisation configurations without magnetic field and in a presence of a tiny out-of-plane field of 100 mT, are demonstrated in Figure 2-7. Let us say first, based on the zero field data, that the optical pumping is effective not only for free exciton resonances, but appears to be equally robust for the entire band of 'localised/bound' excitons. An apparent distinction between these two cases is seen, however, upon application of a magnetic field perpendicular to the surface of the monolayer. A significant enhancement of the polarisation degree (roughly

twice) is observed for 'bound/localised' excitons, but the neutral exciton state exhibits no such change. This finding strongly supports the existence of a mechanism, which limits the general efficiency of optical pumping, but can be lifted by the application of a small magnetic field for the 'localised/bound' excitons, but not for free bright exciton states.

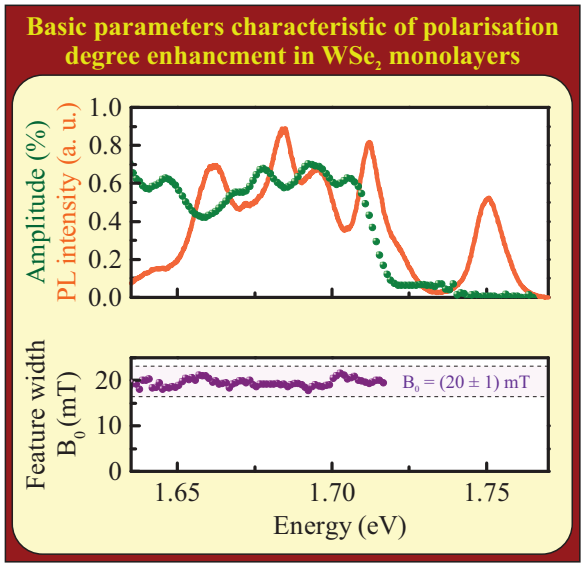

Figure 2-8: **The feature, revealed by the investigation of the evolution of the polarisation degree of 'bound/localised' excitons with out-of-plane magnetic field, can be reproduced by a Lorentzian-like function, mimicking similar effect observed for real spins in conventional semiconductors. The formula which was used, $1-\alpha/(1+(B/B_0)^2)$, introduces two basic parameters: the amplitude α and characterisitic field B_0. The dependence of parameters α and B_0 on the emission energy is presented in top and bottom panels, respectively. In the top graph, the PL spectrum of the investigated WSe_2 monolayer is presented as well, for comparison.**

So far, it has been demonstrated that the strong long-range electron-hole exchange interaction is one of the reasons for the disorientation of the valley pseudo-spin **[85–89]**. However, the strength of exchange coupling depends on the configuration of the spins in the considered states. It has been demonstrated, that the exchange coupling is particularly effective for bright exciton states, but, in the simplest approximation, it vanishes for the electric-dipole forbidden (optically dark) excitons. However, more detailed theoretical treatments reveal finite residual exchange coupling even for the dark excitons, yet its strength is predicted to be orders of magnitude lower than for the bright excitons **[90]**. Consequently, the sc-TMD monolayers with with an optically inactive ground state are expected to display a significantly suppressed relaxation of the valley pseudo-spin. Indeed, the optical pumping effects are quite robust in WSe_2, WS_2 and MoS_2 monolayers and practically non-existent in $MoSe_2$ and $MoTe_2$ monolayers under continuous wave (CW) excitation.

The impact of aforementioned exchange interaction on the electronic states may be considered as equivalent to a presence of an effective magnetic field oriented in the plane of the monolayer. Therefore, the application of the out-of-plane field of a sufficient strength could compensate the exchange interaction, resulting in even better preservation of the valley pseudo-spin. Indeed, the experimental results from Figure 2-9 clearly demonstrate that the value of the characteristic field B_0, indicative of the width of the feature seen in polarisation degree vs magnetic

field dependence, becomes larger when the magnetic field is applied along a direction tilted from the out-of-plane axis (**z**) by the angle α. This finding suggests that the observed field modulation of the pseudospin relaxation has a similar magnetic anisotropy as the valley Zeeman effect, which is mostly sensitive only to the out-of-plane component B_z.

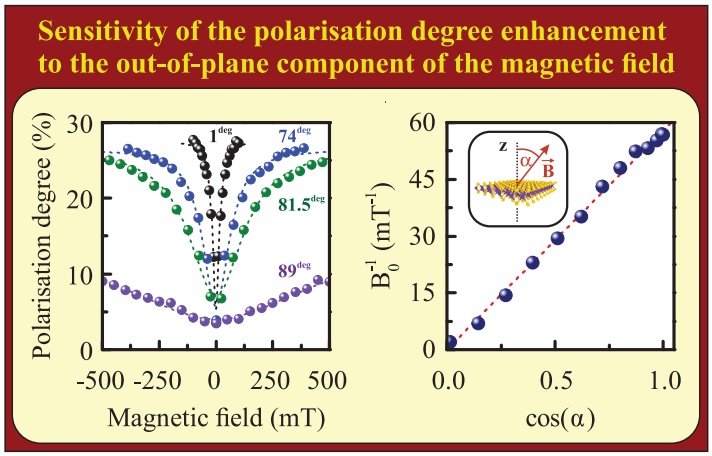

Figure 2-9: **The dependence of the circular polarisation degree on the magnetic field for a PL line at 1.695 eV, arbitrarily selected from the band of 'bound/localised' excitons in WSe_2 monolayer, is presented in the left graph for different orientations of the field vector. Various configurations are characterised by the angle α between the magnetic field vector and the out-of-plane direction (z). As presented in the right graph, the inverse of the charactersitic field B_0 correlates perfectly with $\cos(\alpha)$, which implies that the observed enhancement of polarisation arises solely due to the out-of-plane component of the magnetic field.**

The assumption, that the exchange coupling is the major factor responsible for quenching of optical orientation, must be further specified, to indicate at which electronic level does the majority of depolarisation occurs. In case of the WSe_2 material, one can think of three possibilities: bright excitons, dark excitons or directly at the level of 'localised/bound' excitons. The assumption that only one of these levels can be considered as relevant is strongly supported by experimental evidence. For instance, as demonstrated in Figure 2-8, the characteristic field B_0 of the polarisation degree enhancement was found to be completely independent on the emission energy. Noting the fact that particular PL lines forming the band of 'localised/bound' excitons exhibit drastically different values of g-factors (from -5 to -13), we therefore exclude the possibility of depolarisation at the 'localised/bound' states. Bright excitons, on the other hand, have a well established g-factors equal to about -4. However, in 'darkish' systems they form *de facto* excited states and for that reason they are extremely short-lived. If we introduce a depolarisation rate γ_{depol} associated with the exchange coupling, we would expect it to be significantly smaller than the rate of the bright excitons recombination ($\gamma_{\mathrm{depol}} \ll \gamma^{\mathrm{rec}}_{\mathrm{bright}}$). Therefore, at lower magnetic field fields the effects of the valley depolarisation should be small (hence high degree of polarisation degree seen for bright states) and field-independent. Eventually, the depolarisation at the levels of dark excitons seems most plausible, especially because they constitute the ground state of the system, occupied by the excitons for the majority of time.

The presented concepts are based, to a large degree, on the dynamics of relevant processes. Therefore, time-resolved optical investigations seem appropriate to further develop/verify these ideas. Figure 2-10 illustrates the PL transients traced on a streak camera under circularly polarised excitation (σ^+) and detected in both circular polarisations (σ^+ and σ^-). This allowed the investigation of the temporal evolution of the polarisation degree of the 'bound/localised' excitons with sub-nanosecond resolution without magnetic field and in the presence of field of 100 mT. In the absence of the magnetic field, the important loss of the polarisation degree is clearly visible on the time scale of 100 ps after the laser pulse, and afterwards ($>$ 200 ps) the polarisation degree sets at practically constant level. Remarkably, the initial loss of the polarization degree is fully suppressed upon the application of a tiny magnetic field, when polarisation degree remains constant in time but at the significantly higher level.

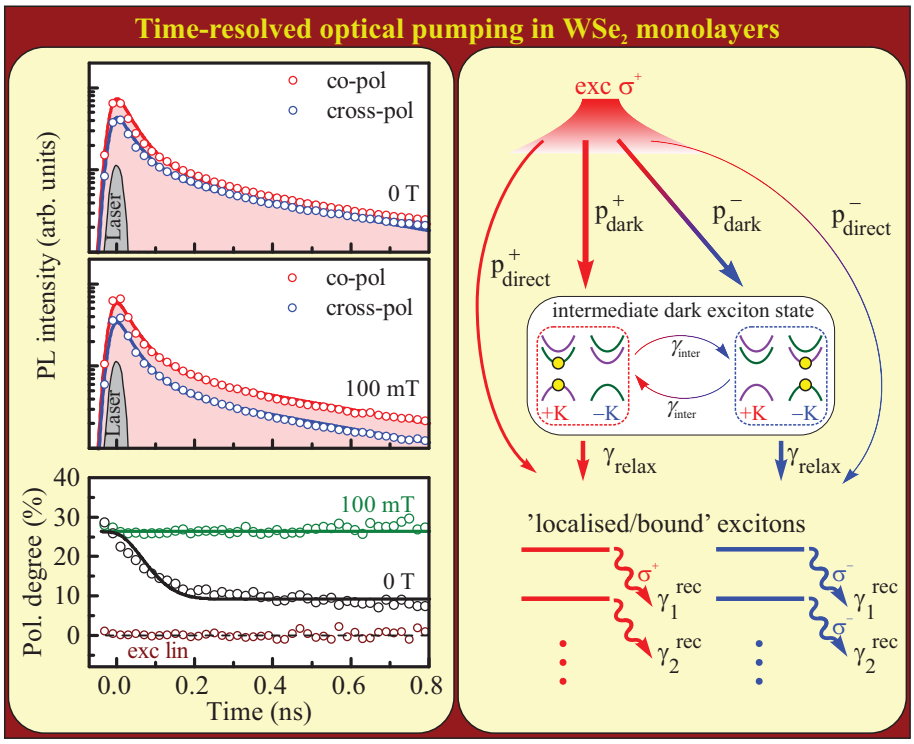

Figure 2-10: **Time-resolved PL of the 'localised/bound' excitons integrated over the emission energy ranging from 1.65 eV to 1.71 eV is presented. The temporal profiles were measured under σ^+ polarised pulsed excitation at 1.91 eV in two circular polarisations of detection without magnetic field and in a small field of 100 mT. The circular polarisation degree of the 'localised/bound' excitons as a function of time after the laser pulse was established in both cases. The solid lines represent the fitted curves based on the rate-equation model described in the text. In the right panel, a scheme of the states and transitions included in the rate-eqation model is shown.**

The scheme of the minimal rate-equation model which accounts for our time-resolved data is presented in Figure 2-10. We assume that the electron-hole pairs, initially photo-created by a σ^+ polarised laser pulse in the K+ valley, relax instantaneously, in part towards the intermediate dark exciton state and in another part directly towards the states of 'localised/bound' excitons, so that a population of these states is established:

$$\begin{cases} N^{\pm}_{\text{dark}}(t=0) & = p^{\pm}_{\text{dark}} \\ N^{\pm}_{\text{LE},i}(t=0) & = \alpha_i p^{\pm}_{\text{direct}}, \text{ for } i=1,2 \end{cases}$$

The initial populations of the dark and 'localised/bound' excitonic states are denoted by $\text{p}^{\pm}_{\text{dark}}$ and $\text{p}^{\pm}_{\text{direct}}$, respectively, where $\pm$ accounts for K$\pm$ valleys occupations. α_i denotes the relative probabilities of the occupation of both considered 'localised' excitons (LE) at t=0 (with the condition $\alpha_1 + \alpha_2 = 1$). The temporal evolution of these populations for t>0 is described by the following equations, which can be directly inferred from the model scheme in Figure 2-10:

$$\begin{cases} \frac{dN^{\pm}_{\text{dark}}(t)}{dt} & = -\gamma_{\text{relax}} N^{\pm}_{\text{dark}}(t) - \gamma_{\text{inter}} N^{\pm}_{\text{dark}}(t) + \gamma_{\text{inter}} N^{\mp}_{\text{dark}}(t) \\ \frac{dN^{\pm}_{\text{LE},i}(t)}{dt} & = -\gamma^{\text{rec}}_i N^{\pm}_{\text{LE},i}(t) + \beta_i \gamma_{\text{relax}} N^{\pm}_{\text{dark}}(t), \text{ for } i=1,2 \end{cases}$$

Particularly important are the populations of dark excitonic states, which are crucial for the modelled polarisation effects. The initial valley polarisation of dark excitons ($\text{p}^{+}_{\text{dark}} > \text{p}^{-}_{\text{dark}}$ under σ^+ excitation) decays with the rate of γ_{inter} due to the inter-valley scattering processes. In parallel, dark excitons relax further towards the localized excitons (and/or form more complex excitonic objects) with the rate of γ_{relax}. We assume that 'bound/localised' excitons are no longer subjected to efficient inter-valley scattering, in accordance with previous studies of sc-TMDs monolayers and in line with a negligible decay of the polarisation degree on the timescale of $0.5 - 1$ ns in our experiment. For the sake of simplicity, in our model we take into account only two types of 'bound/localised' excitons with different lifetimes. The overall time-dependent PL intensity of both localised excitons in $\sigma^{\pm}$ polarisations can be expressed (up to the normalisation constant) as:

$$\text{I}^{\pm}_{\text{LE}}(t) = \sum_{i=1,2} \gamma^{\text{rec}}_i N^{\pm}_{\text{dark}}(t)$$

This is a minimal assumption required to account for the non-exponential character of the temporal PL profiles, as seen in Figure 2-10. This simplification does not substantially influence the overall character of the calculated transients of the polarisation degree due to a suppression of the inter-valley scattering at the level of localised excitons. The efficiency γ_{inter} of the intervalley scattering of dark excitons is the only parameter assumed to be affected by the magnetic field. Using $1/\gamma_{\text{inter}} = 120$ ps in the absence of the magnetic field and setting

Parameters	p^{+}_{dark}	p^{-}_{dark}	p^{+}_{direct}	p^{-}_{direct}	α_1	α_2	$1/\gamma_1^{rec}$	$1/\gamma_2^{rec}$	$1/\gamma_{inter}$ (B = 0)	$1/\gamma_{relax}$	β_1	β_2
Values	0.467	0.249	0.177	0.107	0.498	0.502	42 ps	683 ps	120 ps	48 ps	0.109	0.891

Table 2.3: **The values of the rate-equation model parameters used to calculate the curves presented in Figure 2-10.**

$\gamma_{inter} = 0$ at B = 100 mT we have reproduced our time-resolved data. The values of all the parameters, used in the rate-equation model, are summarised in Table 2.3.

Chapter 3

Single photon sources in thin sc-TMD flakes

In the past, the investigations of optical properties of conventional two dimensional systems gave birth to a new area of research focused on zero dimensional structures. The imperfections of the interface between quantum wells and surrounding barrier material, such as well-width or composition fluctuations, were found to play a role of charge traps. In the optical studies, such centres, if properly isolated, were seen as single-object light sources. Their capability of effectively confining carriers in all three dimensions **[91]** impacts the properties of localised carriers. As a consequence, the PL response takes form of narrow emission lines due to appearance of discrete atomic-like electronic levels **[92–94]**. Eventually, these objects, known as quantum dots, became an intensely investigated research subject. With the advance of the technology of their fabrication, the initial studies of their general properties were followed by the incorporation of quantum dots into more complex heterostructures.

When looking at the development of optical studies of thin layers of sc-TMD, one could come to the conclusion that it currently undergoes a similar evolution. Narrow lines emitting centres (NLECs) have been found to be unintentionally created in exfoliated **[95–100]** and chemically fabricated **[101]** WSe_2 flakes. Similarly to quantum dots, the NLECs reveal a signature of single photon emission, which is a highly desirable property. It is relevant for the investigations of the carrier dynamics in solids, because it grants insight into individual recombination events. Moreover, the utility of single photon sources extends beyond condensed matter physics, as fundamental research in quantum optics profits from the control of light emission at the level of individual photons. Here, we will focus on the basic characterization of NLECs in exfoliated

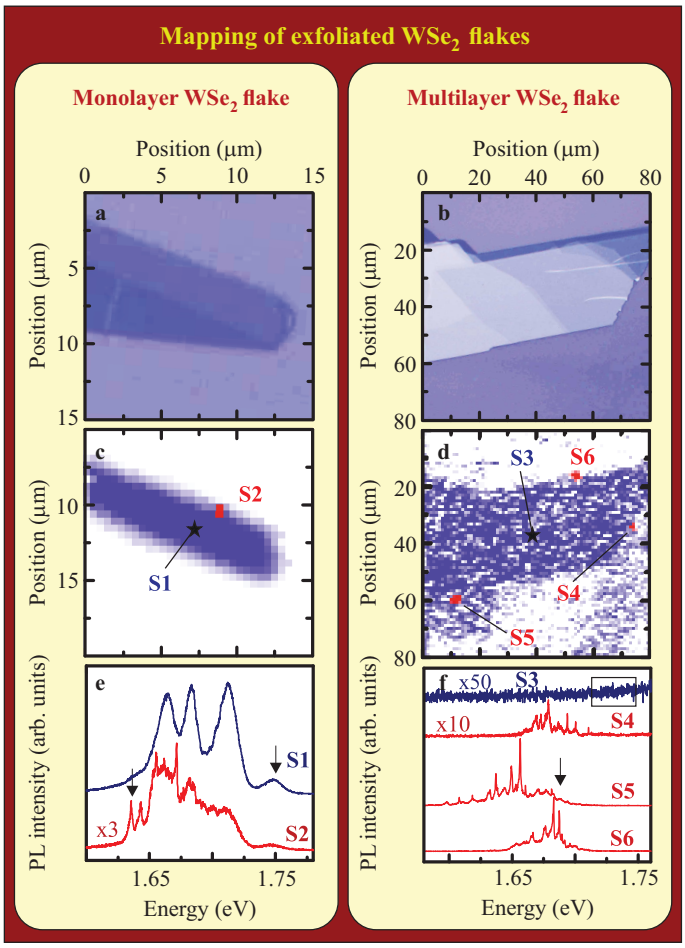

Figure 3-1: **The PL mapping of the surface of WSe_2 flakes with a 514 nm laser beam focalized to a spot of about 1 μm diameter reveals the presence of the narrow lines emitting centres. In the first row, (a, b) two optical images of selected flakes are shown: one with a large monolayer part and the other cosisting of multiple fragments of multilayer thickness (6-9 monolayers). (c) When monitoring the intensity of emission from a monolayer flake, e. g. at the energy of the neutral exciton, one can accurately reproduce the shape of the monolayer part. (d) The multilayer flake does not give a PL signal, however, the integrated intensity over a broder spectral range (marked by a box in the spectrum below) shows a decent contrast between the flake region and the substrate, probably due to scattered light. The spectra taken at selected spots of the two maps are shown in (e, f).**

WSe_2 flakes with the optical methods, followed by the speculations about their origin.

3.1. Appearance of narrow lines emitting centres in exfoliated thin layers of sc-TMD

The exfoliated WSe_2 flakes typically used in the optical studies have lateral size reaching up to several tens of micrometers. In case of monolayers, which appear as separate flakes or can be attached to thicker structures, the μPL spectra measured at the majority of positions on the flake have a form of several broad lines, as discussed previously. However, the thorough mapping of the surface of the flake (at low temperature) with micrometer resolution may uncover distinct locations, in which a drastic change occurs in the character of the emission spectrum. A set of narrow lines (linewidths of the order of 100 μeV) appears on top of the lower energy part of the typical 2D PL spectrum of a monolayer flake. The locations, where NLECs are found, are scarce, well-isolated and the emerging narrow lines tend to appear in groups.

It is important to stress that the presence of NLECs is not limited to monolayers only.

They can also be found in thicker flakes, which can be advantageous due to the absence of the background 2D PL signal from a monolayer, so that the narrow lines can in principle be better resolved. Figure 3-1 presents the results of PL mapping experiments for two selected flakes. The left side of the figure is dedicated to a flake with a monolayer part. The monolayer region can be accurately reproduced in the mapping experiment by monitoring the 2D PL intensity, e. g., at the energy of the free neutral exciton resonance. The vast majority of the area of the flake gives rise to a typical monolayer 2D μPL signal (see the spectrum from the spot S1), however one specific location at the edge of the flake exists (S2), marked by a red spot in the map, where narrow lines appear. The imaging of the multilayer flake is a bit more subtle, since such flakes give practically no PL signal. However, integrating the intensity over the spectral range around 1.75 eV (see spectrum S3) produces a fair contrast between the flake region and the Si/SiO_2 substrate. The signal is due to scattered light, which is of different intensity in the region of the flake and outside it. For this particular structure three locations (S4-S6), also residing at the perimeter of the flake, give rise to the emission in form of narrow lines.

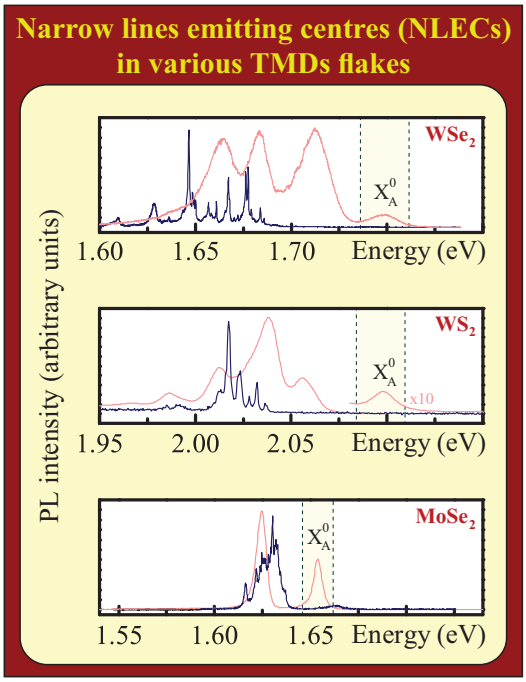

Figure 3-2: **Narrow lines emitting centres may be found in multiple materials belonging to sc-TMD family. Here, the typical PL signal from a monolayer flake (red curve) is compared with a spectrum taken at a location, which shows emission in form of narrow lines (blue curve) for WSe_2, WS_2 and $MoSe_2$ materials. It is worth emphasizing that the narrow emission lines always appear at the energy below the free neutral exciton resonance (X_A^0).**

NLECs can be found in other materials belonging to the sc-TMD familiy **[103, 116]**. In Figure 3-2, the spectra of NLECs are presented for WSe_2, WS_2 and $MoSe_2$ materials, together with the monolayer 2D μPL response for comparison. A common feature of NLECs shared between various sc-TMD materials is the appearance of narrow lines at the energies exclusively below the free neutral exciton resonance. The interpretation of this observation depends on the underlying specific mechanism of carrier localisation. However, generally speaking the exact energy of the emerging discrete states may be dependent on multiple factors, such as compression of the wave functions, enhancement of Coulomb interaction, potentially appearing spin-spin interactions, etc. An appropriate magnitude of particular contributions could push

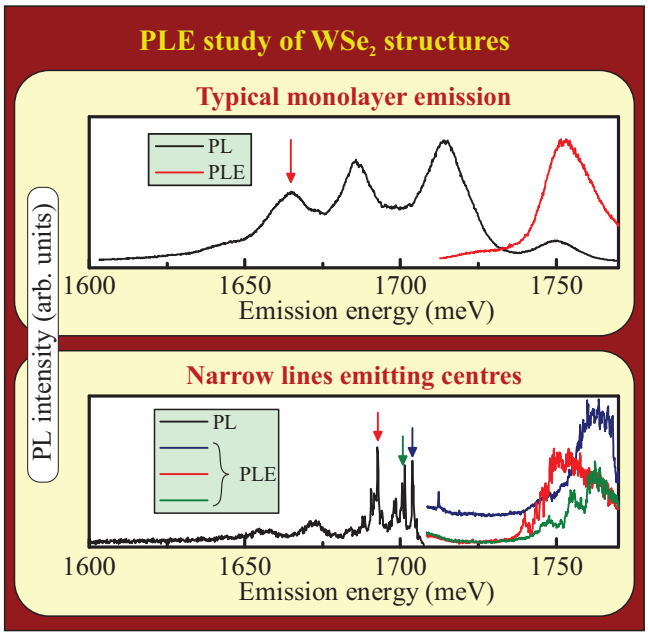

Figure 3-3: **The PLE and PL spectra are compared for monolayer WSe_2 (top image) and a selected NLEC (bottom image). The PL spectrum of the WSe_2 monolayer was measured for non-resonant excitation, with 514 nm laser line, while the PL spectrum of the NLEC comes from PLE measurements, when the laser energy was set around the maximum of emission (∼708 nm). The coloured arrows indicate the energy, at which the intensity was monitored for the corresponding PLE spectra. In case of individual narrow lines, the non-continues abrupt changes of intensity originate from their temporal instability.**

the narrow PL lines of NLECs below the energy of the free neutral exciton resonance. An alternative possibility is that PL lines of NLECs arise exclusively due to charged states and are consequently shifted towards lower energies, by analogy with the free neutral and charged exciton resonances in sc-TMD structures.

3.2. Optical characterization of the NLECs in WSe_2 flakes

Let us begin the analysis of optical properties of NLECs by investigating the properties related to the absorption of light. A direct measurement of reflectance or transmission in case of specimen as small as the NLECs is difficult and usually requires fabrication of specific structures and dedicated experimental set-ups. Instead we will take advantage of the photoluminescence excitation (PLE) technique. It is based on an approach, in which the intensity of the PL signal is monitored as a function of the laser energy for constant excitation power (preferably) in search for the enhanced intensity of emission, which may occur when the laser energy coincides with absorption resonances. Although this method has its limitations (one cannot investigate the ground state absorption), it may still be useful for studying the mechanisms related to the excitation of NLECs. The data discussed here were obtained with a Ti:Sapph laser, which operates from the visible red up to close infrared spectral region.

In the Figure 3-3, the PLE study is presented firstly for the typical 2D-like emission from a monolayer WSe_2 flake. The PL intensity was monitored at an arbitrarily chosen lower energy broad PL line (marked with an arrow in the figure), however it was verified that general

characteristics of the PLE spectrum are identical for different PL lines. In consistency with the previous results, the main feature in the PLE spectrum appears at the energy of the free neutral exciton (which is also seen in the PL and reflectivity spectra). Another structure, although significantly weaker, may also be identified at the lower energy slope of the main neutral exciton line, similarly as the charged exciton resonance manifests itself in the reflective spectra.

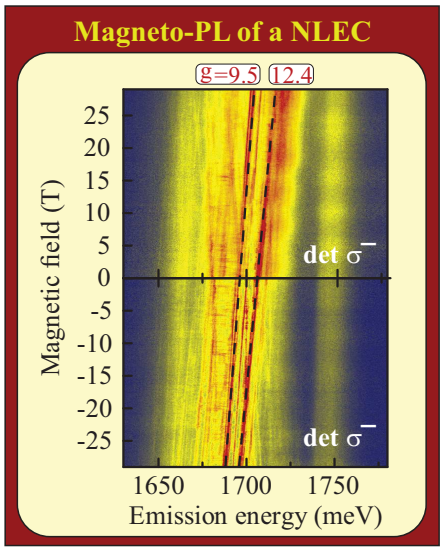

Figure 3-4: **The colour maps show the magnetic field evolution of the PL spectrum for 514 nm laser line excitation in Faraday configuration of a selected NLEC found in a monolayer WSe_2 flake. The magnetic field was applied perpendicular to the surface of the flake. The positive and negative values of the magnetic field correspond to the opposite orientations of its vector. The spectra were detected in σ^- circular polarization. The g-factor values were established for 2 highlighted narrow lines.**

NLECs prove to be a more challenging subject for PLE measurements, as they often exhibit significant random variations of both energy and intensity of emission, what strongly impacts the obtained PLE spectra. However, carefully chosen locations enable monitoring individual narrow lines with no dramatic intensity fluctuations over sufficient periods of time, so that the alternation of the intensity of lines in a PLE experiment comes predominantly from tuning the laser energy. An example of the results for three selected lines are presented in the Figure 3-3. A main finding is that our NLECs exhibit a broad resonances at similar energies as the free neutral exciton resonance seen in the 2D-like PLE spectrum characteristic of WSe_2 monolayers. The inheritance of the NLECs' excitation spectrum may signify that the excitation process involves the absorption of light in the nearby 2D structure followed by the collapse of the photo-created carriers on the discrete states of the NLEC. As discussed later on, the localising potential of NLECs appear to be rather shallow and therefore NLECs may not exhibit excited states, which would allow their resonant excitation.

Continuing our route of comparative analysis, we turn to the magneto-luminescence studies which uncover further links between the properties of WSe_2 monolayers and NLECs. In Figure 3-4 a colour map is presented that illustrates the magnetic field evolution of a PL spectrum of an example NLEC. In this experiment, the emitted light was detected in a set circular polarization (σ^-) and the magnetic field was applied perpendicular to the surface of the flake

in two different polarities, which is in principle equivalent to a measurement when the two opposite circular polarizations are detected while maintaining the orientation of the magnetic field unchanged. The Zeeman splitting of the lines is seen in the spectra obtained for the opposite polarities of the magnetic field therefore g-factors values can be established. As it turns out, the narrow emission lines exhibit suprisingly large g-factor values likewise the lines forming the low energy band (bound excitons) of the typical WSe_2 monolayer PL spectrum. For instance, the two narrow lines marked in the figure have g-factor values equal to -9.5 and -12.4. We have speculated before, that the unusually large Zeeman splitting of bound excitons in WSe_2 monolayers may be related to dark exciton states and it is noteworthy to point out that the presence of local disorder (e. g. in form of various defect centres) could provide mechanisms of their brightening. Such apparent sensitivity to a magnetic field is a feature shared exclusively between NLECs and WSe_2 monolayers, as no fingerprints of so peculiar Zeeman patterns were observed in thicker WSe_2 structures.

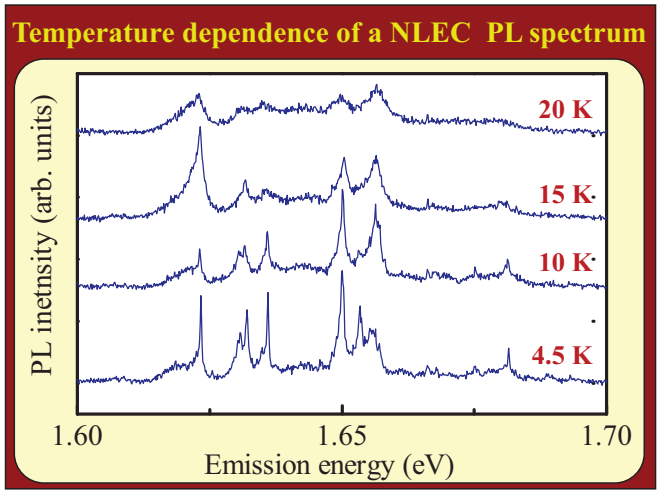

Figure 3-5: **Temperature dependence of the PL spectrum of a selected NLEC in a thick WSe_2 flake under non-resonant excitation conditions (with 514 nm Argon laser line). The increase of the temperature leads to a significant broadening of the PL lines so that they become practically unresolvable at the temperature higher that a few tens of Kelvin.**

With these observations, we have exploited the available experimental data to demonstrate an inheritance of NLECs' properties from WSe_2 structures in form of mono- and multilayers. The proceeding analysis has a sole purpose of completing the optical characterization of NLECs and provide hints regarding their possible origin. We begin with the temperature dependence of a PL spectrum of a selected NLEC shown in Figure 3-5. The increase of the temperature leads to an immediate broadening of the narrow lines in a manner suggesting involvement of phonons **[107, 108]**. Initially, rising the temperature causes an appearance of characteristic sidebands (in form of exponentially decaying tails) on the lower and heigher energy side of the main narrow line. A similar effect is observed in semiconductor quantum dots, where it was established that the sidebands arise due to a coupling mechanism between the excitons and a continuum of acoustic phonons resulting in additional processes with emission or absorption of

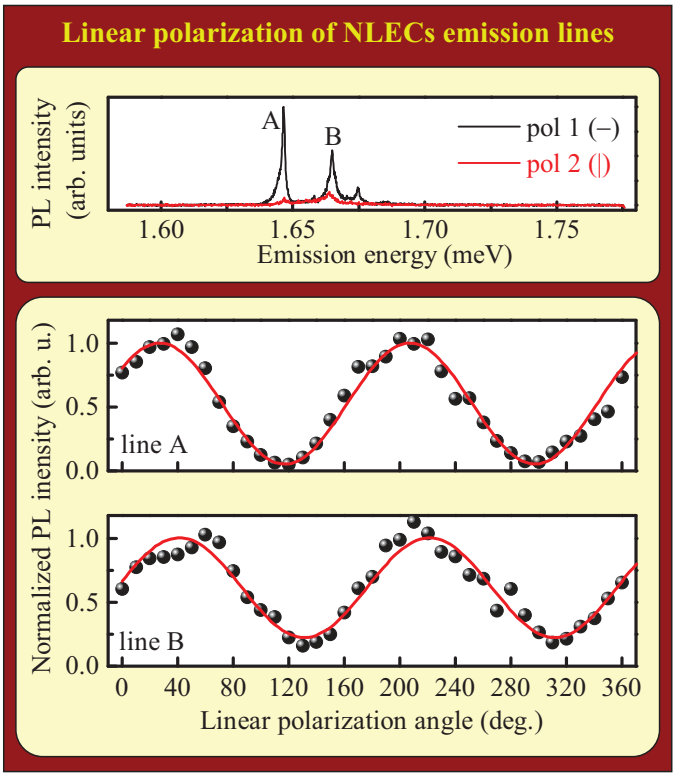

Figure 3-6: **The polarization resolved measurements of photoluminescence show that the emission of NLECs may be fully linearly polarized. The two PL spectra for a selected NLEC (black and red curves in the top image) are detected in perpendicular linear polarizations. For one direction of the detected linear polarization (red curve), the emission lines disappear almost completely. A more detailed analysis of the intensity of the two most robust lines (marked as A and B in the spectrum) as a function of the orientation of the linear polarization axis is presented in the two bottom images. They both show quite high degree of polarization (above 80 %) along slightly different axes (rotated by less than 20 degrees).**

phonons which accompany the main transition (referred to in this context as the zero-phonon line) **[109]**. Following this scenario, we can state that in case of NLECs the zero-phonon line disappears extremely fast with the increase of the temperature, as at 20 K basically only the sidebands remain visible in the PL spectrum. This finding indicates that the trapping potential for charge carriers must be pretty shallow for NLECs, as 20 K corresponds to the energy of only 1.7 meV.

Even though increasing the depth of the potential well in order to push the feasibility of optical studies to higher temperatures is currently an obvious technological challenge, we can carry on with the investigation of our NLECs at helium temperature to learn more about their intrinsic properties. As the next step we will discuss the polarization resolved spectra without the presence of a magnetic field. Figure 3-6 highlights the results of measurements of the PL spectra with linear polarization resolution. Most of the NLECs exhibit a certain degree of linear polarization of their emission lines, however the particular one presented in the figure stands out as an example of a completely linearly polarized emitter. It is clearly illustrated by the two spectra detected in perpendicular linear polarization, as for one direction of the polarisation axis the emission lines practically disappear. Usually, high degree of linear polarization of light sources in solids is indicative of an enhanced electron-hole coupling alongside a distinctive direction, which is most often linked to a geometrical anisotropy of the emitter (e. g. quantum

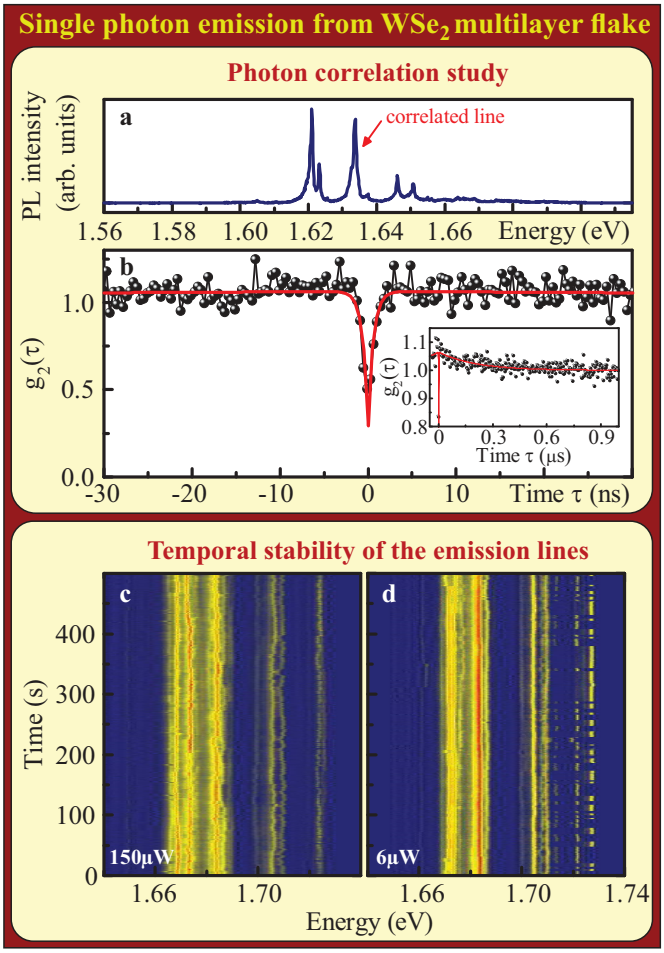

Figure 3-7: **Photon correlation measurements performed in a standard Hanbury Brown and Twiss configuration for individual well-isolated NLEC lines reveal the signature of single photon emission. The top part of the image presents (a) the spectrum of a selected NLEC with the line marked by the arrow for which (b) the correlation function $g_2(\tau)$ is demonstrated uncovering a clear anti-bunching in a nanosecond timescale. The inset presents the same correlation function in wider temporal window to show that a weak bunching in longer timescale appears. The bottom part of the image is devoted to the study of the stability of a NLEC. The set of spectra were recorded (100 ms accumulation) one after another for an extended period of time (about 10 minutes) for (c) lower and (d) higher laser power under the condition of non-resonant excitation (with 514 nm laser line) and presented in a form of colour maps.**

dots exhibiting in-plane ellipticity or quantum wires). A less likely alternative is that it stems from optical pumping, when the polarization of the exciting laser is transferred into electronic excitations and conserved until the recombination process. Here, the latter case is excluded, for instance by varying the detected polarization axis of the NLEC remains unchanged when rotating the linear polarization of the laser.

Finally, we turn to the last and probably most exciting set of optical experiments, which establish that NLECs are single photon emitters. The general interest in this class of light sources comes from the benefits of investigating and controlling the physical processes at the level of individual particles and that includes photons as well. The number of photons emitted simultaneously by any light source is given by a certain statistics (given by e. g. Poissonian or Bose-Einstein distribution) and usually the probability of emitting only a single photon is small. However, a special kind of emitters exists, for which the emission of light is limited mostly to events involving only a single photon. Such particular property can be revealed by the measurements of photon correlations, which basically comes down to detecting the PL signal simultaneously by two fast photodiodes with single photon sensitivity and finding the

probability that they both detect a photon at the same time. In Figure 3-7 a measurement of an example correlation function $g_2(\tau)$ for a selected individual NLEC emission line (marked by an arrow in the spectrum) is presented. An appearance of an antibunching indicates a signature of single photon emission. The depth of the feature, usually established by the value of the correlation function for zero delay between detection events, $g_2(0)$, is directly related to the probability of emitting only a single photon. Typically, an emitter is classified as a single photon source if the depth of the antibunching exceeds 50 % of the background signal, but a perfect source should satisfy the condition $g_2(0) = 0$. In order to establish the quality of our NLEC as a single photon emitter we fitted the correlation function with exponential profiles, but firstly it is necessary to note that in longer timescale a weak bunching appears that could indicate a presence of excited states (no bunching is possible in purely two level system). In order to account for both features the following function was used to describe the correlation function

$$g_2(\tau) = 1 - A_1 * \exp\left(-\left|\frac{\tau}{t_1}\right|\right) + A_2 * \exp\left(-\left|\frac{\tau}{t_2}\right|\right) \tag{3.1}$$

where t_1 is a characteristic decay time related to the antibunching, t_2 describes a characteristic time of the long-timescale bunching, A_1 is the antibunching depth and A_2 is the bunching amplitude. The following values of the parameters were obtained: $A_1 = 0.77 \pm 0.08$, $A_2 = 0.06 \pm 0.01$, $t_1 = 0.6 \pm 0.1$ ns and $t_2 = 0.20 \pm 0.02$ µs. That gives us the value of the correlation function for zero delay $g_2(0) = 0.39$, which shows that the quality of single photon emission from NLECs is far from perfect. However, taking into consideration the early stage of research and little understanding about the actual origin of NLECs there might be room for improvement.

Another issue limiting the functionality of NLECs are temporal instabilities in form of telegraphic noise that affects the emission energy and intensity of lines in sub-second timescale. It is not uncommon for nanoscale sized light sources to exhibit this kind of behaviour which is typically attributed to the influence of charge fluctuation (therefore it is not always considered as a drawback, as such telegraphing emitter may be utilized as a local probe of charge dynamics in so called noise spectroscopy). In an attempt to verify if the telegraphing of lines can be controlled, we have measured the temporal evolution of a PL spectrum under non-resonant excitition with resolution of 100 ms for lower and higher laser power. The results are presented in Figure 3-7**(c–d)** in forms of colour maps. It seems that using lower excitation power, as well as quasi-resonant excitation (not shown here), reduces the temporal instabilities. As a

perspective, one could also consider protecting the surface of the flakes, for instance with exfoliated layers of transparent materials (such as boron nitride) or by depositing dielectric coating.

3.3. Concluding remarks

We have presented a comprehensive optical characterization of NLECs appearing in exfoliated WSe_2 structures. The uncovered single photon nature of these emitting centres offers additional functionalities that may be considered when inventing new types of van der Vaals heterostructures. Although multiple challenges remain to be unraveled, many of them of technological nature, already the firsts attempts of designing more complex structures and performing more detailed experiments have been made. For instance, the possibility of the electrical pumping of NLECs **[103–105]** (as well as typical monolayer emission from different sc-TMD **[110–113]**) has been demonstrated by incorporating a WSe_2 flake into a tunneling diode device with graphene flakes used as the electrodes and boron nitride flakes serving as insulating barriers. Regarding recent progress in the domain of more advanced optical properties, an evidence of cascaded emission from biexciton-exciton consecutive recombination has been observed in the study of photon cross-correlations **[114]**.

The most intriguing puzzle at present concerns obviously the origin of NLECs. In spite of abundant experimental data that is currently available, various statements regarding their creation are still speculative. In view of the emergence of NLECs exclusively at the edges of the flakes in our samples, we made attempts to investigate the morphology of the flakes around their perimeter. In order to do so, a WSe_2 flake was deposited on a graphene film of locally varying monolayer and bilayer thickness formed on a carbon plane of a SiC crystal to provide a suitable conducting substrate for STM studies. Two types of experiment have been performed. The atomically-resolved STM images (not shown here) have been obtained on the flat regions of the WSe_2 flake, showing a triangular lattice structure with the interatomic distances 3.3 Å, in agreement with the crystallographic parameter of the material **[35]**. The large scale lower resolution images uncover much richer material for speculations as generally the edges of exfoliated flakes appear to be heavily damaged so that multiple defects appear in the form of wrinkles, folds or bubbles of air trapped between the flake and the substrate. One of the structures that particularly caught our attention was a piece of a WSe_2 monolayer of

nanometre dimensions attached to a bilayer part of the flake. The STM images illustrating the appearance of this defect is presented in Figure 3-8, together with the description of its most likely formation process. Only one place with such small monolayer was found and the evident anisotropy of its shape brings to mind our liner polariation studies. We have made attempts to perform PL mapping on this flake and indeed a weak signature of narrow lines emission was found in the region were the nanosized monolayer was seen in the STM studies, however given our micrometer resolution in optical experiments our spatial accuracy cannot make our approach conclusive. An alternative route that could possible be more successful would be to measure the electroluminescence signal directly from under the STM tip, however our set-ups are not compatible for this kind of study.

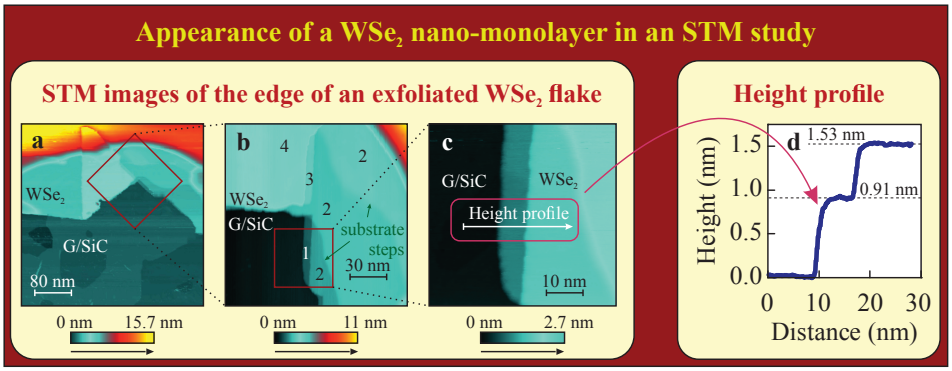

Figure 3-8: **STM images of the edge of a WSe_2 film showing the existence of a nanometer-sized fragment of WSe_2 monolayer at the perimeter of the film. Large scale STM image revealing the morphology of the edge of the WSe_2 bilayer film is shown in (a) and consecutively enlarged in (b) and (c). During the transfer process this area has been unintentionally damaged: the edge has been torn and a piece of triangular shape has been folded onto the film, locally doubling the number of layers. It can be seen that the folded piece locally forms a four-layer area (labelled 4). Besides this, an irregular fringe with a fragment of a monolayer (labelled 1) has been formed; the complementary part forms the upper tri-layer area (labelled 3). The size of the monolayer fragment is 7 nm × 50 nm. The height profile measured along the arrow is presented in (d). The height of the WSe_2 monolayer relative to the graphene plane is 0.91 nm, whereas the height difference between WSe_2 monolayer and bilayer is 0.62 nm, in fair agreement with the interlayer spacing (0.65 nm) in the bulk crystal. [35, 106]**

The quest for uncovering the origin of NLECs may be complicated even more than initially appears as judging by the reported attempts to artificially create such emitting cetntres in WSe_2 flakes it is now more than likely that multiple qualitatively different objects exist that have a similar optical signature of narrow lines emission in the optical spectra. One of the successful approaches to induce a creation of NLECs in a controllable manner was realized by depositing a WSe_2 flake on top of an array on nanopillars so that a pattern of NLECs was created over the whole area of the flake **[115, 116]**. The interpretation of this finding is that the NLECs can be created by large local gradients of strain. However, it is not likely the reason behind the

formation of NLECs in our case or in different attempts to create NLECs, e. g. by scratching the surface of the flake with a STM tip **[98]**. Also, some deviations appear in the reported optical properties, such as a different character of the excitation spectra, as in some samples they appear in a form inherited directly from WSe_2 mono- or multilayer structures **[95, 96]** (a single broad resonance) and in other they resemble a series of excitonic excited states **[98]** (multiple narrow lines). Therefore when testing various hypotheses it is crucial to keep in mind the possibility that qualitatively different NLECs may appear in different studies.

Appendix A

Single photon emitters in boron nitride crystals

A.1. The role of boron nitride in investigations of thin films of sc-TMD and beyond

Hexagonal boron nitride (hBN) is a layered material exhibiting a particular set of properties, which have been exploited in the general research of 2D structures. For instance, a large band gap of almost 6 eV granted it a position as an insulating barrier in tunnelling diode devices based on monolayer flakes of sc-TMD **[103–105]**, which allowed observation of room temperature electro-luminescence from such structures. Moreover, BN crystals in hexagonal form can serve as a fitting substrate for other materials of similar morphology (graphene in particular) **[117–119]**, additionally providing an environment with an intermediate value of the dielectric constant **[120,121]**, $\epsilon \approx 7$, yet noticeably larger than for commonly used Si/SiO_2 substrates. The optical investigations of 2D structures, based on sc-TMD in particular, can further benefit from the transparency of the BN crystals for visible light, as capping the flakes with thin exfoliated films of BN might be used to effectively protect the open-surface systems and prevent, e. g. oxidization processes. Potential enhancement of the quality of the optical signal from sc-TMD flakes and limiting the ageing effects are among the benefits of introducing BN protective layers.

Apart from the presence in the frontlines of the development of van der Waals heterostructures, hBN often appears as a primary object of investigation, however mostly in bulk or multilayer form (although successful attempts to isolate and identify monolayers have been made **[122]**). Until recently, the optical spectroscopy studies of BN crystals were focused mainly

on the energy range around its band gap, which resides in the ultraviolet spectral region and provides a solid method to analyse excitations related closely to the band structure **[123–130]** or shallow defects **[131, 132]**. However, a detailed optical characterisation of a 2D crystal has been proven capable of unveiling unique and unexpected properties, such as appearance of NLECs in thin WSe_2 crystals discussed previously. The following demonstration of similar centres (in terms of their optical response) in BN powder deposited on an alien substrate enriched the family of single photon emitters with yet another new member **[133–140]**. This finding was triggered by the micro-optical characterization of BN crystals, which until recently was not a commonly used approach as the majority of studies devoted to discovering the optical properties of BN material required solely macroscopic investigations. The appearance of NLECs in BN crystals giving rise to emission in visible spectral range immediately invokes a necessity to compare their properties with other colour centres in wide gap materials, such as vacancies in diamond **[141, 142]** or silicon carbide **[143]**. The comprehensive optical characterization of NLECs in BN presented here indeed reveals multiple similarities, but some features remain distinct and intriguing.

With a large variety of presently known single photon sources operating in visible spectral range, such as semiconductor quantum dots **[144, 145]**, single molecules **[146]** or colour centres **[141–143]**, which have been studied in-depth and incorporated into heterostructures, a sound question arises if it is worth the effort and resources to bring new species into this important family of light emitters. A definite answer surely cannot be given at present time, however based on the results reported so far and those brought to attention here, there is no denying that NLECs in BN constitute an appealing system. To compactly summarize their advantages, one could state that they provide robust, multicolour light sources showing the single photon emission up to room temperature, bringing together the two mostly desired properties. Moreover, the utmost facility of sample preparation, requiring only a deposition of BN powder onto a supporting substrate, makes NLECs in BN the most accessible single photon sources with a great potential of building up more complex structures and devices.

A.2. Appearance of single emitting centres in BN powder and exfoliated hBN flakes

The study presented here concern mostly the samples with BN powder in form of 1 μm large grains deposited on Si/SiO_2 substrate. In this case, the process of sample preparation deserves some special attention, because taking into account its simplicity the resulting quality of the

observed optical response is astonishing. After several try-outs (involving dissolving the powder in ethanol, annealing the samples in ambient conditions, etc.), a simple approach to distribute the BN powder on a piece of gelfilm, which acts as a transparent and flexible support typically used in the exfoliation technique of various layered materials (graphite, TMDs and also boron

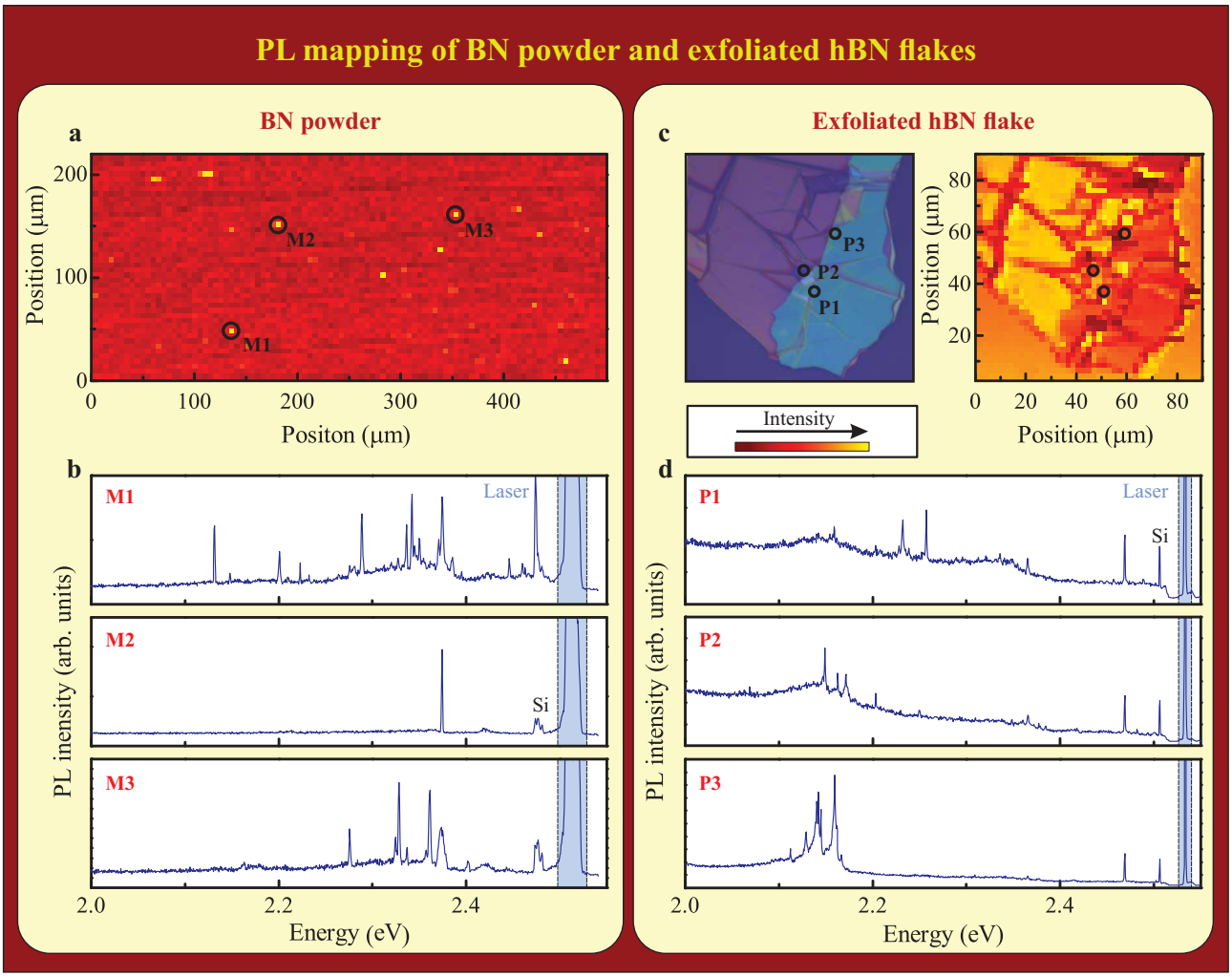

Figure A-1: **The PL mapping experiments, when the surface of the sample is scanned with a laser beam focused to a spot of about 1 μm size, are used to study systematically the appearance of emitting centres in BN. The left panel of the figure presents results obtained for the sample covered with the BN powder. (a) The colour map shows the intensity monitored at the specific energy of 2.374 eV, the choice of which was based on the inspection of individual spectra. The bright pixels in the map represent spots, where an emission line appears at the selected energy value. Therefore the map does not include all the emitting centres in the area, but instead reveals particular ones. (b) Three selected spectra from spots marked in the map (M1-M3) illustrate various patterns of lines originating from the emitting centres. In the right panel the results of mapping obtained for an exfoliated hBN flake are presented. (c) The image from the optical microscope (on the left) is confronted with an counter color plot map of scattered laser light (on the right) to show that the detailes of the flake structure can be reproduced by the mapping. The emitting centres can be found in exfoliated hBN flake as well, as seen in (d) the spectra from selected spots marked in both the optical image and the map (P1-P3).**

nitride), and to press it afterwards against the substrate turned out to be sufficient to observe bright NLECs.

The samples have been characterised in a micro-optical setup, firstly by the PL mapping of their surface at helium temperature, ∼4.2 K, with a laser beam focused to an area of about 1 μm diameter. Indeed, particular spots could be found, of the size below the spatial resolution of the set-up, which give rise to an optical signal in form of narrow spectral lines. A unique pattern of lines represents each spot, appearing sometimes as simple spectra with only a single line, but most often as complex ensembles of lines. They cover a relatively large spectral range in the visible region, reaching up to about 700 nm on the low energy side. As narrow lines can be found at the very edge of the transmission band of the filter used to suppress the laser light, clearly the observation of the high energy lines is limited by the energy of the laser excitation - usually the Ar^+ 488 nm line. A peculiar characteristics of these emitting centres is that, even though particular lines can be robust in intensity, they require a rather high laser excitation power, probably due to sub-bandgap excitation leading to low absorption of the laser light. Typically $1 - 2$ mW of the laser power was delivered to the surface of sample in the mapping experiments, which is comparable to the excitation power typically used for quasi-resonant (below the band gap) excitation of, e. g., semiconductor quantum dots.

Representative results obtained from the μPL mapping of the BN powder sample are presented in the left panel of Figure A-1. The colour map illustrates the spatial distribution of the intensity monitored at a particular energy, 2.374 eV, therefore bright spots reveal places, where a spectral line appears at that chosen energy value. Three selected spectra originating from this map come from places marked as M1-M3. They represent a distinct character of each emitting centre, including the case with only a single spectral line (M2). The distribution of the emitters on the surface of the sample is rather scarce - they tend to appear as single and isolated spots, as demonstrated by the colour map.

Even though the presence of the isolated emitting centres in the BN powder samples is beyond any doubts, one could still argue that their origin may not be related to BN at all. A scenario that the chemical substances used at any step in the production of the BN powder play a substantial role is sound and cannot be *a priori* excluded. A possible route to shed some light on this issue could be the examination of hexagonal BN flakes obtained from bulk crystals - a material of well established crystal structure and composition. Therefore, the hBN flakes exfoliated with a standard method developed mostly during studies of TMDs and graphene

structures, have been deposited on Si/SiO_2 substrates to undergo similar mapping experiments as the BN powder samples. In the right panel of Figure A-1, the results of investigation of a selected flake are summarised. The image from an optical microscope shows, based on the colour contrast with respect to the substrate, that the flake is thick and composed of multiple segments. Most of the characteristics of the flake's shape and structure can be reproduced in the mapping experiment by monitoring, for instance, the intensity of the scattered laser line at the consecutive spatial positions. Such faithful reproduction of the flake's geometry allows us to quite accurately establish a relation between spots in the map and particular places visible in the optical image with precision determined by the size of the laser spot. The centres emitting narrow spectral lines appear also in exfoliated flakes, as seen in the spectra originating from spots P1-P3 indicated in the image and in the map. Generally, the spectra are overall similar to the ones obtained for BN powder sample with the exception that the narrow lines overlap with a broad background of significant intensity, which constitutes a disadvantage for further optical studies. The origin of the background signal is most likely related to the bulk luminescence. Even though it predominantly resides in the UV region, its tails may reach into visible spectral range as well. The observation of narrow lines emitting centres in exfoliated hBN flakes provides a solid argument in favour of the hypothesis, that their origin is related to defects in BN material. However, due to superior quality of the spectra obtained for BN powder samples, they were used in all the proceeding investigations.

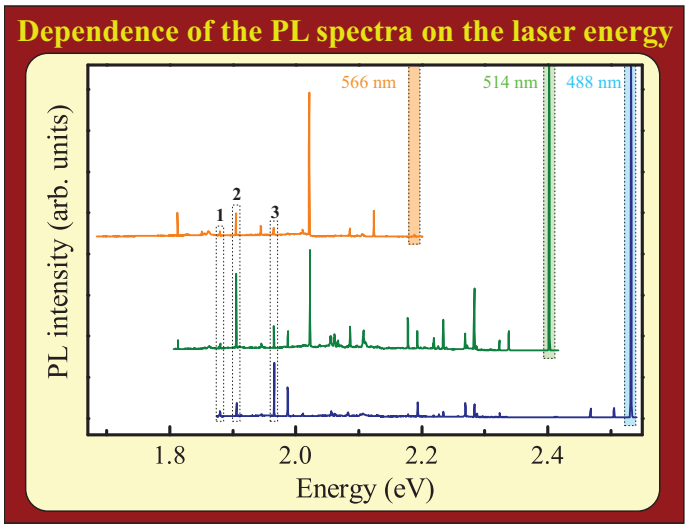

Figure A-2: **The influence of the laser energy on the photoluminescence spectra are studied for a selected emitter in BN powder sample. The three spectra are obtained for excitation with Ar^+ laser lines (488 nm and 514 nm) and with a rhodamine dye laser set at 566 nm. The three highlighted lines exhibit different behavior when changing the excitation energy. The intensity of line nr 1 remains constant, the line nr 2 has an apparent maximum for intermediate excitation and the line nr 3 progressively disappears when the laser energy approaches the emission energy.**

As a first step towards the characterization of the optical properties of the emitting centres in BN, we examine the dependence of their optical spectra on the energy of the laser excitation. In Figure A-2 three spectra for the same location are presented, obtained under the

excitation of 488 nm and 514 nm argon laser lines and 566 nm rhodamine dye laser line with a comparable excitation power of about 0.5 mW. An evident influence of the excitation energy on the intensity of individual lines can be observed. Multiple lines are seen in all three spectra at exactly the same energy, which provides a direct evidence that they appear indeed due to photoluminescence and not a Raman scattering process. Some of the lines clearly exhibit markings of a resonant character, for instance the most robust line in the spectrum for 566 nm excitation is barely visible in the spectrum for 488 nm excitation. Besides that, particular lines can demonstrate various dependence on the excitation energy. The intensity of the line marked as 1 is roughly constant for all three excitations. The line number 2 has an apparent maximum of intensity for the intermediate excitation. At the same time the intensity of line number 3 progressively decreases when the excitation energy approaches the emission energy. Such diversified behaviour of the emitting states must signify a complex energetic structure of the associated defects, which should be studied systematically and in details. Some preliminary attempts to unveil the energetic landscape and the nature of the light-matter coupling for the emitting centres in BN are discussed here through the analysis of the excitation spectra combined with the inspection of polarisation properties.

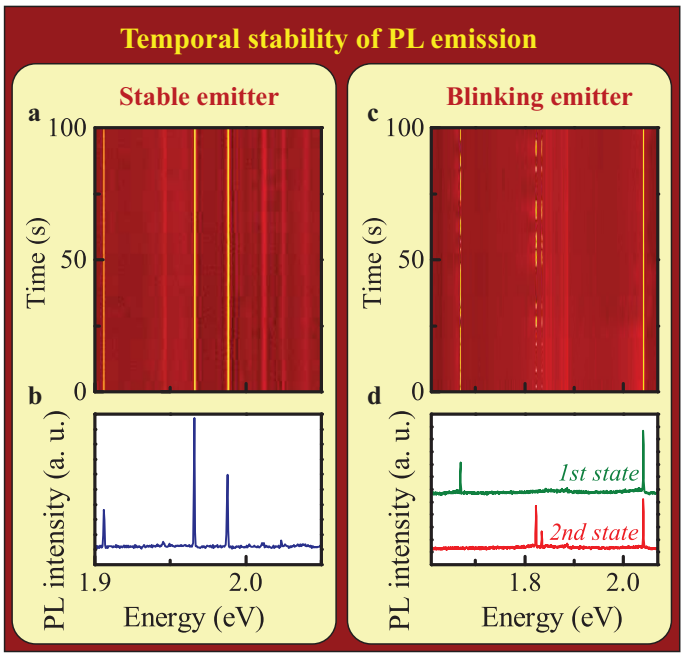

Figure A-3: **The stability of photoluminescence signal is investigated by consecutively recording the PL spectra, one after the other. (a) The temporal evolution in form of a colour map of (b) a spectrum for a selected emitting centre in BN powder shows the existence of emitters with perfect stability regarding the intensity and emission energy. In some rare cases, the emitting centres randomly fluctuate in time between two well-defined states as seen in (c) a temporal evolution of the PL spectrum of another emitter in BN powder. Here, the highest energy line remains stable while the three lower energy lines apparently originate from two metastable states illustrated by (d) two spectra taken at different moments in time.**

From the point of view of more advanced spectroscopic experiments, as well as potential utility of the emitting centres in BN, the matter of their stability plays a fundamentally important role. Also in this aspect, the BN emitters provide a ground for further exploration. A vast majority of them give rise to narrow lines, which exhibit a perfect stability in temporal domain.

That statement is valid for short sub-second timescale, in which no trace of telegraphic noise of the emission lines is observed, as well as longer periods of several hours, when no deterioration of the optical signal occurs during the long-time experiments. A temporal evolution of a spectrum recorded for such a stable emitter is shown in left panel of Figure A-3. However, a small number of emitting centres exhibit peculiar blinking effects, occurring in the timescale of seconds or even tens of seconds. In such a case one can distinguish two states of the emitter, which clearly cannot coexist at the same time. An example of an emitter exhibiting this kind of blinking is presented in the right panel of Figure A-3. Similar effects in other systems, like semiconductor quantum dots, are usually related to the charge fluctuations, however they typically occur at much shorter timescales. The investigation of the switchable centres may allow the identification of charged states as well as grant an insight into the dynamics of local variation of the electric field in the vicinity of the emitting centres, which may prove a valuable asset in uncovering their characteristics through more subtle spectroscopic tools, such as charge noise spectroscopy.

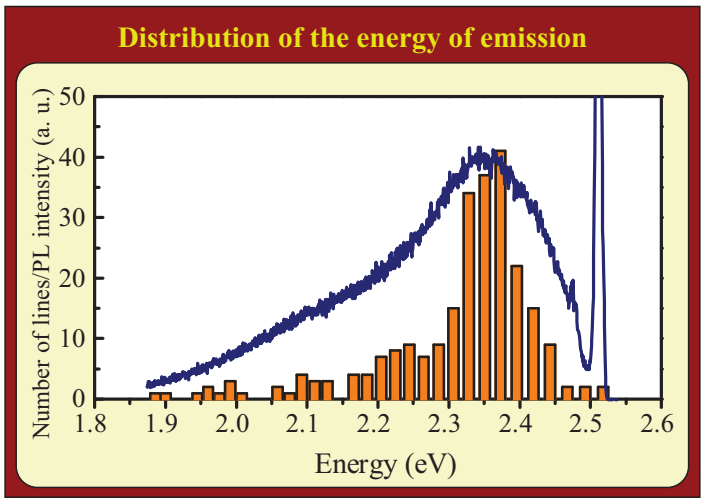

Figure A-4: **The statistical data presenting the number of emission lines at different energy values in BN powder samples, obtained by analysing the spectra of about 80 emitters, shows a clear maximum at about 2.35 eV. The distribution of the occurrence of the narrow lines can be confronted with a spectrum showing a different kind of optical response seen in BN powder samples. It consists of a single broad feature and appears in almost identical form at multiple places in BN powder samples. An apparent correspondence exists between the broad band emission spectrum and the emission energy distribution of individual emitting centres.**

To conclude the initial characterisation of the emitters in BN it is noteworthy to mention, that the narrow spectral lines are not the only optical response observed in BN powder samples. At multiple spots, also broad features appear at the energy covering similar region as the emission in form of narrow lines. In order to provide a more quantitative measure of comparison, the statistics of the appearance of the narrow lines at particular energy for about 80 emitting centres has been investigated. The results in form of a histogram are presented in Figure A-4. On top of the statistical data, a spectrum is presented showing an example of a broad feature, one of the most commonly found in the BN powder samples. The observed correspondence

may serve as a motivation to consider a hypothesis, that apart from rare individual emitting centres also ensembles of them, which give rise to broad emission bands exist in our samples.

A.3. Characterisation of resonances by the photoluminescence excitation and polarisation resolved experiments

A viable option to deepen the insight into the interaction between the emitting centres in BN and light is the investigation of the excitation spectra. In the approach presented here, the intensity of individual lines is monitored, when the laser energy is continuously tuned through the available spectral range, from 560 nm to 610 nm, offered by a rhodamine dye laser. The representative results of the photoluminescence excitation (PLE) measurements for a selected spot on a BN powder sample can be seen in Figure A-5.

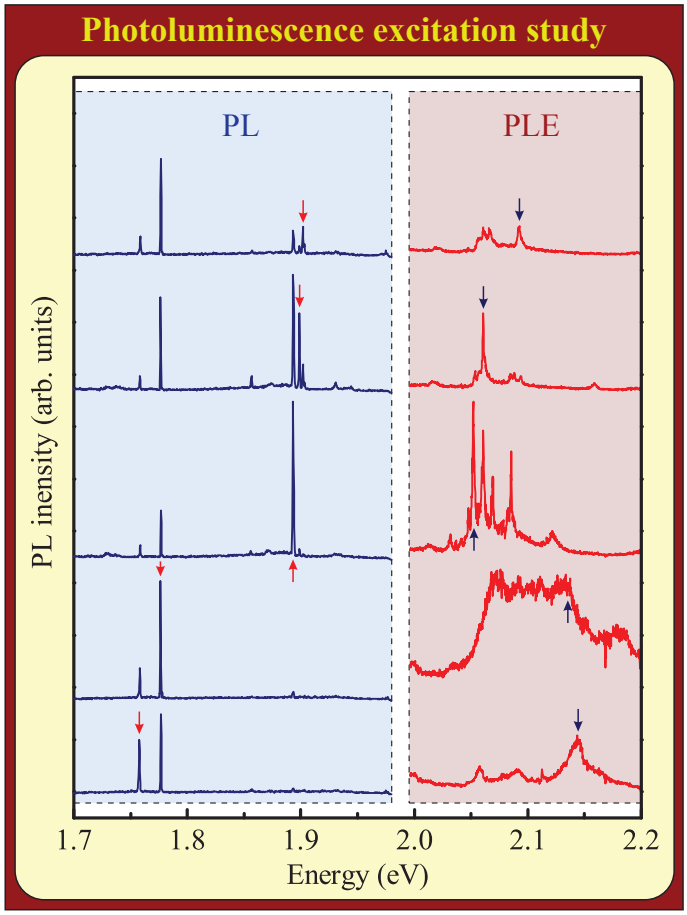

Figure A-5: **The PL spectra obtained for a selected emitting centre in BN powder for different laser energies (blue curves) are confronted with the excitation spectra (red curves), measured with a tunable rhodamine dye laser, to unveil a different character of the emission lines. Here, each of the excitation spectra was obtained for an individual line marked on the adjacent PL spectrum by the red arrow. Complementarily, each of the PL spectra was obtained for the laser energy marked by the blue arrow on the adjacent excitation spectrum.**

The photoluminescence (PL) spectrum here is composed mainly of five lines in the presented energy range and the PLE spectra are shown for each of them. An immediate observation is that the character of the excitation spectra may be qualitatively different for particular lines. The lower energy doublet, two PL lines between 1.75 and 1.8 eV, arises apparently due to non-resonant states, in the sense that the intensity of this pair of lines remains significant through the full excitation energy range. On top of that, both of them exhibit a certain type of resonant response. In the PLE spectrum of the lower energy line one can distinguish several rather weak and broad resonances while for the more robust, higher energy line a kind

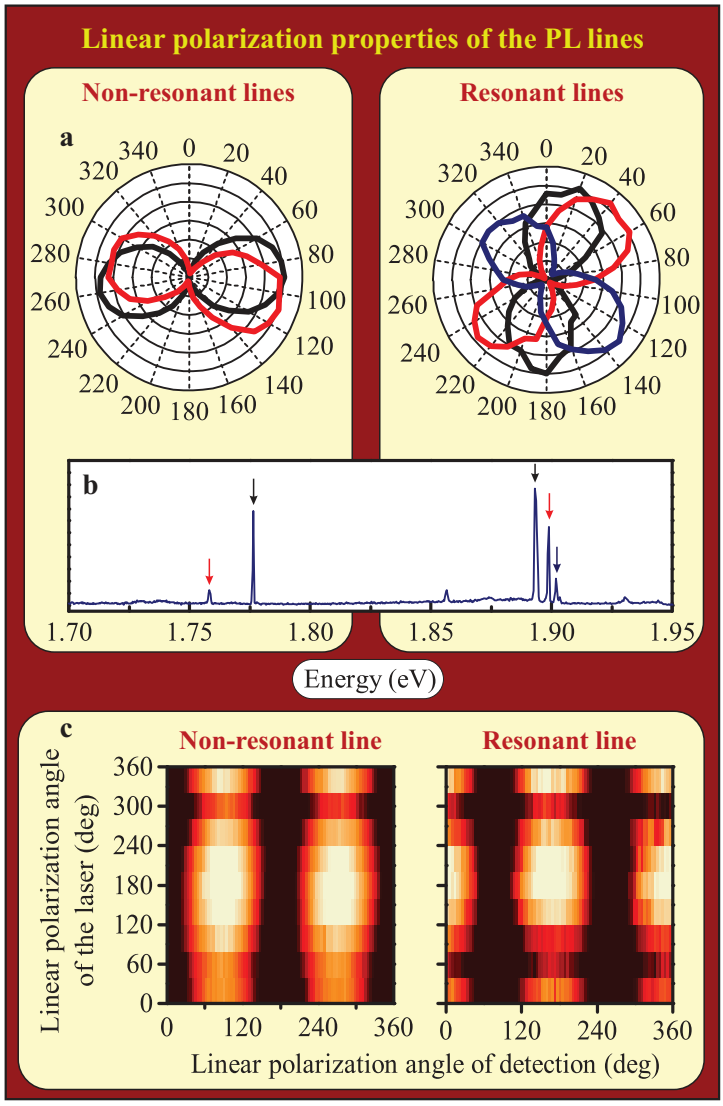

Figure A-6: **The narrow lines originating from emitting centres in BN are usually completely linearly polarized. (a) The polar plots demonstrate the dependence of the intensity of the PL lines on the angle of the linear polarisation in detection for lines recognised as non-resonant and resonant (based on the PLE measurements). Particular curves appearing in the polar plots correspond to the lines marked with arrows in (b) the PL spectrum based on a colour code (independently for lower energy non-resonant and higher energy resonant lines). Each line has its own distinct axis of polarisation, most clearly seen when inspecting the polarisation properties of the emission signal. However, the BN powder emitters also exhibit sensitivity to the polarisation properties of the laser used for their excitation. To illustrate that, one line from the 'non-resonant' doublet and 'resonant' triplet was selected (both lines are marked separately by black arrows in the PL spectrum) and (c) colour maps of the intensity of the lines were plotted as a function of the linear polarisation angle of the laser (vertical axis) and the detected PL signal (horizontal axis).**

of an extensive band appears in the excitation spectrum, similar to one commonly seen in the presence of a continuum of excited states. On the other hand, the triplet of lines, seen around 1.9 eV, reveals strictly resonant characteristics. For these three lines, narrow resonances appear with the linewidth comparable to the one of the PL lines, a feature most clearly pronounced for the lowest energy line of the triplet. Outside of the resonant energies, all three lines almost completely vanish from the PL spectrum, which enables to a certain degree a selective and independent excitation of these emission lines.

In order to complete the characterization of the intrinsic properties of the emitting centres in BN we analyse their polarisation properties measured for the same spot, which served as the example to present the PLE studies. By taking advantage of the familiarity of the PL spectrum we demonstrate the polarisation data in Figure A-6 separately for resonant and non-resonant

emission lines (simply for clarity as no substantial differences arise from this distinction). All five emission lines appearing in the PL spectrum are completely linearly polarised, each line along its own intrinsic axis. First of all, this signifies, that the linear polarisation of these lines originates from the internal properties of the emitting states, determined probably by some kind of anisotropy, rather than inherited from the linear polarisation of the exciting laser light. At this point, there is no particular proof that all the lines seen in the spectrum originate from the same emitter, though it is reasonable to assume that it is so. If that is the case, the linear polarisation data presented here may serve as an indication of the presence of fine structure splitting, as, for instance, the two highest energy lines of the resonant triplet are polarized perpendicularly to each other and the splitting beteen them is rather small ($\sim$3.2 meV).

The emission spectra of the narrow line emitting centres in BN reveal also a sensitivity to the direction of the linear polarisation of the laser used for excitation. Clearly the absorption of light by the emitter can be tuned by rotating the linear polarisation axis of the laser, as seen in Figure A-6c, in which the intensity of a selected resonant and non-resonant line is presented as a function of the linear polarisation angle for both excitation and detection as a colour plot. This finding, combined with the results of the PLE study, shows that there exist at least two possible ways of distinguishing individual emitters from ensembles, which exploit the excitation selectivity related to the laser polarisation and energy.

A.4. Influence of external conditions: temperature end magnetic field dependence

We proceed with the discussion of the dependence (or lack thereof) of the optical properties of the emitting centres in BN powder on varying external conditions such as temperature and a magnetic field. In Figure A-7a the evolution of the PL spectrum is presented in a temperature range from 10 - 296 K. The intensity, emission energy and linewidth is analysed for a selected line at $\sim$1.998 eV and the results are presented in Figure A-7b. The influence of temperature on the properties of PL lines is pretty standard for localized emitting centres in solids. The intensity is quenched, the emission energy is red-shifted and the lines are broadened at higher temperature. Apart from this typical evolution of individual narrow lines, an appearance of an additional feature becomes apparent, when the temperature of the sample exceeds about 200 K. A broad band suddenly emerges covering completely the visible spectral region where the narrow lines are found. The intensity of this background signal grows drastically with further increase of the temperature. The presence of a similar feature is commonly observed for

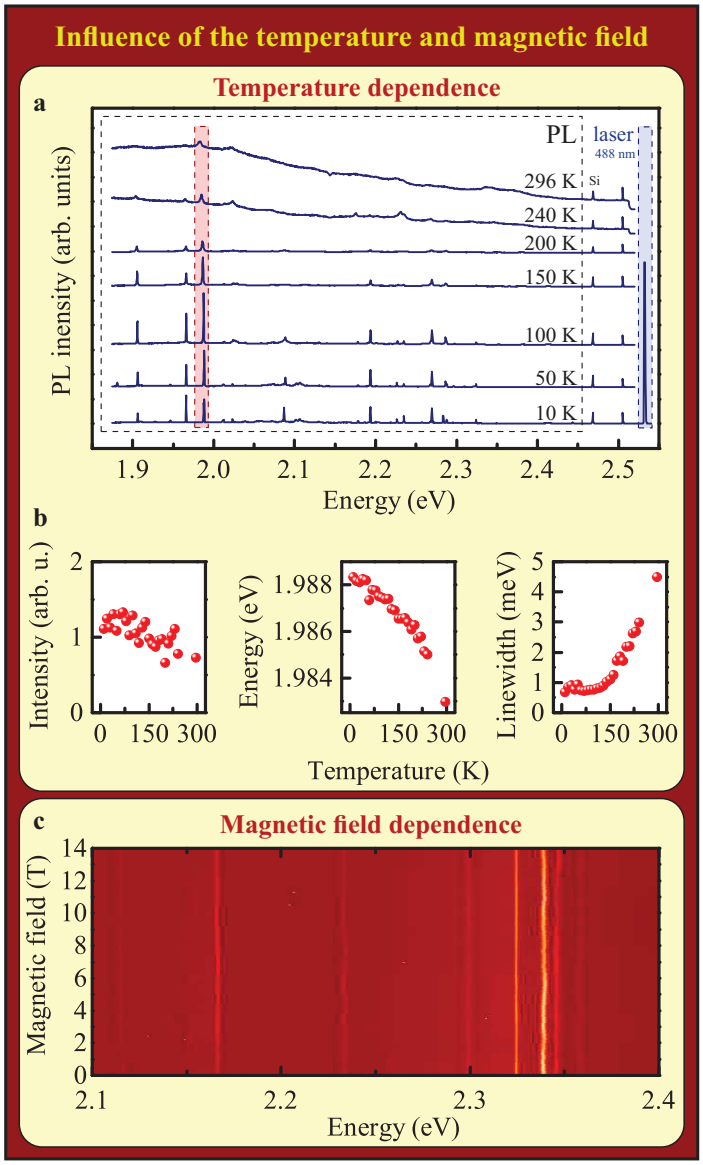

Figure A-7: **The investigation of the influence of external conditions, such as temperature or magnetic field, is a standard way to learn about the properties of light emitters in solids. Firstly, we present the PL spectra for a selected emitting centre in BN as a function of temperature. A feature commonly appearing in defect centres in wide gap materials and present here as well is a broad band emission which gains in intensity with the increase of the temperature. Even though a presence of such spectrally broad background hinders the observation and analysis of individual lines, in some cases it is possible to trace the evolution of a particular line from helium up to room temperature, which we do here for the line at 1.988 eV (at low temperature) which is highlighted in the spectrum. For this line we present the dependence of its (b) intensity, emission energy and linewidth. (c) The measurements of the magnetic field dependence, performed on multiple randomly selected emitting spots, have proven so far that the emitting centres in BN are completely insensitive to the application of a magnetic field in the investigated field regime (up to 14 T).**

various colour centres in wide gap materials. It is attributed to the phonon assisted transitions which accompany the zero-phonon line. However, this may not be the case for emitters in BN powder. Firstly, the broad band does not appear at all at low temperatures, which would imply that phonons responsible for its emergence become involved at temperatures as high as 200 K, which is unlikely. Taking into account the fact, that the intensity of the background emission grows in time, when exposing the emitter with laser excitation for extended periods of time at a set temperature, we currently consider the possibility that it comes from damaging the crystal due to heating it with the laser of a significant power.

The results of the magneto-optical studies are much more puzzling, because the emitters in BN powder (as well as exfoliated hBN crystals) appear to be completely insensitive to the application of a magnetic field in the range up to 14 T. The results of measurements for a

selected emitter in BN powder sample are presented in Figure A-7. No signature of a field-induced splitting is observed for any of the lines nor a noticeable impact of the field on their intensity. This property is common for all measured emitting centres. Any possible explanations of this observation currently remain highly speculative. Nonetheless, we would like to point out two simple concepts leading to the disappearance of Zeeman effects for optical transitions. The basic ideas behind them are presented schematically in Figure A-8. The first scenario is based on a coupling between electrons. Let us imagine that the resonances seen in our experiments are related to optical transitions between vacuum and many body states. If the involved electrons would form antiferromagnetically coupled pairs, then the energy of the electronic states could be magnetic field independent. In such scenario one can expect an appearance of higher energy triplet state, which in the simplest case of two electrons with 1/2 spin splits into three components. A feasible route to verify this hypothesis is extension of the magneto-optical studies to higher fields in search for, e. g. anti-crossings induced by a potential transformation of the ground electronic state from singlet into triplet configuration. An alternative idea simply takes into consideration a Zeeman splitting of individual electronic states of exactly the same magnitude, what leads to the compensation of the magnetic field splitting for the optical transitions. If the optical selection rules would favour the transitions exclusively between the two higher and the two lower branches of the relevant electronic states, then the resonances seen in the optical spectra could be insensitive to the magnetic field.

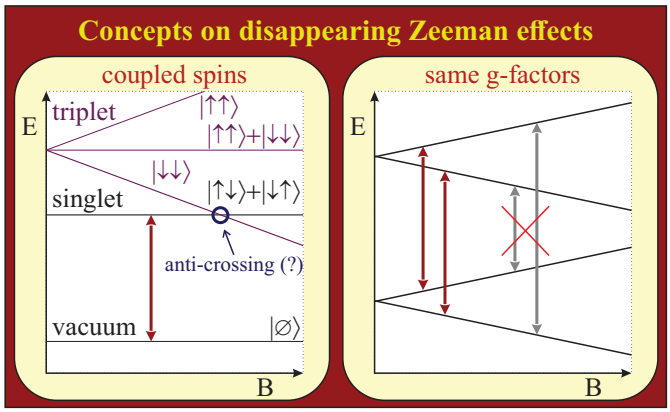

Figure A-8: **A pictorial representation of two simple cases of electronic states, which could lead to complete disappearance of the Zeeman effects for optical transitions. The first possibility is based on transition between two magnetic-field-independent states, e. g. from a vaccum state to a singlet state of two coupled electrons. This scenario is shown in the left panel of the figure, in which a presence of a higher energy triplet state is marked as well. Effects of coupling between singlet and triplet states could be revealed at higher magnetic fields. A second sceniario is demonstrated in the right panel. It considers a simple case, when the same value of the Zeeman splitting of two electronic states, combined with proper selection rules, leads to field independent optical transitions.**

A.5. Photon correlation study - single photon emission from helium to room temperature

The photon correlation functions measured for single, well isolated PL lines from defect centres in BN clearly confirm their single photon emission character. A robust anti-bunching is seen, which reveals its characteristic time to reside in tens of nanoseconds timescale. This value constitutes the upper limit for the PL decay time and is comparable with other single photon emitters in solids. Another feature, which is observed in the correlation functions in longer timescales (of the order of microseconds) is a bunching with unusually large amplitude. That is a peculiar trait of the NLECs in BN crystals of currently unknown origin. A bunching in a correlation function may appears due to charge fluctuations, which induce small variations in the energy of the electronic states relevant for the optical transitions. Alternatively, a bunching may also arise in multilevel systems, where the transitions between particular states are accounted for by rate equation models. We believe the latter explanation is more likely to be valid for NLECs in BN, based on the decent stability of their PL lines and the typical multiline optical response. The photon correlation measurements were done in broad temperature range from helium up to room temperature. The experimental correlation functions, presented in Figure A-9(a), were described by the same formula which was used for NLECs in WSe_2 structures:

$$g_2(\tau) = 1 - A_1 * \exp\left(-\left|\frac{\tau}{t_1}\right|\right) + A_2 * \exp\left(-\left|\frac{\tau}{t_2}\right|\right) \tag{A.1}$$

where t_1 is an exponential temporal constant characterising the antibunching, t_2 is an exponential temporal constant characterising the long timescale bunching, A_1 is the antibunching depth and A_2 is the bunching amplitude. The temperature dependence of the particular parameters is presented in Figure A-9(b). The quality of single photon emission of NLECs in BN is exceptionally good. It may be represented by the renormalised value of the correlation function at zero time delay: $g_2(0) \rightarrow g_2(0)/(1+A_2) = (1-A_1+A_2)/(1+A_2)$. The renormalisation is necessary to preserve the interpretation of the value of the $g_2(0)$ parameter as the probability of emitting more than one photon in the presence of a bunching of significant amplitude. The excellent quality of the NLECs in BN is seen in the low value of the renormalised $g_2(0)$, especially at low temperature (roughly below 200 K) when it does not exceed 5 %. At higher temperatures the value of the renormalised $g_2(0)$ increases significantly due to the emergence

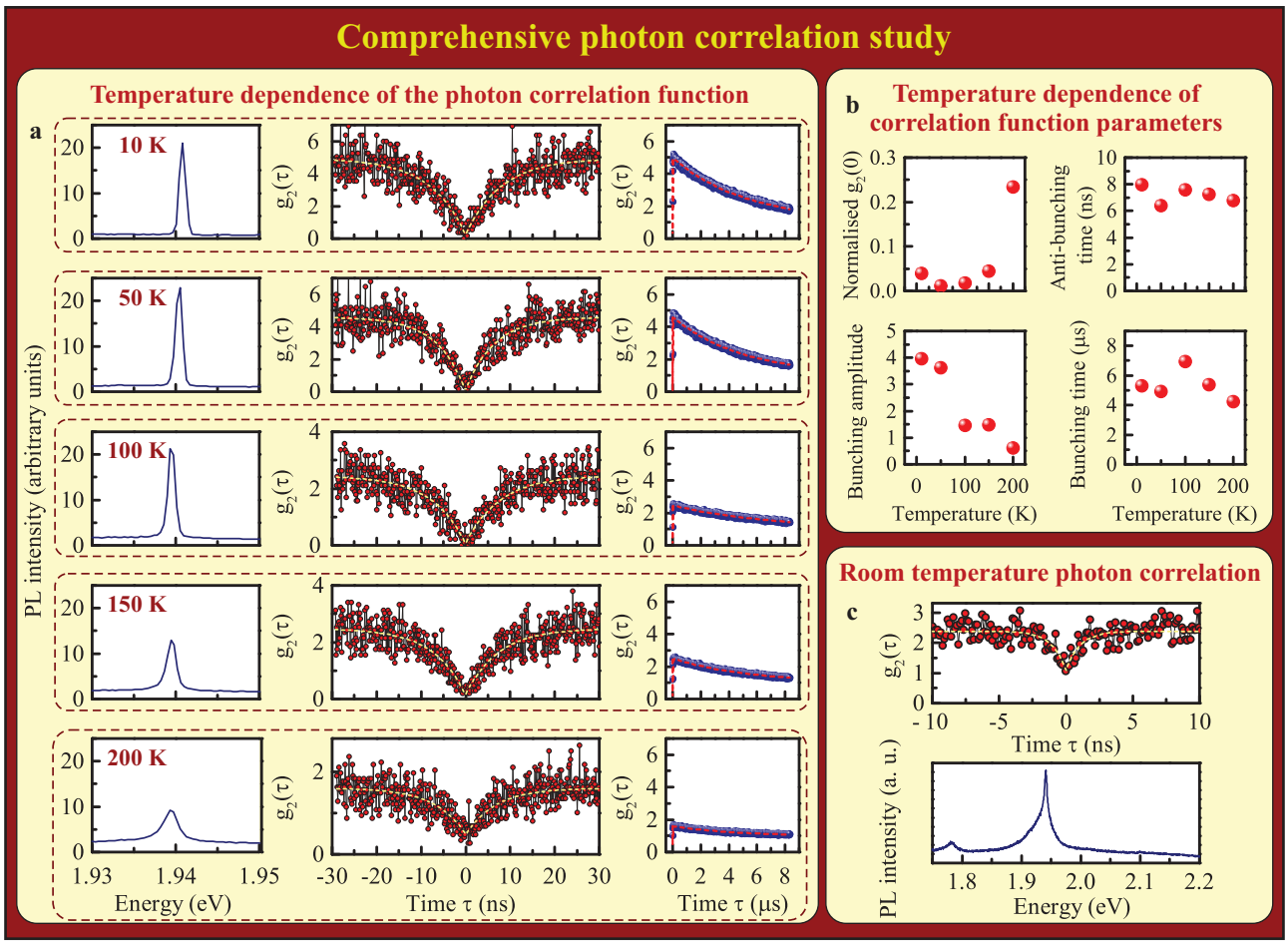

Figure A-9: **The study of photon correlations in a broad temperature range shows that NLECs in BN are remarkably good quality single photon sources. Firstly, for a single location we present (a) the temperature dependence in sub-room-temperature range (10 - 200 K) of the PL spectrum showing a selected PL line, then photon correlation function measured for this line in short timescale (tens of nanoseconds) illustrating the presence of the anti-bunching and photon correlations in long timescale (tens of microseconds) revealing an appearance of a robust bunching. For a different location (b) the photon correlation function and the PL spectrum at room temperature is shown. It is noteworthy to point out, that in order to reproduce ambient conditions of operation, the helium flow was stopped and the sample was left to termalize to the actual temperature of the environment. Finally, (c) the basic parameters describing the short timescale anti-bunching and long timescale bunching, namely their amplitude and characteristic time, are presented as a function of temperature for the data presented in (a).**

of the spectrally broad background signal. It is important to stress that this observation does not necessarily imply the deterioration of the single photon emission capabilities of NLECs in BN at higher temperature. It simply signifies that the appearing background signal does not come entirely from the same transition which at low temperature appears in form of a narrow, well isolated line. An example of such a situation could be a temperature activated emergence of huge phonon sidebands, which would accompany each individual narrow line. Their merging into a singly extensive PL band could definitely limit the possibility of detecting signal exclu-

sively from an individual optical transition. Nevertheless, the progress in understanding the origin and properties of NLECs in BN may point out the ways to better isolate the luminescence coming from individual PL lines at higher temperatures and restore the almost perfect character of single photon emission even up to room temperature.

Another parameter which is evidently sensitive to the variation of the temperature is the amplitude of the bunching. It noticeable diminishes by about five times when increasing the temperature from 10 to 200 K, but given the uncertain origin of the bunching feature this observation is difficult to interpret. We would just state a remark, which follows the multi-state rate equation system scenario, that the rise of the temperature may substantially increase the ratio between the non-radative and radiative processes. Therefore the dynamics of the population and depopulation of the emitting states can be expected to be highly sensitive to temperature. The two remaining parameters, i. e. characteristic temporal constants related to the antibunching and the bunching appear to be practically independent on the temperature.

Finally, the photon correlation was measured at room temperature for a NLEC in BN at a new location to demonstrate the possibility of room temperature operation. The $g_2(\tau)$ function and the PL spectrum showing the correlated emission line is presented in Figure A-9c. These data demonstrates that in spite of the high temperature background one can still observe single photon emission from NLECs in BN in ambient conditions. The value of the renormalised $g_2(0)$ was found to be 0.46, which satisfies the generally acknowledged criterion for a single photon source ($g_2(0) < 0.5$) .

A.6. Concluding remarks

The number of experiments described and interpreted here provide a comprehensive characterisation of the optical properties of NLECs in BN. Our current understanding is that these appealing emitters originate from the optical transitions between discrete electronic states located deep in the bandgap, which emerge due to structural defects. The observation of a unique set of lines, which appear at different energies at each particular location in our samples, suggests that these defects take various forms. They may be related to boron and/or nitride vacancies, presence of additional atoms at inter-atomic sites of the lattice or combinations of both. Such defects could also induce local distortion of the lattice manifesting itself as translation or rotation of the positions of the closest atoms.

The question about the exact origin of the NLECs in BN is also connected with the puzzling

observation of the emission from single defects under excitation with relatively large micrometer sized laser beam. It is counter-intuitive that among millions of illuminated atoms every so often single emitting defects are found. Our current impression, based on the statistical analysis of the distribution of the emission energy of the PL lines from multiple NLECs and appearance of broad emission bands at some locations, is that the density of such emitting defects is highly inhomogeneous. As we have speculated, the broader structures may arise due to the optical response of the ensembles of NLECs. A possible explanation of the observation of single, isolated centres may also be related, perhaps partially, to the existence of strict optical selection rules required to effectively excite the transitions within particular defects. Our preliminary study of NLECs in BN indicate that at least two conditions may apply for some transitions. One of them was discovered in the PLE measurements, where a resonant character of some PL lines was revealed. Certain lines were disappearing completely when the laser energy was tuned out of very specific, well defined values. A second property, which allows some degree of selectivity in excitation of different transitions, was uncovered in linear polarisation resolved measurements. The efficiency of the light emission from NLECs in BN was found to be highly sensitive to the direction of the linear polarisation of the laser implying that absorption is polarisation dependent. Each PL line exhibited its own directions of polarisation axes corresponding to the maximum and the minimum of the absorption. Therefore, combining these two features, one can imagine that in typically used excitation conditions with set wavelength and direction of linear polarisation of the laser, most of the NLECs give practically none PL response.

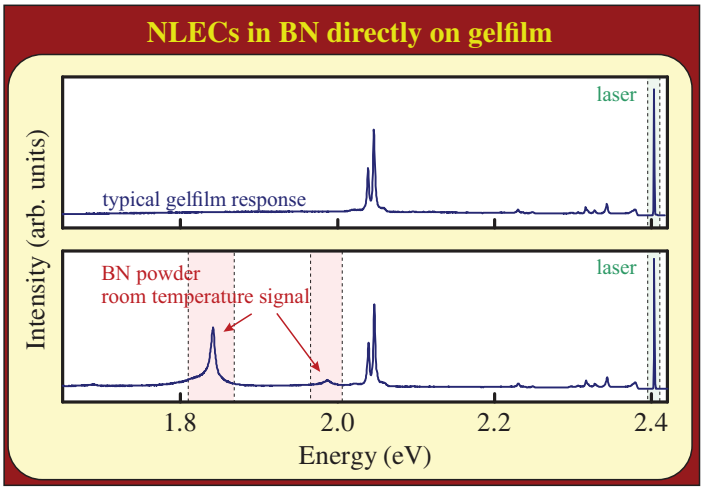

Figure A-10: **The typical optical response of an elastometric stamp (an elastic, transparent film of gel-like consistency) under Argon laser line 514 nm excitation is presented in the top graph. BN powder has been distributed over a piece of such film (attached afterwards on a glass slide) resulting in the observation of the optical signature of NLECs at ambient conditions on specific spacial locations as demonstrated in the bottom graph. The NLECs can be found on the film in a similar manner as on the Si/SiO_2 substrates covered with BN powder, by scanning its surface with micrometre-sized laser beam.**

In terms of perspectives, NLECs in BN are expected to become a blooming field of research

due to their basic traits uncovered so far. Bringing up an analogy with the development of NLECs in sc-TMDs structures, one can note that the possibility of electrical pumping is an obvious next step towards realising the awaiting technological challenges. However, new directions also emerge, which lead to unexplored, as of yet, routes. For instance, the presence of NLECs in powder form of BN at room temperature ensures that the design of future structures is not limited to conventional substrates. One may think of more versatile media on which BN powder could be deposited. Figure A-10 shows an optical response of a NLEC in BN residing on a piece of an elastometric stamp commonly used in exfoliation techniques. Such preliminary results validate the feasibility of realising completely new ideas, such as single photon emitters on transparent and elastic supports.

Summary

The content of this thesis was built around rather simple experimental observations regarding optical investigations of thin films of semiconducting transition metal dichalcogenides (sc-TMD) materials. The interest in the properties of such type of structures has raised quite recently. It can be seen as a direct follow-up of the extremely successful graphene research, however the results of preliminary studies have already brought up the unexpected and appealing findings, which stimulate the broad efforts focused on investigation of a large class of layered structures. The currently conducted research on atomically thin layers of materials other than graphite, given its early stages, remains at the very basic level. Consequently, our understanding of the electronic properties of such systems constantly evolves, as more and more experimental observations are reported, accompanied by the attempts to confront them with theoretical concepts. However, quite often new findings bring up more puzzles than actual answers to the recurring questions **[147]**.

Here, we have presented a systematic study of the optical response of exfoliated sc-TMD structures based on the measurements of photoluminescene and reflectivity spectra. In **Chapter 1**, the general characterisation of sc-TMD layers is discussed, including the investigation of the impact of the number of layers and temperature on the excitonic resonances observed in the optical spectra. The presented data are interpreted in terms of the evolution of the band structure with the thickness of the flakes, accompanied by the modifications of the Coulomb interaction. The variation of the energy of the resonances and their corresponding linewidth increase induced by the rise of the temperature in absorption-type experiments is accounted for by standard formalism developed for traditional semiconductors, which is based on coupling mechanisms between electrons and phonons. On the other hand, the temperature dependence of the photoluminescence spectra reveal quite surprising features, which differentiate various materials belonging to sc-TMD family. In this work, $MoSe_2$ and WSe_2 monolayers are compared, for which the luminescence spectra at low temperature are strikingly different. The

enhancement of the emission intensity characteristic of WSe_2 material at higher temperature contrasts strongly with conventional quenching of intensity observed in $MoSe_2$ material. This observation has been interpreted as a consequence of two types of spin alignment in the conduction sub-bands. This finding signifies, that the excitonic states visible in the luminescence spectra of WSe_2 and $MoSe_2$ monolayers are formed from electrons occupying different conduction states. Consequently, the optically active excitons in $MoSe_2$ material may be considered as the ground state of the system. On the other hand, the radiately recombining excitons in WSe_2 material are composed of electrons locked on the higher energy conduction states, therefore in this case there exist lower energy optically inactive dark states. This distinction was used to classify the sc-TMD materials into 'bright' and 'darkish' families.

In **Chapter 2** the characterisation is extended to include the analysis of Zeeman effects. A simple empirical model is developed to describe the linear with magnetic field terms, which shift the individual electronic states in the fundamental sub-bands. Eventually, three contributions were considered, which account for spin, orbital and valley-type effects. The magnitude of the corresponding parameters was estimated in multiple ways, e. g. by the analysis of the polarisation degree of the charged exciton resonance in the absorption-type investigations. This enabled the evaluation of the g-factor of an individual electronic state in the conduction band. In terms of photoluminescence studies, the $MoSe_2$ monolayers exhibit conventional behaviour. The values of the g-factors mimic the ones seen in the reflectivity measurements. On the other hand, WSe_2 monolayers reveal again surprising traits. The lower energy emission lines, forming the band of 'localised/bound' excitons, show extremely large Zeeman splittings. We have speculated that this feature is related to optical transitions involving dark exciton states.

Finally, the appearance of narrow lines emitting centres (NLECs) in exfoliated WSe_2 structures at low temperatures was discussed in **Chapter 3**. A comprehensive analysis of their properties was presented. This included the comparison of the excitation spectra of the NLECs and the 2D-like response of monolayers, the temperature and magnetic field evolution of the NLECs' emission lines and their polarisation properties. The measurements of photon correlations revealed the single photon emission character of NLECs. It is still not clear what is the exact origin of NLECs, nonetheless some possibilities were considered. They were partially based of scanning tunnelling microscope (STM) studies, which uncovered the presence of nano-sized monolayers at the perimeter of an exfoliated WSe_2 flake.

A similar characterisation for NLECs found in another representative of the class of two

dimensional materials - boron nitride (BN) - was presented in **Appendix A**. It this case the emission in form of narrow lines comes most probably from structural defects in a similar manner as in other wide gap materials such as diamond or silicon carbide. These NLECs were also found to be single photon sources, however in this case the capabilities of light emission are sustained up to room temperature. Therefore, they appear to be quite appealing objects from the point of view of their potential functionalities. Apart from that, NLECs in BN revealed a multitude of optical properties, which may be helpful in learning what kind of defects they actually are. Their emission strength turned out to be highly sensitive to the polarisation and energy of the laser used for excitation. Thus, the strict selection rules may also be relevant for the explanation of the surprisingly small spatial density of the emitting defects.

List of publications

The Author of this thesis has co-authored the following articles during the period of his PhD studies (October 2012 - May 2016).

List of publications related to this work:

- A. Arora, M. Koperski, K. Nogajewski, J. Marcus, C. Faugeras, M. Potemski, **Excitonic resonances in thin films of WSe_2: from monolayer to bulk material.**, Nanoscale **7**, 10421-10429 (2015).

- A. Arora, K. Nogajewski, M. Molas, M. Koperski, M. Potemski, **Exciton band structure in layered $MoSe_2$: from a monolayer to the bulk limit.**, Nanoscale **7**, 20769-20775 (2015).

- M. Koperski, K. Nogajewski, A. Arora, V. Cherkez, P. Mallet, J.-Y. Veuillen, J. Marcus, P. Kossacki, M. Potemski, **Single photon emitters in exfoliated WSe_2 structures.**, Nature Nanotechnology **10**, 503-506 (2015).

- T. Smoleński, M. Goryca, M. Koperski, C. Faugeras, T. Kazimierczuk, A. Bogucki, K. Nogajewski, P. Kossacki, M. Potemski, **Tuning Valley Polarization in a WSe_2 Monolayer with a Tiny Magnetic Field.**, Phys. Rev. X **6**, 021024 (2016).

- T. Jakubczyk, V. Delmonte, M. Koperski, K. Nogajewski, C. Faugeras, W. Langbein, M. Potemski, J. Kasprzak, **Radiatively Limited Dephasing and Exciton Dynamics in $MoSe_2$ Monolayers Revealed with Four-Wave Mixing Microscopy.**, Nano Lett. **16 (9)**, 5333-5339 (2016).

- M. Koperski, M. R. Molas, A. Arora, K. Nogajewski, A. O. Slobodeniuk, C. Faugeras, M. Potemski, **Optical properties of atomically thin transition metal dichalcogenides: Observations and puzzles.** arXiv:1612.05879 (2016). *(review paper to be published in Nanophotonics)*

List of publications on other topics:

- A. H. Trojnar, M. Korkusinski, U. C. Mendes, M. Goryca, M. Koperski, T. Smolenski, P. Kossacki, P. Wojnar, P. Hawrylak, **Fine structure of a biexciton in a single quantum dot with a magnetic impurity.**, Phys. Rev. B **87**, 205311 (2013).

- M. Koperski, M. Goryca, T. Kazimierczuk, T. Smoleński, A. Golnik, P. Wojnar, P. Kossacki, **Introducing single Mn^{2+} ions into spontaneously coupled quantum dot pairs.**, Phys. Rev. B **89**, 075311 (2014).

- M. Goryca, M. Koperski, P. Wojnar, T. Smoleński, T. Kazimierczuk, A. Golnik, P. Kossacki, **Coherent Precession of an Individual 5/2 Spin.** Phys. Rev. Lett. **113**, 227202 (2014).

- J. Kobak, T. Smoleński, M. Goryca, M. Papaj, K. Gietka, A. Bogucki, M. Koperski, J.-G. Rousset, J. Suffczyński, E. Janik, M. Nawrocki, A. Golnik, P. Kossacki, W. Pacuski, **Designing quantum dots for solotronics.**, Nature Communications **5**, 3191 (2014).

- M. Goryca, M. Koperski, T. Smoleński, Ł. Cywiński, P. Wojnar, P. Plochocka, M. Potemski, P. Kossacki, **Spin-lattice relaxation of an individual Mn^{2+} ion in a CdTe/ZnTe quantum dot.**, Phys. Rev. B **92**, 045412 (2015).

- T. Smoleński, M. Koperski, M. Goryca, P. Wojnar, P. Kossacki, T. Kazimierczuk, **Optical study of a doubly negatively charged exciton in a CdTe/ZnTe quantum dot containing a single Mn^{2+} ion.**, Phys. Rev. B **92**, 085415 (2015).

- M. Koperski, T. Smoleński, M. Goryca, P. Wojnar, M. Potemski, P. Kossacki, **Magnetic-field-induced abrupt spin-state transition in a quantum dot containing magnetic ions.**, Phys. Rev. B **94**, 245439 (2016).

- J. Kobak, A. Bogucki, T. Smoleńnski, M. Papaj, M. Koperski, M. Potemski, P. Kossacki, A. Golnik, W. Pacuski, **Direct determination of zero-field splitting for single Co^{2+} ion embedded in a CdTe/ZnTe quantum dot.**, arXiv:1610.05732 (2016).

Bibliography

[1] K. S. Novoselov, D. Jiang, F. Schedin, T. J. Booth, V. V. Khotkevich, S. V. Morozov, A. K. Geim, **Two-dimensional atomic crystals.** Proc. Natl. Acad. Sci. U.S.A. **102**, 10451 (2005).

[2] W. Jaegermann, C. Pettenkofer, B. A. Parkinson, **Cu and Ag deposition on layered p-type WSe_2: Approaching the Schottky limit.**, Phys. Rev. B **42**, 7487 (1990).

[3] R. Schlaf, A. Klein, C. Pettenkofer, W. Jaegermann, **Laterally inhomogeneous surface-potential distribution and photovoltage at clustered In/WSe_2 (0001) interfaces.**, Phys. Rev. B **48**, 14242 (1993).

[4] F. Rose, M. O. Goerbig, and F. Piéchon, **Spin- and valley-dependent magneto-optical properties of MoS_2.**, Phys. Rev. B **88**, 125438 (2013).

[5] J. S. Bunch, A. M. van der Zande, S. S. Verbridge, I. W. Frank, D. M. Tanenbaum, J. M. Parpia, H. G. Craighead, P. L. McEuen, **Electromechanical Resonators from Graphene Sheets.**, Science **315**, 490 (2007).

[6] N. Morell, A. Reserbat-Plantey, I. Tsioutsios, K. G. Schädler, F. Dubin, F. H. L. Koppens, A. Bachtold, **High Quality Factor Mechanical Resonators Based on WSe_2 Monolayers.**, Nano Lett. **16 (8)**, 5102 (2016).

[7] M. Chhowalla, H. S. Shin, G. Eda, L.-J. Li, K. P. Loh, H. Zhang, **The chemistry of two-dimensional layered transition metal dichalcogenide nanosheets.**, Nature Chemistry **5**, 263-275 (2013).

[8] D. Voiry, A. Goswami, R. Kappera, C. C. C. e Silva, D. Kaplan, T. Fujita, M. Chen, T. Asefa, M. Chhowalla, **Covalent functionalization of monolayered transition metal dichalcogenides by phase engineering.**, Nature Chemistry **7**, 45-49 (2015).

[9] G. Li, A. Luican, E. Y. Andrei, **Scanning Tunneling Spectroscopy of Graphene on Graphite**, Phys. Rev. Lett. **102**, 176804 (2009).

[10] J. H. Park, S. Vishwanath, X. Liu, H. Zhou, S. M. Eichfeld, S. K. Fullerton-Shirey, J. A. Robinson, R. M. Feenstra, J. Furdyna, D. Jena, H. G. Xing, A. C. Kummel, **Scanning Tunneling Microscopy and Spectroscopy of Air Exposure Effects on Molecular Beam Epitaxy Grown WSe_2 Monolayers and Bilayers.**, ACS Nano, **10 (4)**, 4258-4267 (2016).

[11] W. Yao, D. Xiao, Q. Niu, **Valley-dependent optoelectronics from inversion symmetry breaking.**, Phys. Rev. B **77**, 235406 (2008).

[12] Z. Y. Zhu, Y. C. Cheng, U. Schwingenschlögl, **Giant spin-orbit-induced spin splitting in two-dimensional transition-metal dichalcogenide semiconductors.**, Phys. Rev. B **84**, 153402 (2011).

[13] A. Molina-Sánchez, D. Sangalli, K. Hummer, A. Marini, L. Wirtz, **Effect of spin-orbit interaction on the optical spectra of single-layer, double-layer, and bulk MoS_2.**, Phys. Rev. B **88**, 045412 (2013).

[14] K. Kośmider, J. W. González, J. Fernández-Rossier, **Large spin splitting in the conduction band of transition metal dichalcogenide monolayers.**, Phys. Rev. B **88**, 245436 (2013).

[15] G. Wang, C. Robert, A. Suslu, B. Chen, S. Yang, S. Alamdari, I. C. Gerber, T. Amand, X. Marie, S. Tongay, B. Urbaszek, **Spin-orbit engineering in transition metal dichalcogenide alloy monolayers.**, Nature Communications **6**, 10110 (2015).

[16] A. Castellanos-Gomez, M. Buscema, R. Molenaar, V. Singh, L. Janssen, H. S. J. van der Zant, G. A. Steele, **Deterministic transfer of two-dimensional materials by all-dry viscoelastic stamping**, 2D Mater. **1**, 011002 (2014).

[17] M. Amani, D.-H. Lien, D. Kiriya, J. Xiao, A. Azcatl, J. Noh, S. R. Madhvapathy, R. Addou, S. KC, M. Dubey, K. Cho, R. M. Wallace, S.-C. Lee, J.-H. He, J. W. Ager III X. Zhang, E. Yablonovitch, A. Javey, **Near-unity photoluminescence quantum yield in MoS_2**, Science **350**, 1065-1068 (2015).

[18] D. W. Latzke, W. Zhang, A. Suslu, T.-R. Chang, H. Lin, H.-T. Jeng, S. Tongay, J. Wu, A. Bansil, A. Lanzara, **Electronic structure, spin-orbit coupling, and interlayer interaction in bulk MoS_2 and WS_2**, Phys. Rev. B **91**, 235202 (2015).

[19] M. M. Ugeda, A. J. Bradley, S.-F. Shi, F. H. da Jornada, Y. Zhang, D. Y. Qiu, W. Ruan, S.-K. Mo, Z. Hussain, Z.-X. Shen, F. Wang, S. G. Louie, M. F. Crommie, **Giant bandgap renormalization and excitonic effects in a monolayer transition metal dichalcogenide semiconductor.**, Nature Materials **13**, 1091 (2014).

[20] A. Chernikov, T. C. Berkelbach, H. M. Hill, A. Rigosi, Y. Li, O. B. Aslan, D. R. Reichman, M. S. Hybertsen, T. F. Heinz, **Exciton Binding Energy and Nonhydrogenic Rydberg Series in Monolayer WS_2**, Phys. Rev. Lett. **113**, 076802 (2014).

[21] K. He, N. Kumar, L. Zhao, Z. Wang, K. F. Mak, H. Zhao, J. Shan, **Tightly Bound Excitons in Monolayer WSe_2.**, Phys. Rev. Lett. **113**, 026803 (2014).

[22] H. M. Hill, A. F. Rigosi, C. Roquelet, A. Chernikov, T. C. Berkelbach, D. R. Reichman, M. S. Hybertsen, L. E. Brus, T. F. Heinz, **Observation of Excitonic Rydberg States in Monolayer MoS_2 and WS_2 by Photoluminescence Excitation Spectroscopy.**, Nano Lett. **15 (5)**, 2992 (2015).

[23] D. Y. Qiu, F. H. da Jornada, S. G. Louie, **Optical Spectrum of MoS_2: Many-Body Effects and Diversity of Exciton States.**, Phys. Rev. Lett. **111**, 216805 (2013).

[24] A. J. Bradley, M. M. Ugeda, F. H. da Jornada, D. Y. Q, W. Ruan, Y. Zhang, S. Wickenburg, A. Riss, J. Lu, S.-K. Mo, Z. Hussain, Z.-X. Shen, S. G. Louie, M. F. Crommie, **Probing the Role of Interlayer Coupling and Coulomb Interactions on Electronic Structure in Few-Layer $MoSe_2$ Nanostructures**, Nano Lett. **15 (4)**, 2594 (2015).

[25] B. Zhu, X. Chen, X. Cuia, **Exciton Binding Energy of Monolayer WS_2.**, Sci Rep. **5**, 9218 (2015).

[26] A. Chernikov, A. M. van der Zande, H. M. Hill, A. F. Rigosi, A. Velauthapillai, J. Hone, T. F. Heinz, **Electrical Tuning of Exciton Binding Energies in Monolayer WS_2.**, Phys. Rev. Lett. **115**, 126802 (2015).

[27] D. Y. Qiu, F. H. da Jornada, S. G. Louie, **Screening and many-body effects in two-dimensional crystals: Monolayer MoS_2.**, Phys. Rev. B **93**, 235435 (2016).

[28] A. Ramasubramaniam, **Large excitonic effects in monolayers of molybdenum and tungsten dichalcogenides**, Phys. Rev. B **86**, 115409 (2012).

[29] K. F. Mak, C. Lee, J. Hone, J. Shan, T. F. Heinz, **Atomically Thin MoS_2: A New Direct-Gap Semiconductor.** Phys. Rev. Lett. **105**, 136805 (2010).

[30] A. Splendiani, L. Sun, Y. Zhang, T. Li, J. Kim, C.-Y. Chim, G. Galli, F. Wang, **Emerging Photoluminescence in Monolayer MoS_2.**, Nano Lett. **10 (4)**, 1271 (2010).

[31] P. Tonndorf, R. Schmidt, P. Böttger, X. Zhang, J. Börner, A. Liebig, M. Albrecht, C. Kloc, O. Gordan, D. R. T. Zahn, S. M. de Vasconcellos, R. Bratschitsch, **Photoluminescence emission and Raman response of monolayer MoS_2, $MoSe_2$, and WSe_2**, Optics Express **21**, 4908 (2013).

[32] W. Zhao, Z. Ghorannevis, L. Chu, M. Toh, C. Kloc, P.-H. Tan, G. Eda, **Evolution of Electronic Structure in Atomically Thin Sheets of WS_2 and WSe_2**, ACS Nano, **7 (1)**,791 (2013).

[33] C. Ruppert, O. B. Aslan, T. F. Heinz, **Optical Properties and Band Gap of Single- and Few-Layer $MoTe_2$ Crystals.**, Nano Lett. **14 (11)**, 6231 (2014).

[34] I. G. Lezama, A. Arora, A. Ubaldini, C. Barreteau, E. Giannini, M. Potemski, A. F. Morpurgo, **Indirect-to-Direct Band Gap Crossover in Few-Layer $MoTe_2$.** Nano Lett. **15 (4)**, 2336 (2015).

[35] J. A. Wilson, A. D. Yoffe, **The transition metal dichalcogenides discussion and interpretation of the observed optical, electrical and structural properties.** Adv. Phys. **18**, 193 (1969).

[36] R. Coehoorn, C. Haas, J. Dijkstra, C. J. F. Flipse, R. A. de Groot, A. Wold, **Electronic structure of $MoSe_2$, MoS_2, and WSe_2. I. Band-structure calculations and photoelectron spectroscopy.**, Phys. Rev. B **35**, 6195 (1987).

[37] R. Coehoorn, C. Haas, R. A. de Groot, **Electronic structure of $MoSe_2$, MoS_2, WSe_2. II. The nature of the optical band gaps.**, Phys. Rev. B **35**, 6203 (1987).

[38] A. Kormányos, G. Burkard, M. Gmitra, J. Fabian, V. Zólyomi, N. D. Drummond, V. Fal'ko, **k·p theory for two-dimensional transition metal dichalcogenide semiconductors.**, 2D Materials **2**, 022001 (2015).

[39] H. Rostami, A. G. Moghaddam, R. Asgari, **Effective lattice Hamiltonian for monolayer MoS_2: Tailoring electronic structure with perpendicular electric and magnetic fields.**, Phys. Rev. B **88**, 085440 (2013).

[40] F. Zahid, L. Liu, Y. Zhu, J. Wang, H. Guo, **A generic tight-binding model for monolayer, bilayer and bulk MoS_2**, AIP Advances **3**, 052111 (2013).

[41] G.-B. Liu, W.-Y. Shan, Y. Yao, W. Yao, D. Xiao, **Three-band tight-binding model for monolayers of group-VIB transition metal dichalcogenides.**, Phys. Rev. B **88**, 085433 (2013).

[42] E. Cappelluti, R. Roldán, J. A. Silva-Guillén, P. Ordejón, F. Guinea, **Tight-binding model and direct-gap/indirect-gap transition in single-layer and multilayer MoS_2.**, Phys. Rev. B **88**, 075409 (2013).

[43] R. Roldán, M. P. López-Sancho, F. Guinea, E. Cappelluti, J. A. Silva-Guillén, P. Ordejón, **Momentum dependence of spin-orbit interaction effects in single-layer and multi-layer transition metal dichalcogenides.**, 2D Materials **1**, 034003 (2014).

[44] T. Cheiwchanchamnangij, W. R. L. Lambrecht, **Quasiparticle band structure calculation of monolayer, bilayer, and bulk MoS_2**, Phys. Rev. B **85**, 205302 (2012).

[45] A. Kuc, N. Zibouche, T. Heine, **Influence of quantum confinement on the electronic structure of the transition metal sulfide TS_2.**, Phys Rev B **83**, 245213 (2011).

[46] H. Terrones, F. López-Urías, M. Terrones, **Novel hetero-layered materials with tunable direct band gaps by sandwiching different metal disulfides and diselenides.**, Scientific Reports **3**, 1549 (2013).

[47] G.-B. Liu, D. Xiao, Y. Yao, X. Xude, W. Yao, **Electronic structures and theoretical modelling of two-dimensional group-VIB transition metal dichalcogenides.**, Chem. Soc. Rev. **44**, 2643 (2015).

[48] Y. Zhang, T.-R. Chang, B. Zhou, Y.-T. Cui, H. Yan, Z. Liu, F. Schmitt, J. Lee, R. Moore, Y. Chen, H. Lin, H.-T. Jeng, S.-K. Mo, Z. Hussain, A. Bansil, Z.-X. Shen, **Direct observation of the transition from indirect to direct bandgap in atomically thin epitaxial $MoSe_2$.**, Nature Nanotechnology **9**, 111 (2014).

[49] W. Zhao, R. M. Ribeiro, M. Toh, A. Carvalho, C. Kloc, A. H. Castro Neto, G. Eda, **Origin of Indirect Optical Transitions in Few-Layer MoS_2, WS_2, WSe_2.**, Nano Lett. **13 (11)**, 5627 (2013).

[50] M. Manca, M. M. Glazov, C. Robert, F. Cadiz, T. Taniguchi, K. Watanabe, E. Courtade, T. Amand, P. Renucci, X. Marie, G. Wang, B. Urbaszek, **Enabling valley selective exciton scattering in monolayer WSe_2 through upconversion.**, arXiv:1701.05800 (2017).

[51] W. Y. Liang, **Optical anisotropy in layer compounds.**, J. Phys. C: Solid State Phys. **6**, 551 (1973).

[52] A. R. Beal, W. Y. Liang, **Excitons in 2H-WSe_2 and 3R-WS_2.**, J. Phys. C: Solid St. Phys. **9**, 2459 (1976).

[53] A. R. Beal, H. P. Hughes, **Kramers-Kronig analysis of the reflectivity spectra of 2H-MoS_2, 2H-$MoSe_2$ and 2H-$MoTe_2$.**, J. Phys. C: Solid State Phys. **12**, 881 (1979).

[54] H. Peelaers, C. G. Van de Walle, **Effects of strain on band structure and effective masses in MoS_2.**, Phys. Rev. B **86**, 241401(R) (2012).

[55] A. R. Beal, J. C Knights, W. Y. Liang, **Transmission spectra of some transition metal dichalcogenides. II. Group VIA: trigonal prismatic coordination.**, J. Phys. C: Solid State Phys. **5**, 3540 (1972).

[56] K. P. O'Donnell, X. Chen, **Temperature Dependence of Semiconductor Band Gaps.**, Appl. Phys. Lett. **58**, 2924 (1991).

[57] S. Rudin, T. L. Reinecke, B. Segall, **Temperature-Dependent Exciton Linewidths in Semiconductors.**, Phys. Rev. B **42**, 11218 (1990).

[58] G. Wang, L. Bouet, D. Lagarde, M. Vidal, A. Balocchi, T. Amand, X. Marie, B. Urbaszek, **Valley dynamics probed through charged and neutral exciton emission in monolayer WSe_2**, Phys. Rev. B **90**, 075413 (2014).

[59] C. R. Zhu, K. Zhang, M. Glazov, B. Urbaszek, T. Amand, Z. W. Ji, B. L. Liu, X. Marie, **Exciton valley dynamics probed by Kerr rotation in WSe_2 monolayers.**, Phys. Rev. B **90**, 161302(R) (2014).

[60] C. Robert, D. Lagarde, F. Cadiz, G. Wang, B. Lassagne, T. Amand, A. Balocchi, P. Renucci, S. Tongay, B. Urbaszek, X. Marie, **Exciton radiative lifetime in transition metal dichalcogenide monolayers.**, Phys. Rev. B **93**, 205423 (2016).

[61] A. Arora, M. Koperski, K. Nogajewski , J. Marcus, C Faugeras, M. Potemski, **Excitonic resonances in thin films of WSe_2: from monolayer to bulk material.**, Nanoscale **7**,10421 (2015).

[62] A. Arora, K. Nogajewski, M. Molas, M. Koperski, M. Potemski, **Exciton band structure in layered $MoSe_2$: from a monolayer to the bulk limit.** Nanoscale **7**, 20769 (2015).

[63] X.-X. Zhang, Y. You, S. Y. F. Zhao, T. F. Heinz, **Experimental Evidence for Dark Excitons in Monolayer WSe_2.**, Phys. Rev. Lett. **115**, 257403 (2015).

[64] P. Kossacki, J. Cibert, D. Ferrand, Y. Merle d'Aubigné, A. Arnoult, A. Wasiela, S. Tatarenko, J. A. Gaj, **Neutral and positively charged excitons: A magneto-optical study of a p-doped $Cd_{1-x}Mn_xTe$ quantum well.**, Phys. Rev. B **60**, 16018 (1999).

[65] V. Ciulin, P. Kossacki, S. Haacke, J.-D. Ganiére, B. Deveaud, A. Esser, M. Kutrowski, T. Wojtowicz, **Radiative behavior of negatively charged excitons in CdTe-based quantum wells: A spectral and temporal analysis.**, Phys. Rev. B **62**, R16310(R) (2000).

[66] P. Kossacki, **Optical studies of charged excitons in II-VI semiconductor quantum wells.**, Journal of Physics: Condensed Matter **15 (13)**, R471 (2003).

[67] Y. Li, J. Ludwig, T. Low, A. Chernikov, X. Cui, G. Arefe, Y. D. Kim, A. M. van der Zande, A. Rigosi, H. M. Hill, S. H. Kim, J. Hone, Z. Li, D. Smirnov, T. F. Heinz, **Valley Splitting and Polarization by the Zeeman Effect in Monolayer $MoSe_2$.**, Phys. Rev. Lett. **113**, 266804 (2014).

[68] G. Aivazian, Z. Gong, A. M. Jones, R.-L. Chu, J. Yan, D. G. Mandrus, C. Zhang, D. Cobden, W. Yao, X. Xu, **Magnetic control of valley pseudospin in monolayer WSe_2.**, Nature Physics **11**, 148 (2015).

[69] D. MacNeill, C. Heikes, K. F. Mak, Z. Anderson, A. Kormányos, V. Zólyomi, J. Park, D. C. Ralph, **Breaking of Valley Degeneracy by Magnetic Field in Monolayer $MoSe_2$.**, Phys. Rev. Lett. **114**, 037401 (2015).

[70] G. Wang, L. Bouet, M. M. Glazov, T. Amand, E. L. Ivchenko, E. Palleau, X. Marie, B. Urbaszek, **Magneto-optics in transition metal diselenide monolayers.**, 2D Materials **2**, 034002 (2015).

[71] A. Srivastava, M. Sidler, A. V. Allain, D. S. Lembke, A. Kis, A. Imamoglu, **Valley Zeeman effect in elementary optical excitations of monolayer WSe_2.**, Nature Physics **11**, 141-147 (2015).

[72] A. Kormányos, V. Zólyomi, N. D. Drummond, G. Burkard, **Spin-Orbit Coupling, Quantum Dots, and Qubits in Monolayer Transition Metal Dichalcogenides**, Phys. Rev. X **4**, 011034 (2014).

[73] D. V. Rybkovskiy, I. C. Gerber, M. V. Durnev, **Atomically inspired k·p approach and valley Zeeman effect in transition metal dichalcogenide monolayers**, arXiv:1610.02695 (2016).

[74] A. V. Stier, K. M. McCreary, B. T. Jonker, J. Kono, S. A. Crooker, **Exciton diamagnetic shifts and valley Zeeman effects in monolayer WS_2 and MoS_2 to 65 Tesla**, Nat. Commun. **7**, 10643 (2016).

[75] A. A. Mitioglu, P. Plochocka, Á. Granados del Aguila, P. C. M. Christianen, G. Deligeorgis, S. Anghel, L. Kulyuk, D. K. Maude, **Optical Investigation of Monolayer and Bulk Tungsten Diselenide (WSe_2) in High Magnetic Fields** Nano Lett. **15**, 4387 (2015).

[76] A. A. Mitioglu, K. Galkowski, A. Surrente, L. Klopotowski, D. Dumcenco, A. Kis, D. K. Maude, P. Plochocka, **Magnetoexcitons in large area CVD-grown monolayer MoS_2 and $MoSe_2$ on sapphire**, Phys. Rev. B **93**, 165412 (2016).

[77] A. Arora, R. Schmidt, R. Schneider, M. R. Molas, I. Breslavetz, M. Potemski, R. Bratschitsch, **Valley Zeeman Splitting and Valley Polarization of Neutral and Charged Excitons in Monolayer $MoTe_2$ at High Magnetic Fields**, Nano Lett. **16**, 3624 (2016).

[78] B. Fallahazad, H. C. P. Movva, K. Kim, S. Larentis, T. Taniguchi, K. Watanabe, S. K. Banerjee, E. Tutuc, **Shubnikov-de Haas Oscillations of High-Mobility Holes in Monolayer and Bilayer WSe_2: Landau Level Degeneracy, Effective Mass, and Negative Compressibility.**, Phys. Rev. Lett. **116**, 086601 (2016).

[79] F. Meier, B. P. Zakharchenya (eds.), **Optical orientation: modern problems in condensed matter sciences.** Vol. **8**. Elsevier Science (1984).

[80] K. F. Mak, K. He, J. Shan, T. F. Heinz, **Control of valley polarization in monolayer MoS_2 by optical helicity.**, Nature Nanotechnology **7**, 494-498 (2012).

[81] T Cao, G. Wang, W. Han, H. Ye, C. Zhu, J. Shi, Q. Niu, P. Tan, E. Wang, B. Liu, J. Feng, **Valley-selective circular dichroism of monolayer molybdenum disulphide.**, Nature Communications **3**, 887 (2012).

[82] H. Zeng, J. Dai, W. Yao, D. Xiao, X. Cui, **Valley polarization in MoS_2 monolayers by optical pumping.**, Nature Nanotechnology **7**, 490-493 (2012).

[83] A. M. Jones, H. Yu, N. J. Ghimire, S. Wu, G. Aivazian, J. S. Ross, B. Zhao, J. Yan, D. G. Mandrus, D. Xiao, W. Yao, X. Xu, **Optical generation of excitonic valley coherence in monolayer WSe_2.**, Nature Nanotechnology **8**, 634-638 (2013).

[84] T. Smoleński, M. Goryca, M. Koperski, C. Faugeras, T. Kazimierczuk, A. Bogucki, K. Nogajewski, P. Kossacki, M. Potemski, **Tuning Valley Polarization in a WSe_2 Monolayer with a Tiny Magnetic Field**, Phys. Rev. X **6**, 021024 (2016).

[85] M. M. Glazov, T. Amand, X. Marie, D. Lagarde, L. Bouet, B. Urbaszek, **Exciton fine structure and spin decoherence in monolayers of transition metal dichalcogenides.**, Phys. Rev. B **89**, 201302(R) (2014).

[86] T. Yu, M. W. Wu, **Valley depolarization due to intervalley and intravalley electron-hole exchange interactions in monolayer MoS_2.**, Phys. Rev. B **89**, 205303 (2014).

[87] H. Dery, Y. Song, **Polarization analysis of excitons in monolayer and bilayer transition-metal dichalcogenides.**, Phys. Rev. B **92**, 125431 (2015).

[88] T. Yan, X. Qiao, P. Tan, X. Zhang, **Valley depolarization in monolayer WSe_2.**, Scientific Reports **5**, 15625 (2015).

[89] M. M. Glazov, E. L. Ivchenko, G. Wang, T. Amand, X. Marie, B. Urbaszek, B. L. Liu, **Spin and valley dynamics of excitons in transition metal dichalcogenide monolayers.**, Phys. Status Solidi B **252**, 2349 (2015).

[90] A. O. Slobodeniuk, D. M. Basko, **Spin-flip processes and radiative decay of dark intravalley excitons in transition metal dichalcogenide monolayers.**, 2D Materials **3**, 035009 (2016).

[91] C. W. Snyder, B. G. Orr, D. Kessler, L. M. Sander, **Effect of strain on surface morphology in highly strained InGaAs film**, Phys. Rev. Lett. **66**, 3032 (1991).

[92] J. -Y. Marzin, J. -M. Gérard, A. Izraël, D. Barrier, G. Bastard, **Photoluminescence of Single InAs Quantum Dots Obtained by Self-Organized Growth on GaAs**, Phys. Rev. Lett. **73**, 716 (1994).

[93] A. Zrenner, L. V. Butov, M. Hagn, G. Abstreiter, G. Böhm, G. Weimann, **Quantum dots formed by interface fluctuations in AlAs/GaAs coupled quantum well structures**, Phys. Rev. Lett. **72**, 3382 (1994).

[94] D. Gammon, E. S. Snow, B. V. Shanabrook, D. S. Katzer, D. Park, **Fine Structure Splitting in the Optical Spectra of Single GaAs Quantum Dots**, Phys. Rev. Lett. **76**, 3005 (1996).

[95] M. Koperski, K. Nogajewski, A. Arora, V. Cherkez, P. Mallet, J.-Y. Veuillen, J. Marcus, P. Kossacki, M. Potemski, **Single photon emitters in exfoliated WSe_2 structures**, Nature Nanotechnology **10**, 503 (2015).

[96] A. Srivastava, M. Sidler, A. V. Allain, D. S. Lembke, A. Kis, A. Imamoğlu, **Optically active quantum dots in monolayer WSe_2**, Nature Nanotechnology **10**, 491 (2015).

[97] C. Chakraborty, L. Kinnischtzke, K. M. Goodfellow, R. Beams, A. N. Vamivakas, **Voltage-controlled quantum light from an atomically thin semiconductor**, Nature Nanotechnology **10**, 507 (2015).

[98] P. Tonndorf, R. Schmidt, R. Schneider, J. Kern, M. Buscema, G. A. Steele, A. Castellanos-Gomez, H. S. J. van der Zant, S. Michaelis de Vasconcellos, R. Bratschitsch, **Single-photon emission from localized excitons in an atomically thin semiconductor**, Optica **2**, 347 (2015).

[99] S. Kumar, A. Kaczmarczyk, B. D. Gerardot, **Strain-Induced Spatial and Spectral Isolation of Quantum Emitters in Mono- and Bilayer WSe_2**, Nano Lett. **15**, 7567 (2015).

[100] J. Kern, I. Niehues, P. Tonndorf, R. Schmidt, D. Wigger, R. Schneider, T. Stiehm, S. Michaelis de Vasconcellos, D. E. Reiter, T. Kuhn, R. Bratschitsch, **Nanoscale Positioning of Single-Photon Emitters in Atomically Thin WSe_2**, Adv. Mater. **28**, 7101, (2016).

[101] Y.-M. He, G. Clark, J. R. Schaibley, Y. He, M.-C. Chen, Y.-J. Wei, X. Ding, Q. Zhang, W. Yao, X. Xu, C.-Y. Lu, J.-W. Pan, **Single quantum emitters in monolayer semiconductors**, Nature Nanotechnology **10**, 497 (2015).

[102] A. Branny, G. Wang, S. Kumar, C. Robert, B. Lassagne, X. Marie, B. D. Gerardot, B. Urbaszek, **Discrete quantum dot like emitters in monolayer $MoSe_2$: Spatial mapping, magneto-optics, and charge tuning**, Appl. Phys. Lett. **108**, 142101 (2016).

[103] C. Palacios-Berraquero, M. Barbone, D. M. Kara, X. Chen, I. Goykhman, D. Yoon, A. K. Ott, J. Beitner, K. Watanabe, T. Taniguchi, A. C. Ferrari, M. Atatüre, **Atomically thin quantum light-emitting diodes**, Nature Communications **7**, 2978 (2016).

[104] G. Clark, J. R. Schaibley, J. Ross, T. Taniguchi, K. Watanabe, J. R. Hendrickson, S. Mou, W. Yao, X. Xu, **Single Defect Light-Emitting Diode in a van der Waals Heterostructure**, Nano Lett. **16**, 3944 (2016).

[105] S. Schwarz, A. Kozikov, F. Withers, J. K. Maguire, A. P. Foster, S. Dufferwiel, L. Hague, M. N. Makhonin, L. R. Wilson, A. K. Geim, K. S. Novoselov, A. I. Tartakovskii, **Electrically pumped single-defect light emitters in WSe_2**, 2D Materials **3**, 025038 (2016).

[106] W. Jaegermann, H. Tributsch, M. M. Benameur, **Interfacial properties of semiconducting transition metal chalcogenides**, Prog. Surf. Sci. **29**, 1 (1988).

[107] Y.-M. He, S. Höfling, C. Schneider, **Phonon induced line broadening and population of the dark exciton in a deeply trapped localized emitter in monolayer WSe_2**, Optics Express **24**, 8066 (2016).

[108] S. Kumar, M. Brotóns-Gisbert, R. Al-Khuzheyri, A. Branny, G. Ballesteros-Garcia, J. F. Sánchez-Royo, B. D. Gerardot, **Resonant laser spectroscopy of localized excitons in monolayer WSe_2**, Optica **3**, 882 (2016).

[109] L. Besombes, K. Kheng, L. Marsal, H. Mariette, **Acoustic phonon broadening mechanism in single quantum dot emission**, Phys. Rev. B **63**, 155307 (2007).

[110] R. S. Sundaram, M. Engel, A. Lombardo, R. Krupke, A. C. Ferrari, Ph. Avouris, M. Steiner, **Electroluminescence in Single Layer MoS_2.**, Nano Lett. **13 (4)**, 1416 (2013).

[111] J. S. Ross, P. Klement, A. M. Jones, N. J. Ghimire, J. Yan, D. G. Mandrus, T. Taniguchi, K. Watanabe, K. Kitamura, W. Yao, D. H. Cobden, X. Xu, **Electrically tunable excitonic light-emitting diodes based on monolayer WSe_2 p-n junctions**, Nature Nanotechnology **9**, 268 (2014).

[112] F. Withers, O. Del Pozo-Zamudio, A. Mishchenko, A. P. Rooney, A. Gholinia, K. Watanabe, T. Taniguchi, S. J. Haigh, A. K. Geim, A. I. Tartakovskii, K. S. Novoselov, **Light-emitting diodes by band-structure engineering in van der Waals heterostructures**, Nature Materials **14**, 301 (2015).

[113] F. Withers, O. Del Pozo-Zamudio, S. Schwarz, S. Dufferwiel, P. M. Walker, T. Godde, A. P. Rooney, A. Gholinia, C. R. Woods, P. Blake, S. J. Haigh, K. Watanabe, T. Taniguchi, I. L. Aleiner, A. K. Geim, V. I. Fal'ko, A. I. Tartakovskii, K. S. Novoselov, **WSe_2 Light-Emitting Tunneling Transistors with Enhanced Brightness at Room Temperature.**, Nano Lett. **15 (12)**, 8223 (2015).

[114] Y.-M. He, O. Iff, N. Lundt, V. Baumann, M. Davanco, K. Srinivasan, S. Höfling, C. Schneider, **Cascaded emission of single photons from the biexciton in monolayered WSe_2**, Nature Communications **7**, 13409 (2016).

[115] C. Palacios-Berraquero, D. M. Kara, A. R.-P. Montblanch, M. Barbone, P. Latawiec, D. Yoon, A. K. Ott, M. Loncar, A. C. Ferrari, M. Atatüre, **Large-scale quantum-emitter arrays in atomically thin semiconductors**, arXiv:1609.04244 (2016).

[116] A. Branny, S. Kumar, R. Proux, B. D. Gerardot, **Deterministic strain-induced arrays of quantum emitters in a two-dimensional semiconductor**, arXiv:1610.01406 (2016).

[117] C. R. Dean, A. F. Young, I. Meric, C. Lee, L. Wang, S. Sorgenfrei, K. Watanabe, T. Taniguchi, P. Kim, K. L. Shepard, J. Hone, **Boron nitride substrates for high-quality graphene electronics**, Nature Nanotechnology **5**, 722 (2010).

[118] J. Xue, J. Sanchez-Yamagishi, D. Bulmash, P. Jacquod, A. Deshpande, K. Watanabe, T. Taniguchi, P. Jarillo-Herrero, B. J. LeRoy, **Scanning tunnelling microscopy and spectroscopy of ultra-flat graphene on hexagonal boron nitride**, Nature Materials **10**, 282 (2011).

[119] M. Okada, T. Sawazaki, K. Watanabe, T. Taniguch, H. Hibino, H. Shinohara, R. Kitaura, **Direct Chemical Vapor Deposition Growth of WS_2 Atomic Layers on Hexagonal Boron Nitride**, ACS Nano **8**, 8273 (2014).

[120] L. H. Li, E. J. G. Santos, T. Xing, E. Cappelluti, R. Roldán, Y. Chen, K. Watanabe, T. Taniguchi, **Dielectric Screening in Atomically Thin Boron Nitride Nanosheets**, Nano Lett. **15**, 218 (2015).

[121] C. Faugeras, S. Berciaud, P. Leszczynski, Y. Henni, K. Nogajewski, M. Orlita, T. Taniguchi, K. Watanabe, C. Forsythe, P. Kim, R. Jalil, A. K. Geim, D. M. Basko, M. Potemski, **Landau Level Spectroscopy of Electron-Electron Interactions in Graphene**, Phys. Rev. Lett. **114**, 126804 (2015).

[122] R. V. Gorbachev, I. Riaz, R. R. Nair, R. Jalil, L. Britnell, B. D. Belle, E. W. Hill, K. S. Novoselov, K. Watanabe, T. Taniguchi, A. K. Geim, P. Blake, **Hunting for Monolayer Boron Nitride: Optical and Raman Signatures**, Small **7**, 465 (2011).

[123] S. Larach, R. E. Shrader, **Multiband Luminescence in Boron Nitride**, Phys. Rev. **104**, 68 (1956).

[124] A. Zunger, A. Katzir, A. Halperin, **Optical properties of hexagonal boron nitride**, Phys. Rev. B **13**, 5560 (1976).

[125] C. A. Taylor, S. W. Brown, V. Subramaniam, S. Kidner, S. C. Rand, R. Clarke, **Observation of near-band-gap luminescence from boron nitride films**, Applied Physics Letters **65**, 1251 (1994).

[126] K. Watanabe, T. Taniguchi, H. Kanda, **Direct-bandgap properties and evidence for ultraviolet lasing of hexagonal boron nitride single crystal**, Nature Materials **3**, 404 (2004).

[127] D. A. Evans, A. G. McGlynn, B. M. Towlson, M. Gunn, D. Jones, T. E. Jenkins, R. Winter, N. R. J. Poolton, **Determination of the optical band-gap energy of cubic and hexagonal boron nitride using luminescence excitation spectroscopy**, J. Phys.: Condens. Matter **20**, 075233 (2008).

[128] L. Museur, A. Kanaev, **Near band-gap photoluminescence properties of hexagonal boron nitride**, Journal of Applied Physics **103**, 103520 (2008).

[129] A. Pierret, J. Loayza, B. Berini, A. Betz, B. Plaçais, F. Ducastelle, J. Barjon, A. Loiseau, **Excitonic recombinations in h-BN: From bulk to exfoliated layers**, Phys. Rev. B **89**, 035414 (2014).

[130] G. Cassabois, P. Valvin, B. Gil, **Hexagonal boron nitride is an indirect bandgap semiconductor**, Nature Photonics **10**, 262 (2016).

[131] L. Museur, E. Feldbach, A. Kanaev, **Defect-related photoluminescence of hexagonal boron nitride**, Phys. Rev. B **78**, 155204 (2008).

[132] R. Bourrellier, S. Meuret, A. Tararan, O. Stéphan, M. Kociak, L. H. G. Tizei, A. Zobelli,**Bright UV Single Photon Emission at Point Defects in h-BN**, Nano Lett. **16**, 4317 (2016).

[133] T. T. Tran, K. Bray, M. J. Ford, M. Toth, I. Aharonovich, **Quantum emission from hexagonal boron nitride monolayers**, Nature Nanotechnology **11**, 37 (2015).

[134] T. T. Tran, C. Zacherson, A. M. Berhane, K. Bray, R. G. Sandstrom, L. H. Li, T. Taniguchi, K. Watanabe, I. Aharonovich, M. Toth, **Quantum Emission from De-**

fects in Single-Crystalline Hexagonal Boron Nitride, Phys. Rev. Applied **5**, 034005 (2016).

[135] T. T. Tran, C. Elbadawi, D. Totonjian, C. J. Lobo, G. Grosso, H. Moon, D. R. Englund, M. J. Ford, I. Aharonovich, M. Toth, **Robust Multicolor Single Photon Emission from Point Defects in Hexagonal Boron Nitride**, ACS Nano **10**, 7331 (2016).

[136] A. W. Schnell, T. T. Tran, H. Takashima, S. Takeuchi, I. Aharonovich, **Non-linear excitation of quantum emitters in hexagonal boron nitride mulitilayers**, APL Photonics **1**, 091302 (2016).

[137] N. R. Jungwirth, B. Calderon, X. Ji, M. G. Spencer, M. E. Flatté, G. D. Fuchs, **Temperature Dependence of Wavelength Selectable Zero-Phonon Emission from Single Defects in Hexagonal Boron Nitride**, arXiv:1605.04445 (2016).

[138] L. J. Martínez, T. Pelini, V. Waselowski, J. R. Maze, B. Gil, G. Cassabois, V. Jacques, **Efficient single photon emission from a high-purity hexagonal boron nitride crystal**, arXiv:1606.04124 (2016).

[139] N. Chejanovsky, M. Rezai, F. Paolucci, Y. Kim, T. Rendler, W. Rouabeh , F. F. de Oliveira, P. Herlinger, A. Denisekno, S. Yang, I. Gerhardt, A. Finkler, J. H. Smet, J. Wrachtrup, **Topological attributes and photo-dynamics of visible spectrum quantum emitters in hexagonal boron nitride**, arXiv:1608.03114 (2016).

[140] A. L. Exarhos, D. Hopper, R. R. Grote, A. Alkauskas, L. C. Bassett, **Optical Signatures of Quantum Emitters in Suspended Hexagonal Boron Nitride**, arXiv:1609.02641 (2016).

[141] A. Gruber, A. Drabenstedt, C. Tietz, L. Fleury, J. Wrachtrup, C. von Borczyskowski, **Scanning Confocal Optical Microscopy and Magnetic Resonance on Single Defect Centers**, Science **276**, 2012 (1997).

[142] R. Brouri, A. Beveratos, J-P. Poizat, P. Grangier, **Photon antibunching in the fluorescence of individual color centers in diamond**, Opt. Lett. **25**, 1294 (2000).

[143] S. Castelletto, B. C. Johnson, V. Ivády, N. Stavrias, T. Umeda, A. Gali , T. Ohshima, **A silicon carbide room-temperature single-photon source**, Nature Materials **13**, 151 (2014).

[144] M. A. Reed, J. N. Randall, R. J. Aggarwal, R. J. Matyi, T. M. Moore, A. E. Wetsel, **Observation of discrete electronic states in a zero-dimensional semiconductor nanostructure**, Phys. Rev. Lett. **60**, 535 (1988).

[145] P. Michler, A. Kiraz, C. Becher, W. V. Schoenfeld, P. M. Petroff, L. Zhang, E. Hu, A. Imamoglu, **A Quantum Dot Single-Photon Turnstile Device**, Science **290**, 2282 (2000).

[146] B. Lounis, W. E. Moerner, **Single photons on demand from a single molecule at room temperature**, Nature **407**, 491 (2000).

[147] M. Koperski, M. R. Molas, A. Arora, K. Nogajewski, A. O. Slobodeniuk, C. Faugeras, M. Potemski, **Optical properties of atomically thin transition metal dichalcogenides: Observations and puzzles.** arXiv:1612.05879 (2016).